The Structural Record of Mid - Crustal Stress and Pore Fluid Pressure Changes Related to the Earthquake Cycle

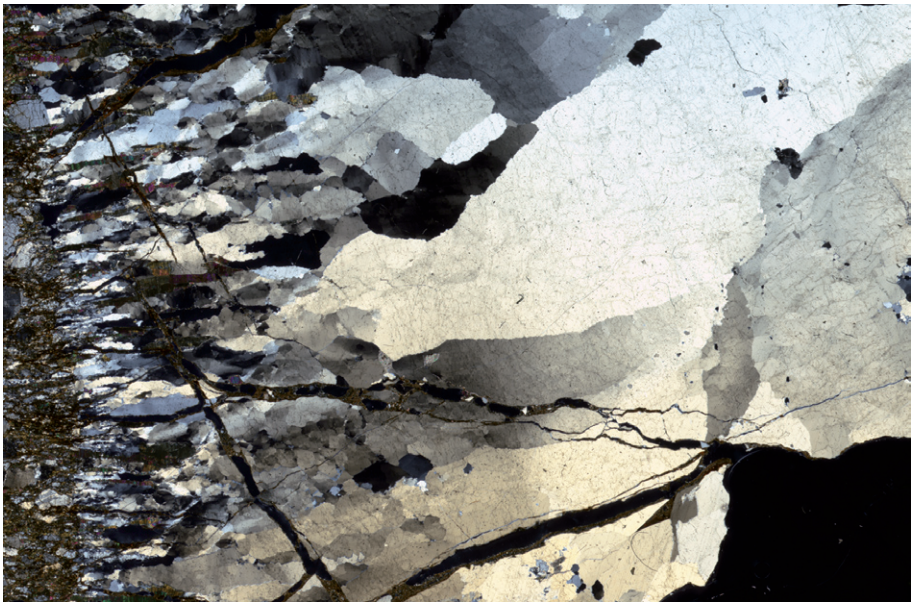

Thesis accepted by the faculty of Geoscience at the Ruhr-University Bochum, Germany, in fulfilment of the requirements for the degree of a Dr. rer. nat.

Jens-Alexander Nüchter

Day of examination:
26.01.2007

Examination committee:

Prof. Dr. B. Stöckhert
Prof. Dr. M. Alber
Dr. habil. T. Meier

Table of contents

Abstract

Metamorphic rocks approaching the crustal scale brittle-ductile transition during exhumation are expected to become increasingly affected by short term stress changes related to seismic activity in the overlying seismogenic layer, while still residing in a long-term viscous environment. Rapid coseismic loading to high stress is expected to cause a transient downward deflection of the crustal scale brittle ductile transition in consequence to the high imposed strain rate. The uppermost horizon of the plastosphere (Scholz, 1990) beneath the fault tip, capable of viscous flow on a long term, will undergo brittle failure in consequence to coseismic loading. The (micro-)structural record of syntaxial monogenetic veins in the high pressure / low temperature metamorphic Styra-Ochi Unit in southern Evia, Greece is investigated to gain insight into rapid stress and pore fluid pressure changes in the middle crust in consequence to the seismic cycle. The following features are characteristic:

1) The veins crosscut the foliation and all pre-existing structures.
2) The veins have formed from tensile fractures, with a typical length on the order of 10^{-1} to 10^{1} m. Vein orientation is uniform on the kilometre scale.
3) Some veins branch symmetrically with an aperture angle of 30°. Symmetrical branching is indicative for unstable fracture propagation approaching the terminal velocity.
4) Fabrics of the vein quartz indicate that the veins formed during a single sealing stage by mineral precipitation in open cavities.
5) The veins show a low aspect ratio of about 10 to 100 and a characteristic lenticular shape, which requires distributed ductile deformation of the host rock.
6) The sealing quartz grains reveal a broad spectrum of microstructural features indicative of crystal plastic deformation at temperatures of about 300 to 350°C and high stress.
7) Fluid inclusions trapped in the vein quartz recorded time series of pore fluid pressure evolution during vein sealing, from markedly sublithostatic pressure at the vein margins (early stage) to quasi lithostatic pressure in the vein centre (final stage).
8) The intensity of inhomogeneous crystal plastic deformation decreases towards the vein centres.

The features indicate that opening of the fractures commenced immediately after crack arrest. It was controlled by ductile deformation of the host rock at temperatures between 300 and 350°C, with fracture-parallel shortening by less than 2%. Quartz crystallized inward from the fracture walls during progressive opening of the fissure and buckling of the walls. Early grown grains record a longer history of deformation than those close to the vein centre, leading to the observed gradient in the intensity of crystal plastic deformation.

Based on the principles of fracture mechanics, the pore fluid pressure in an open cavity must be in equilibrium with the wall normal remote stress σ_3. In an extensional tectonic regime, the maximum principal stress σ_1 is defined by the overburden rock mass and is constant.

The evolution from low to high pore fluid pressure reflects the relaxation of a coseismically induced stress peak. During opening and sealing of the fissure, the, differential stress drops by about 80 to 100 MPa. The timescale of vein sealing compares to the timescale for the decay of the remote stress, which can be approximately predicted using a best guess bulk rock rheology (e.g. a flow law for powerlaw creep of quartz or a constant Newtonian viscosity) and assuming relaxation in a fixed grip mode. For a simple model with a constant viscosity of 10^{21} Pa s, the inferred timescale of vein sealing is on the order of 10^{1} to 10^{2} years.

These findings are consistent with the following scenario: Unstable fracture propagation is the consequence of rapid coseismic loading related to fault slip in the overlying brittle crust. During loading, the pore fluid pressure drops in consequence to distributed damage. Decelerating viscous creep and rise in the pore fluid pressure during postseismic stress relaxation result in fracture opening. Sealing of the fissures to become veins takes place by precipitation of minerals from the pore fluid streaming through the evolving cavity. Opening of fractures and development to a vein is therefore interpreted to be a short-term and episodic process during a stage of postseismic creep. If so, the record of the exhumed rocks provides insight into earthquake-related damage in the uppermost plastosphere, stress and pore fluid pressure changes in the earthquake cycle, and transient crustal properties during postseismic creep and stress relaxation.

1. Introduction

1.1. Problem definition and scope

Major earthquakes are followed up by a transient stage of accelerated postseismic surface deformation, observable by modern geodetic techniques (Arnadottir and Segal, 1994; Pollitz et al., 2001; Bosl and Nur, 2002; Freed and Bürgmann, 2004; Freed et al., 2006; Ellis et al., 2006). Inversion of the surface displacement patterns is generally interpreted to reflect afterslip on the fault plane in seismogenic depth and/or viscous deformation of the half space situated below the brittle ductile transition in consequence to rapid coseismic loading to high stress (e.g. Arnadottir and Segal, 1994; Ivins, 1996; Pollitz et al., 2001; Freed and Bürgmann, 2004; Arnadottir et al., 2005; Freed et al. 2006; Ellis et al., 2006). While the stress in the seismogenic layer is reduced in consequence to seismic slip, very high differential stress may build up locally near and below the lower termination of the fault (e.g. Sibson, 1980; Tse and Rice, 1986; Scholz, 1990; Küster and Stöckhert, 1999; Trepmann and Stöckhert, 2001; Ellis and Stöckhert, 2004a, 2004b; Ellis et al. 2006) in the uppermost part of the plastosphere (Scholz, 1990), otherwise being capable of viscous flow on the long term. Coseismic loading causes a downward deflection of the brittle ductile transition in consequence to the imposed high strain rates (e.g. Sibson, 1980; Scholz, 1990; Küster and Stöckhert 1999; Trepmann and Stöckhert 2001, 2002, 2003; Ellis and Stöckhert 2004a; Rolandone et al. 2004). Therefore, the uppermost horizon of the plastosphere (Scholz, 1990) beneath the fault tip will undergo brittle failure during coseismic loading (Sibson, 1980; Küster and Stöckhert, 1999; Baisch and Bokelmann, 2001; Trepmann and Stöckhert, 2002; Miller et al., 2004). Afterwards, during postseismic stress relaxation, the brittle damage is expected to become reduced by thermally activated sealing and healing processes (Baisch and Bokelmann, 2001; Miller et al., 2004).

Previous investigations on exhumed metamorphic rocks provided evidence for major changes in the fluid pressure in consequence to the seismic cycle (Mullis, 1976; Küster and Stöckhert, 1999; Trepmann and Stöckhert, 2002). High differential stress is not compatible with a lithostatic pore fluid pressure due to the limited strength of the rocks (Etheridge et al., 1984; Kohlstedt et al., 1995). The pore fluid pressure must therefore drop during loading to high stress, and can recover to a near-lithostatic level during postseismic stress relaxation (Mullis, 1976; Trepmann and Stöckhert, 2002).

The nature of seismically induced damage in the middle crust and the related pore fluid pressure changes are poorly constraint due to the lack of direct access and insufficient resolution of geophysical techniques. The structural record of exhumed metamorphic rocks potentially provides the only access to a detailed record of brittle damage and pore fluid pressure changes, though imposed by earthquakes in the geological past, which nucleated in the formerly overlying, now eroded upper crust (Mullis, 1976; Küster and Stöckhert, 1999; Trepmann and Stöckhert, 2002).

The structural record of discordant quartz veins with a low aspect ratio in the metamorphic Styra-Ochi Unit of southern Evia (Greece) is interpreted to result from a stage of brittle failure in the middle crust followed by viscous deformation during stress relaxation. Such veins are considered as recorders of coseismic brittle failure followed up by postseismic stress relaxation and damage reduction by sealing. A detailed study of the structural record of the veins on the mesoscopic and microscopic scale provides detailed insight into material behaviour and conditions during the seismic cycle. The characteristic timescale of postseismic stress relaxation and recovery of pore fluid pressure can be estimated. The present study is based on the principle of uniformitarianism. It is expected that the processes recorded by metamorphic rocks millions of years ago in the geological past are identical to those governing postseismic phenomena and surface deformation in present days.

1.2. Objectives of the present thesis

The discordant veins in the Styra-Ochi Unit in southern Evia are expected to result from brittle failure in consequence to almost instantaneous coseismic loading, followed up by fracture opening and mineral precipitation into the evolving cavity during postseismic stress relaxation. Therefore, the veins are potential recorders of transient stress and pore fluid pressure cycles in the middle crust, imposed by seismic activity in the middle crust. The objectives of the present thesis are as follows:

- To examine evidence for the switch between brittle failure and viscous creep as a function of the imposed stress and strain rate in the middle crust.
- To estimate postseismic finite strain from the geometry of the veins.
- To assess the history of pore fluid pressure from fluid inclusions trapped in the vein sealing grains.
- To draw conclusions on the magnitude of imposed differential stress and the characteristic stress history.
- To gain information about the timescale of postseismic stress relaxation and pore fluid pressure recovery.

1.3. Organization of the thesis

Following this brief introduction, the thesis is composed of three individual manuscripts ready to be submitted to scientific journals. Therefore, some chapters are repeated in the individual manuscripts, because they are required in each individual paper for the discussion.

The second chapter outlines the evidence for the switch between unstable tensile crack propagation and viscous low finite strain deformation of the host rock from the mesoscopic and microscopic structural record of the veins.

In the third chapter gradients in the microstructural record of the vein sealing quartz are investigated to support the model of progressive fracture parallel shortening of the host rock during the stage of vein sealing.

In chapter four, the pore fluid pressure changes during progressive widening and sealing of the vein are investigated by microthermometric analysis of primary fluid inclusions trapped in the vein quartz. It is demonstrated that the fluid pressure can be used as a stress gauge. Based on the results of this study, the timescale of stress relaxation, vein sealing, and pore fluid pressure recovery is discussed.

References

Arnadottir, T., Segal, P. (1994): The 1989 Loma-Prieta earthquake imaged from inversion of geodetic data.- J. Geophys. Res., 99: 21835-21855.

Arnadottier, T., Jónsson, S., Pollitz, F., Jiang, W., Feigl, K. L. (2005): Postseismic deformation following the June 2000 earthquake sequence in the soutj iceland seismic zone.- J. Geophys. Res, 110(B12): doi: 10.1029.

Baisch, S., Bokelmann, G.H.R. (2001): Seismic waveform attributes before and after the Loma Prieta earthquake: Scattering change near the earthquake and temporal recovery.- J. Geophys. Res., 106(B8): 16323-16337.

Bosl, W. J., Nur, A. (2002): Aftershocks and pore fluid diffusion following the 1992 Landers earthquake.- *J. Geophys. Res*, *107*(B12): doi: 10.1029/2001JB000155.

Ellis, S., Stöckhert, B. (2004a): Imposed strain localization in the lower crust on seismic timescales. Earth Planets Space, 56(12): 1103-1109.

Ellis, S., Stöckhert, B. (2004b): Elevated stresses and creep rates beneath the brittle-ductile transition caused by seismic faulting in the upper crust.- J. Geophys. Res., 109(5), B05407.

Ellis, S., Beavan, J., Eberhart-Phillips, D., Stöckhert, B. (2006): Simplified models of the Alpine Fault seismic cycle: stress transfer in the mid-crust.- Geophys. J. Int., 166(1): 386-402.

Etheridge, M.A., Wall, V.J., Cox, S.F. (1984): High fluid pressures during regional metamorphism and deformation: implications for mass transport and deformation mechanisms.- J. Geophys. Res., 89: 4344-4358.

Freed, A.M., Bürgmann, R. (2004): Evidence of powerlaw flow in the Mojave desert mantle.- Nature, 430: 548-551.

Freed, A.M., Bürgmann, R., Calais, E., Freymueller, J., Hreinsdóttir, S. (2006): Implications of deformation following the 2002 Denali, Alaska, earthquake for postseismic relaxation processes and lithospheric rheology.- J. Geophys. Res., 111(B1), doi: 10.1029.

Ivins, E.R. (1996): Transient creep of a composite lower crust 2. A polymineralic basis for rapidly evolving postseismic deformation modes.- J. Geophys. Res., 101: 28005-28028.

Küster, M., Stöckhert, B. (1999): High differential stress and sublithostatic pore fluid pressure in the ductile regime - microstructural evidence for short-term post-seismic creep in the Sesia Zone, Western Alps.- Tectonophysics, 303: 263-277.

Kohlstedt, D. L., Evans, B., Mackwell, S. J. (1995): Strength of the lithosphere: Constraints imposed by laboratory experiments.- J. Geophys. Res., 100(B9): 17587-17602.

Miller, S. A., Collettini, C., Chiaraluce, L., Cocco, M., Barchi, M., Kaus, B. J. P. (2004): Aftershocks driven by a high-pressure CO2 source at depth.- Nature, 427: 714-727.

Mullis, J. (1976): Daas Wachstumsmillieu der Quarzkristalle im Val d´lliez.- Schweizerische Mineralogische und Petrographische Mitteilungen, 56(2): 219-268.

Pollitz, F.F., Wicks, C., Thatcher, W. (2001): Mantle flow beneath a continental strike-slip fault: postseismic deformation after the 1999 Hector Mine earthquake.- Science, 293: 1814-1818.

Rolandone, F., Bürgmann, R., Nadeau, R.M. (2004): The evolution of the seismic-aseismic transition during the earthquake cycle; constraints from the time-dependent depth distribution of aftershocks.- Geophys. Res. Lett., 31(23).

Sibson, R.H. (1980): Transient discontinuities in ductile shear zones.- J. Struct. Geol., *2*: 165-171.

Scholz, C.H. (1990): The mechanics of earthquake and faulting.- Cambridge University press.

Trepmann, C.A., Stöckhert, B. (2001): Mechanical twinning of jadeite: an indication of synseismic loading beneath the brittle-plastic transition.- Int. J. Earth Sci., 90(1): 4-13.

Trepmann, C.A., Stöckhert, B. (2002): Cataclastic deformation of garnet; a record of synseismic loading and postseismic creep.- J. Struct. Geol., 24(11): 1845-1856.

Trepmann, C.A., Stöckhert, B. (2003): Quartz microstructures developed during non-steady state plastic flow at rapidly decaying stress and strain rate.- J. Struct. Geol., 25(12): 2035-2051.

Tse, S.T., Rice, J.R. (1986): Crustal earthquake instability in relation to the depth variation of frictional slip properties.- J. Geophys. Res., 91(9): 9452-9472.

2. Fracturing and single-event vein formation in the middle crust – the record of coseismic loading and postseismic creep

Abstract

Metamorphic rocks approaching the crustal scale brittle-ductile transition (BDT) during exhumation are expected to become increasingly affected by short term stress fluctuations related to seismic activity in the overlying seismogenic layer, while still residing in a long-term viscous environment. The (micro-)structural record of monogenetic syntaxial quartz veins in high pressure metamorphic rocks from southern Evia, Greece, is investigated to gain insight into the processes and conditions just beneath the long-term BDT. The following features are characteristic: 1) The veins crosscut the foliation and all pre-existing structures; 2) the veins have formed from tensile cracks, with a typical length on the order of 10^{-1} to 10^{1} m; 3) some veins branch symmetrically with an aperture angle of 30°, indicating high crack propagation rates on the order of Raleigh wave speed; 4) fabrics of the vein quartz show that the veins formed during a single sealing stage by mineral precipitation in open cavities; 5) the veins show a low aspect ratio of about 10 to 100 and a characteristic lenticular shape, which requires distributed ductile deformation of the host rock; 6) the fabrics of the sealing quartz indicate crystal plastic deformation at temperatures of about 300 to 350°C. Crack opening and concomitant sealing, commencing immediately after crack arrest, was controlled by ductile deformation of the host rock at temperatures between 300 and 350°C. Crack parallel shortening is less than 2%. The structural and microstructural record reflects an isothermal switch from brittle failure and high speed crack propagation to decelerating viscous creep. The high stress - low finite strain event is interpreted to record the seismic cycle, with rapid coseismic loading followed by postseismic stress relaxation, controlled by viscous creep of the host rock. The record of the exhumed rocks provides insight into the characteristics of earthquake-related damage in the uppermost plastosphere and transient crustal properties during postseismic stress relaxation, with details of history and spatial resolution only accessible in such fossil systems.

2.1. Introduction

Exhumed metamorphic rocks provide insight into processes and conditions at deeper levels of the crust, which are not accessible to direct observation with high resolution and details. Upon exhumation, originally deep seated crust has to pass the brittle ductile transition zone (BDT). Approaching the BDT from below in a tectonically active region means that the rocks get more and more affected by cyclic stress changes related to seismic activity in the overlying seismogenic layer (schizosphere sensu Scholz, 1990). Numerical models show that a crustal volume beneath the tip of a fault is loaded to high stress during major earthquakes (Ellis and Stöckhert, 2004a; Ellis and Stöckhert, 2004b). These stresses are relaxed during a subsequent episode of viscous postseismic creep that contributes to deformation recorded at the surface by modern geodetic techniques (e.g. Arnadottir and Segal, 1994; Peltzer et al., 1996; Pollitz et al., 2001; Freed and Bürgmann, 2004; Freed et al., 2006; Ellis et al., 2006). On a local scale, coseismic loading can be understood as deformation in a fixed grip mode: A certain volume of the crust is distorted elastically by only a few percent within a few seconds. The amount of strain accumulated during postseismic stress relaxation by viscous creep is expected to correspond to the amount of elastic distortion, quasi-instantaneously induced by coseismic slip

on the overlying fault. Hence, structures and fabrics of exhumed metamorphic rocks reflecting coseismic loading and postseismic stress relaxation are expected to bear the characteristics of high stress–low strain events. Microstructural evidence for such events have been reported from the Sesia Zone, Western Alps (Küster and Stöckhert, 1999; Trepmann and Stöckhert, 2001, 2002, 2003) and are interpreted to record major earthquakes at ancient faults in the meanwhile eroded upper crust.

Stress changes during rapid coseismic deformation of the middle crust cause a downward deflection of the brittle ductile transition in consequence of the high imposed strain rate (Fig. 1) (e.g. Tse and Rice, 1986; Scholz, 1990; Küster and Stöckhert 1999; Ellis and Stöckhert 2004a). The uppermost horizon of the plastosphere (Scholz, 1990) beneath the fault tip, capable of viscous flow on a long term, will undergo brittle failure in consequence to coseismic loading (Fig. 1). The temporary downward deflection of the long-term brittle-ductile transition and the subsequent restoration to its original level are documented by the time-dependent depth distribution of aftershocks related to the 1992 M 7.3 Landers earthquake (Rolandone et al. 2004). There, an instantaneous coseismic downward shift in the vertical distribution of hypocenters is followed by recovery to the long term depth distribution within about 10 years (Fig. 2).

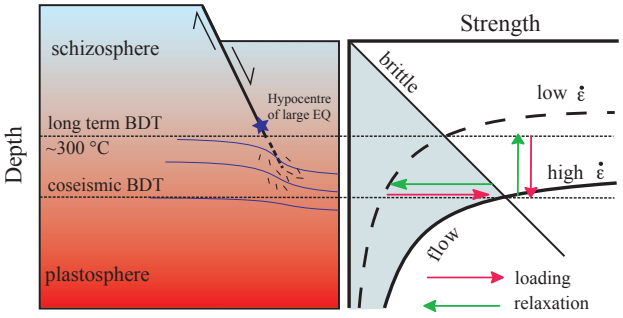

Fig. 1: Scheme illustrating of the effects of coseismic loading and postseismic creep. Coseismic loading results in a downward deflection of the crustal scale brittle ductile transition in consequence to the high imposed strain rate. During postseismic stress relaxation, the brittle ductile transition recovers to the long term depth.

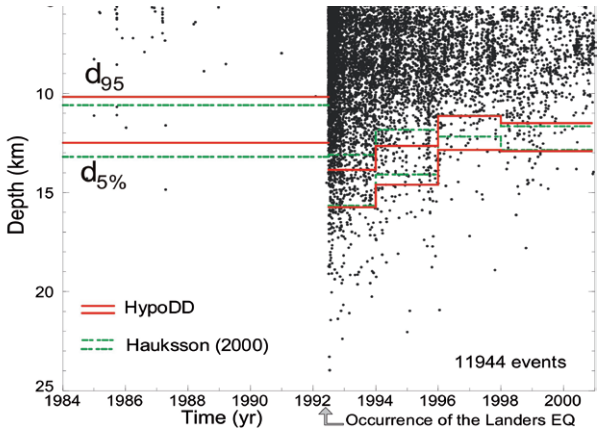

Fig. 2: The depth distribution of aftershocks reflects an instantaneous downward deflection of the brittle ductile transition in consequence to the June 28, 1992 M 7.3 Landers earthquake, followed up by recovery to the long term depth (Rolandone et al. 2004).

Previous reports on the record of seismically induced stress cycles in rocks once situated in the middle crust near the tip of a seismically active fault focused on microstructural features. These comprise fabrics indicating localized crystal plastic deformation at high stress (Trepmann and Stöckhert, 2001, 2003) or brittle failure (Trepmann and Stöckhert, 2002), followed up by creep at decreasing stress. In the present paper, I investigate what is suspected to be the record of the seismic cycle on the mesoscopic scale. The objective is distributed deformation in an extensive volume of middle crust in the vicinity of a seismogenic fault, not that of localized deformation

within a shear zone extending downwards from the fault. The characteristic properties of lenticular discordant quartz veins widespread in high pressure - low temperature metamorphic rocks exposed on Evia Island (Greece) are interpreted to record such episodic deformation, implying an isothermal switch from coseismic brittle failure to postseismic viscous creep. Such processes of non-steady state deformation are expected to contribute to the short-term surface deformation recorded by modern geodetic techniques, related to the earthquake cycle.

2.2. Geological setting

The Styra-Ochi Unit in southern Evia Island, Greece, is part of the high pressure - low temperature (HP-LT) metamorphic internal Cyclades belt, situated in the backarc region of the active Hellenic subduction zone. The structure of the Cyclades is governed by extensional tectonics and crustal thinning since the Early Miocene (Le Pichon and Angelier, 1981; Jolivet and Faccenna, 2000), driven by continuing roll back of the Hellenic subduction zone (Meulenkamp et al. 1988). In the Cyclades, extensional deformation is localized in a single major (e.g. Lister et al., 1984; Faure et al., 1991) or several (e.g. Gautier and Brun, 1994) detachment faults. For the major part, the hanging wall block is eroded, except for remnants on the islands of Tinos, Kea, and Paros (e.g. Gautier and Brun, 1994). The Styra-Ochi Unit in southern Evia is composed of a variety of siliciclastic and carbonate-rich marine metasediments, with metamorphosed basaltic to rhyolitic volcanic and intrusive rocks. During its earlier history, the Styra-Ochi Unit in southern Evia underwent pervasive deformation and HP-LT metamorphic overprint at about 400°C and 1 GPa (Klein-Helmkamp, 1996), indicating maximum burial to a depth of about 30 to 35 km. It was exhumed as a coherent unit, interpreted to represent the footwall block of a metamorphic core complex. The structures developed during that stage reflect a continuous evolution from ductile to brittle extensional deformation within a uniform kinematic framework (Gautier and Brun, 1994; Klein-Helmkamp, 1996). The veins investigated in the present study formed during exhumation and postdate HP-LT metamorphism.

2.3. Description of the crack patterns and the quartz veins developed from the cracks

Veins originate as cracks. As such, the stage of brittle failure and crack propagation is to be set apart from the stage of opening and sealing, i.e. vein formation. Information on the length of the original crack, its orientation and shape, and its relation to pre-existing structures is readily obtained from the geometry of the vein walls, with the filling material virtually removed. The processes of opening of the crack and sealing with material crystallizing from the pore fluid (e.g. Yardley, 1984) are recorded by the shape of the vein and the microstructures of the sealing minerals.

The veins of interest crosscut the foliation and all former syn-metamorphic structures and fabrics, including schistosity (Figs. 3, 4a, b), shearband foliation (Fig. 3), and pre-existing earlier veins parallel to the foliation (Fig. 4a). Schistosity, representing a plane of low tensile strength, is crosscut by the cracks at a variable, locally acute angle (Fig. 3). Some veins branch

symmetrically with an aperture angle of about 30° (Fig. 4c). The branches are straight and seem to be not influenced by pre-existing structures of the host rock. Conjugate crack sets and a shear offset parallel to the vein walls is not observed (Figs. 3, 4). The geometry suggests tensile failure (mode I) and opening normal to the least principal stress, σ_3. The orientation of the vein walls, hence of the original cracks, is more or less uniform all over the Styra-Ochi Unit in southern Evia, an area of more than 500 km^2. They trend about NW to NNW and are nearly vertical (Fig. 5). The orientation is consistent with a stress field characterized by $\sigma_1 = \sigma_v$ and σ_3 at about NE to ENE at the stages of fracturing and vein formation (Fig. 5). The length of most veins ranges between 10^{-1} m and 10^{1} m, which is taken to reflect the characteristic length scale of the cracks. Most veins show a symmetric lense shape with a low aspect ratio between 10 and 30 (Fig. 4, 14b). Some veins are more irregular in shape, showing swelling and pinching (Fig. 4b).

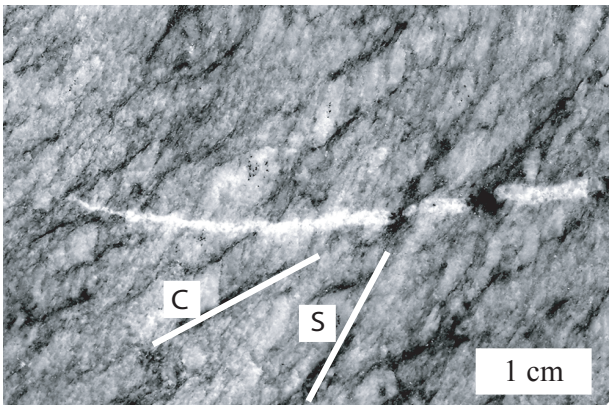

Fig. 3: The vein crosscuts the foliation (S and C-planes) at an acute angle. The vein tip is sharp.
Photograph from the polished sample EN 62.

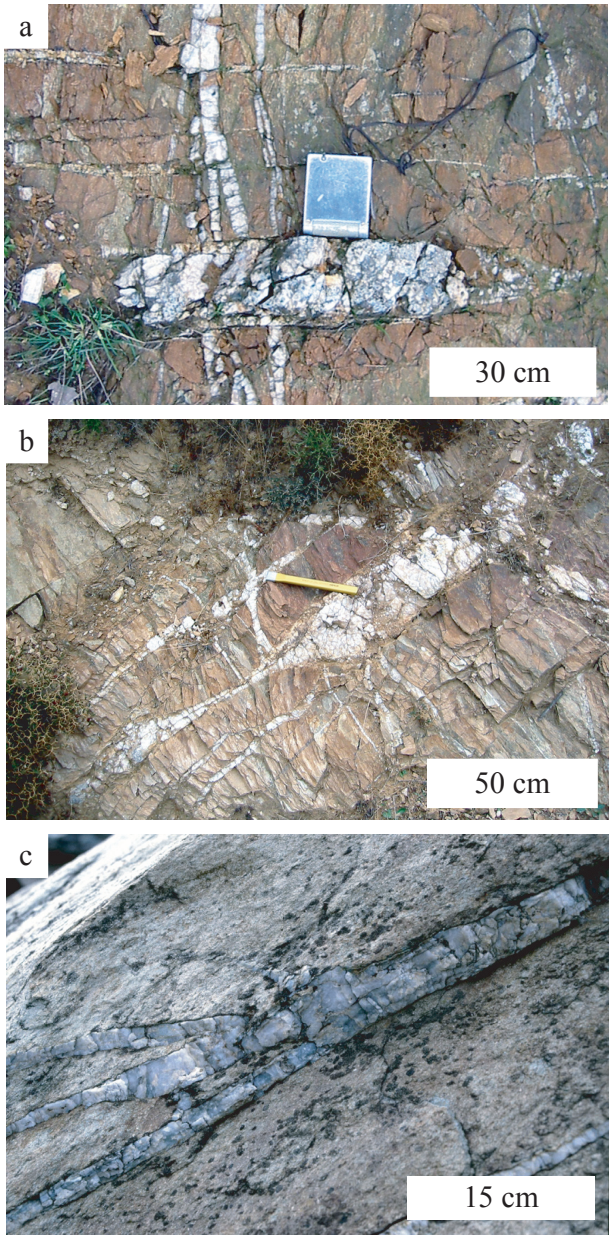

Fig. 4 (right): Discordant quartz veins in the Styra-Ochi Unit.
a) A lens-shaped vein with a low aspect ratio of about 12 crosscuts pre-existing concordant veins.
b) Vein with irregular shape showing swelling and pinching.
c) Symmetrically branching vein with the characteristic aperture angle of about 30°.

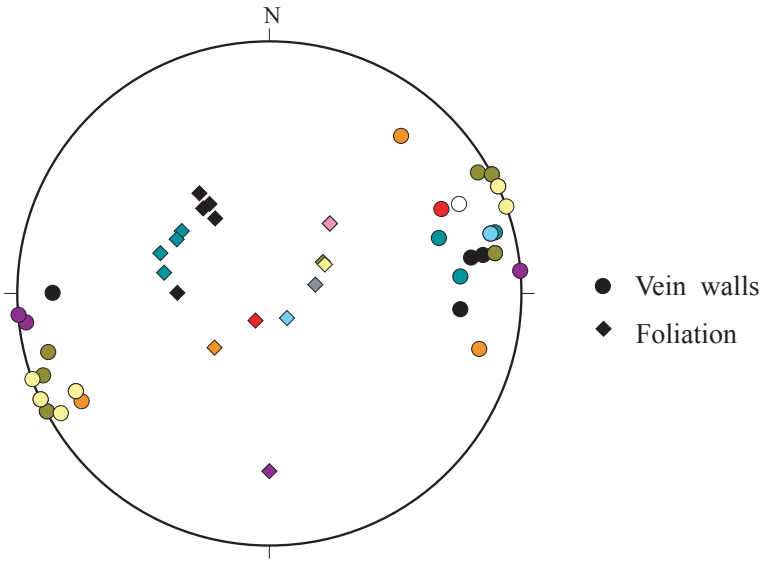

Fig. 5: Stereographic plot (lower hemisphere) of poles to the foliation and to the vein walls at different locations in the Styra-Ochi Unit of southern Evia (Greece). The data cover an area of more than 500 km^2.

2.4. Microfabrics of vein quartz

2.4.1. Methods

The microfabrics of the veins were investigated by optical and scanning electron microscopy. The samples were cut normal to the host rock foliation and normal to the vein wall. The microstructures were examined in thin section (30 µm thick) with a polarizing microscope. The scanning electron microscope (SEM)-based technique of electron backscatter diffraction (EBSD), using polished thin sections, yields microstructural information with a resolution on the µm scale and provides information on the spatial distribution of the full crystallographic orientation. EBSD-investigations were carried out using a SEM (LEO 1530) equipped with field emission gun and forescatter detector. For EBSD analysis, the thin sections were chemically polished using a silicon suspension (SYTON®) to minimise surface damage, then coated with carbon to limit charging effects. The SEM was operated at an acceleration voltage of 20 kV and a working distance of 25 mm, with the thin section tilted at an angle of 70° with respect to the beam.

2.4.2. Primary quartz microfabrics related to sealing

The veins are predominantly sealed by quartz, in places associated with additional minor albite and zoisite. Grains bearing crystallographically controlled facets are common (Fig. 6). At the vein margins, quartz tends to form elongate crystals with a shape and crystallographic preferred orientation of the c-axes about normal to the vein wall (Fig. 7 a, b; Fig. 8 a (I, II), b (I, II)). Close to the vein walls, the c-axis orientation distribution of the vein sealing quartz is diffuse with multiple weak maxima (Fig. 8 a (I), b (I)). With increasing distance to the vein walls, the number of these maxima reduces and the crystallographic preferred orientation (CPO) with a c-axis maximum about normal to the vein walls becomes more and more pronounced (Fig. 8 a (I), b (I)). The shape preferred orientation (SPO) of the long axis of the quartz grains corresponds to the CPO of the c-axes (Fig. 7 a, b; Fig. 8 a (II), b (II)). With increasing distance to the vein walls, the grain size increases gradually (Figs. 7 a, b; 8 a (III), b (III)) and reaches up to several centimetres in the centre of the vein (Fig. 9). Residual open vugs with crystallographically controlled faces are common (Fig. 10a). In contrast, inclusion trails parallel to the vein walls (Durney and Ramsay, 1973; Ramsay, 1980; Cox and Etheridge 1983; Fisher and Bryne, 1990; Fisher and Brantley, 1992; Fisher et al., 1995) are systematically absent.

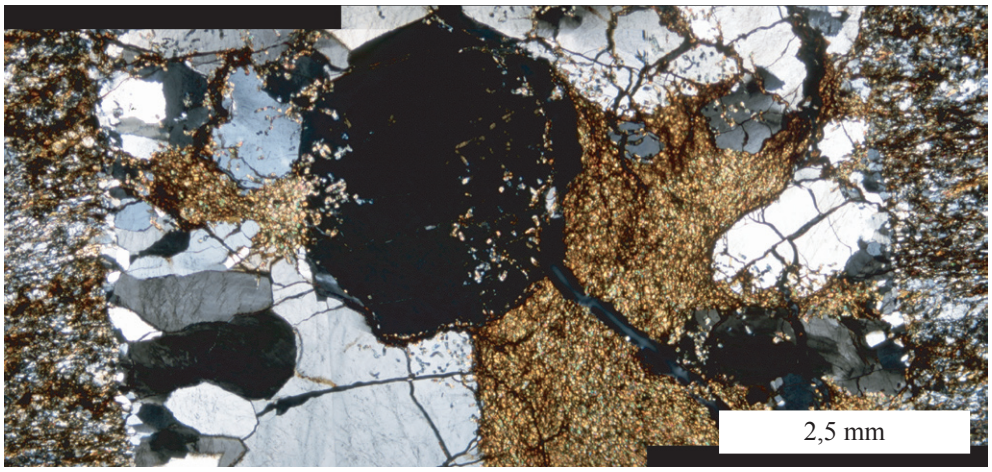

Fig. 6: Growth competition between crystals grown from the vein wall towards the vein centre. Some grains show crystallographically controlled facets. Micrograph with crossed polarizers.

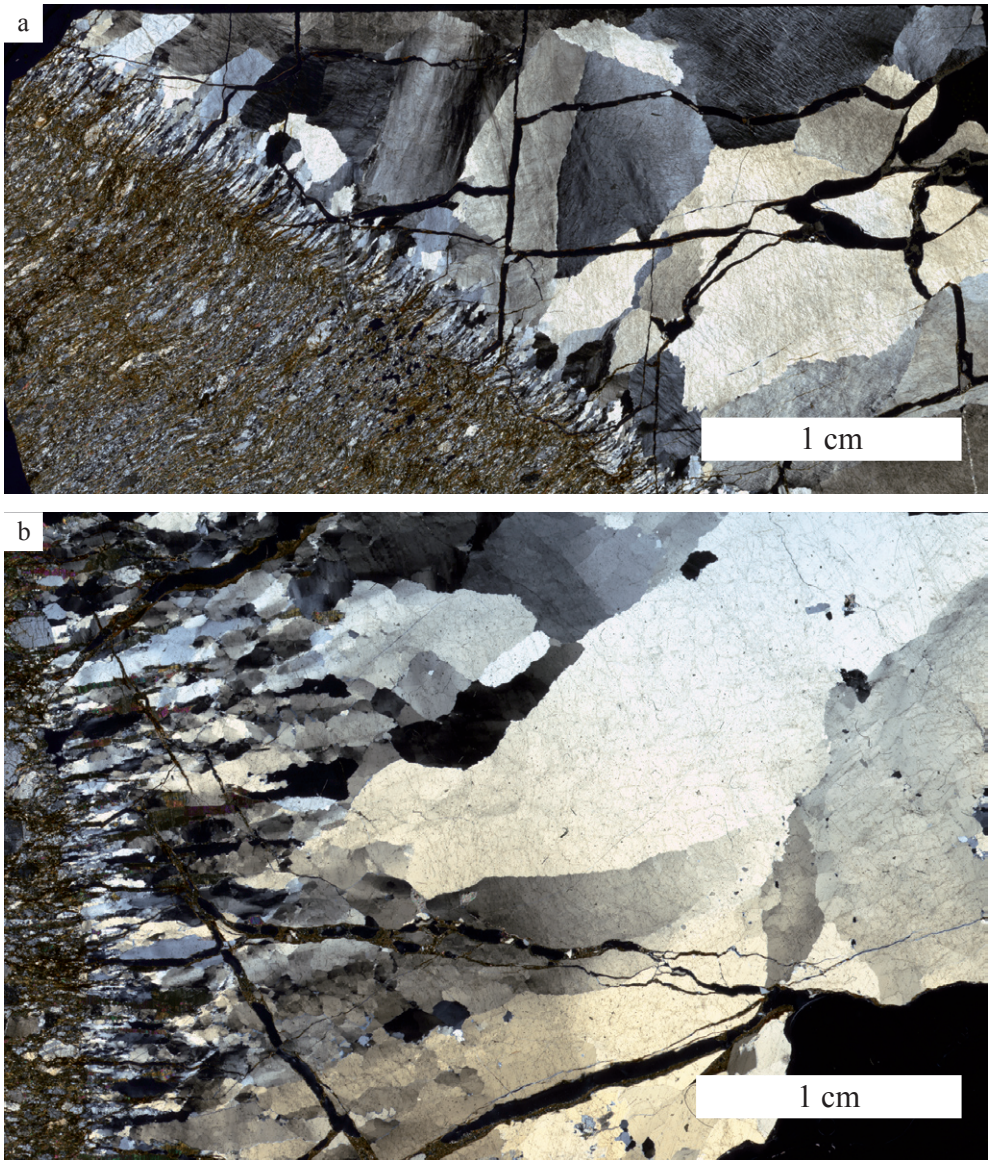

Fig. 7: Microfabrics of vein sealing quartz. With increasing distance to the vein walls, the grain size increases. The quartz grains show a shape preferred orientation with their long axes about normal to the vein walls, undulatory extinction, subgrains and sutured grain boundaries. A) Vein EN 4; B) Vein EN 45.
Thin sections scanned with crossed polarizers.

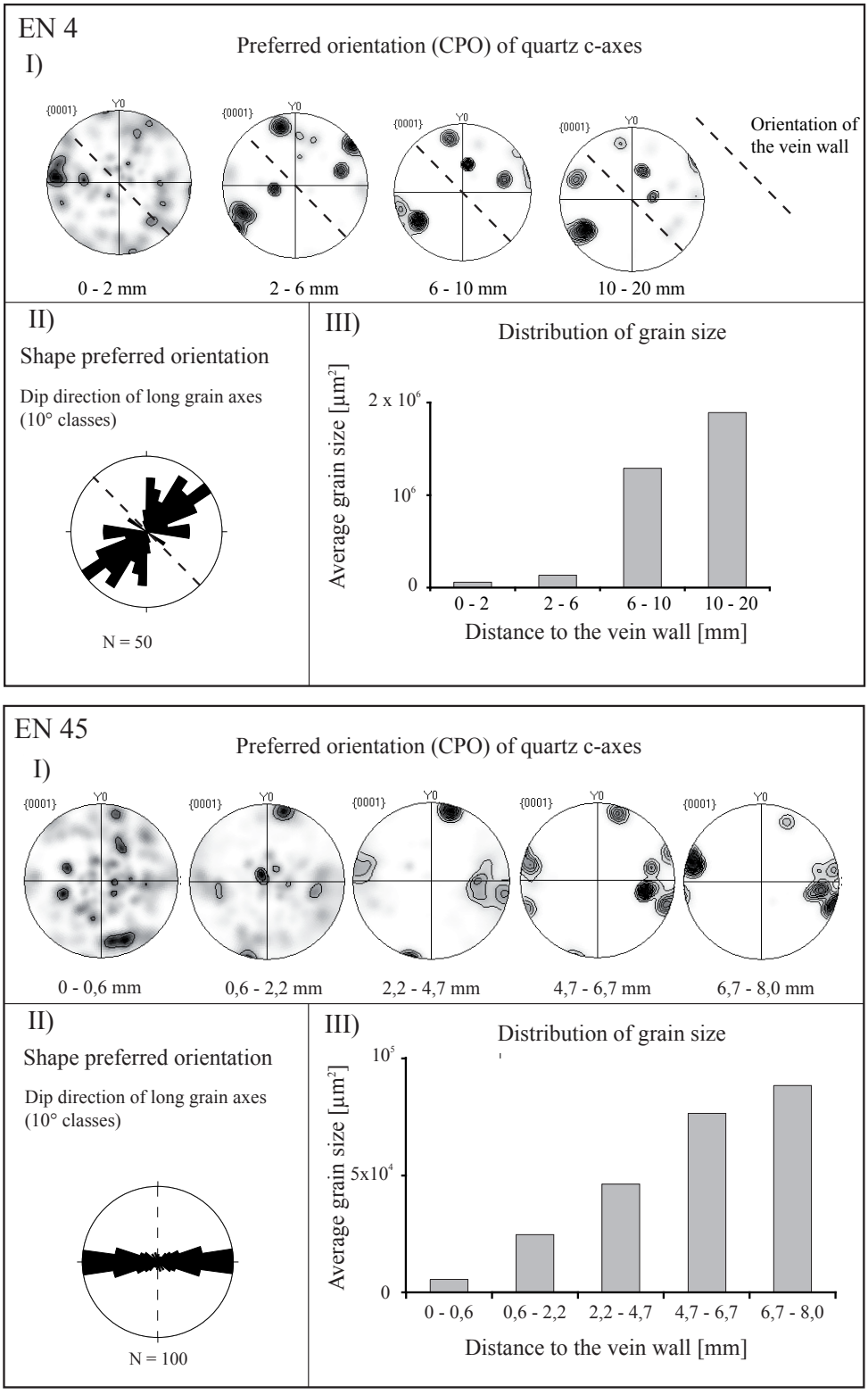

Figs. 8: Grain shape and orientation data acquired by EBSD for the area displayed in Fig. 7.

I) Development of a more pronounced quartz c-axes preferred orientation with increasing distance to the vein walls. II) Shape preferred orientation of the quartz crystals. III) Increase in quartz grain size with increasing distance to the vein walls. A) Vein EN 4 (Fig. 7a), B) Vein EN 45 (Fig. 7b).

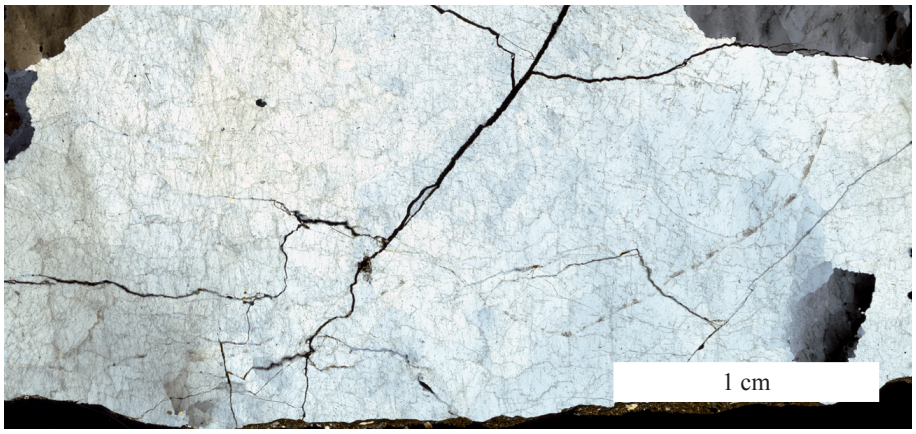

Fig. 9: Centimetre-sized quartz crystals at the centre of vein EN 45. The grains show undulatory extinction. Scanned thin section with crossed polarizers.

2.4.3. Microfabrics of vein quartz related to crystal plastic deformation

The coarse quartz grains in the veins show microstructures indicative of deformation by dislocation glide, least so in the vicinity of the open vugs. Inhomogeneous crystal plastic deformation is revealed by marked undulatory extinction, deformation bands and deformation lamellae (Figs. 7, 10). Microstructures indicating thermally activated annealing comprise subgrains and sutured high-angle grain boundaries indicative of migration recrystallization (strain-induced grain boundary migration) (Figs. 7, 10b, c). New grains formed by recrystallization are restricted to the outermost zone of the veins (Fig. 7) and are absent in their centre (Figs. 7, 9). On the grain scale, finite strain is very low; most grains appear almost undistorted with their original shape largely preserved.

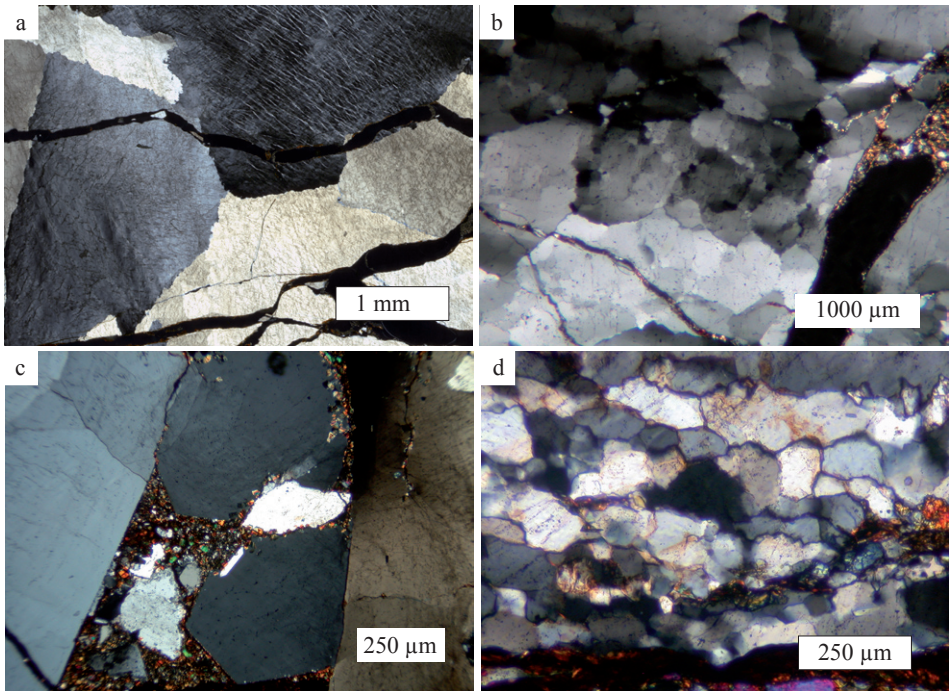

Fig. 10: Microfabrics of the vein sealing quartz crystals showing undulatory extinction (a, b, c), subgrains (b) and deformation bands (a), least so in the vicinity of the central open vugs (c). Recrystallized grains are restricted to the vein margins (d).
Micrographs with crossed polarizers.

2.5. Discussion

2.5.1. Crustal level of fracturing and vein formation

The veins crosscut all syn-metamorphic structures of the host rock and the original vein shape appears to be at best little modified by later deformation. Hence, the cracks and the resulting veins postdate the pervasive ductile deformation during HP / LT metamorphism. The orientation of the veins indicates that tensile fracturing and vein formation occurred in an extensional tectonic environment. The structural record indicates that the veins do not represent deep-seated syn-metamorphic structures, but must have formed during exhumation and cooling.

The widespread record of recrystallization in the vein quartz microstructures suggests deformation at elevated temperatures. The correlation between thermochronometry and natural quartz microstructures (e.g. Voll, 1976; Dunlap et al., 1997; Stöckhert et al., 1999; Brix et al., 2002), supported by the extrapolation of experimental flow laws to slow geological strain rates (e.g. Hirth et al., 2001), provides a base to estimate these temperatures. For deformation of the vein quartz, the microfabrics point to temperatures similar to or slightly above 300°C, a temperature commonly predicted for the long-term brittle-ductile transition in continental crust (Strehlau and Meissner, 1987; Ranalli and Murphy, 1987). As there is no evidence for a complex thermal history in the Styra-Ochi Unit (Klein-Helmkamp, 1996) and uniform cooling during exhumation can be assumed, this means that brittle failure and opening of the cracks to become veins must have taken place at temperatures near to or somewhat above 300°C. The thermobarometric results (Klein-Helmkamp, 1996) indicate that the P-T conditions approached a geotherm of roughly 30°C/km upon exhumation, in accordance with exhumation in an extensional environment. More precise information on the geotherm at the stage of interest being not available, the temperatures similar to 300°C are assumed to have prevailed at a depth of similar to 10 km.

2.5.2. The stage of loading, initiation and propagation of cracks

In the following, compressive stresses are denoted by positive and tensile stresses by negative values, as commonplace in structural geology. The resistance of rock to brittle failure is governed by the distribution of preexisting voids, like sharp flaws, (micro-)cracks and blunt pores, as well as grain and interphase boundaries, at which the applied remote stress is intensified (Griffith, 1920; Irwin, 1948, 1956, 1957). The magnitude of stress in the material at a distance r to a crack tip under tensile load is proportional to the static stress intensity factor K_I and to $r^{-1/2}$ (Irwin, 1948, 1956, 1957). Stress is strongly intensified near a crack tip. The static tensile stress intensity factor depends on the magnitude of tensile stress acting normal to the crack, σ_n, and the crack length L (Irwin, 1948, 1956, 1957):

$$K_I = -\sigma_n \sqrt{\pi L/2} \qquad (1)$$

The stress intensity factor K_I is independent of the void geometry (Crager and Paris, 1967). The stress intensification around a crack tip drives crack propagation. Hence, K_I is also referred to as the tensile crack extension force (e.g. Atkinson, 1987; Anderson, 1995). If K_I reaches a certain material constant, the fracture toughness K_{IC} (Irwin, 1961), the material fails by initiation of unstable crack propagation. The fracture toughness rises with increasing blunting of the crack tip and is maximum for spherical voids (e.g. Anderson, 1995; Bertram and Kalthoff, 2003). As K_{IC} is exclusively defined for sharp crack tips (Irwin, 1961), the fracture toughness at blunt voids is referred to K^*_{IC} (e.g. Anderson, 1995; Bertram and Kalthoff, 2003). During unstable crack propagation, the value of the static stress intensity factor K_I increases with crack length for σ_n = const (eq. 1). Since the first law of thermodynamics must be obeyed, the excess in crack extension force, K_I, is converted into kinetic energy (Anderson, 1995). The kinetic energy controls the crack speed (Atkinson, 1987; Anderson, 1995). For high speed crack propagation, the kinetic energy may also allow crack propagation to continue for a short while when K_I has fallen to below K_{IC}. Therefore, high speed cracks get arrested when K_I reaches the arrest toughness $K_{IA} < K_{IC}$ (e.g. Anderson, 1995).

The energy approach of Griffith (1920) and Irwin (1956, 1957) implies that incremental crack propagation can be described as a release of strain energy. The energy release rate, G, is correlated with the rate of crack tip propagation (e.g. Atkinson, 1987). The energy is dissipated by the formation of two new surface increments and the inelastic damage in the process zone around the crack tip (e.g. Anderson, 1995; Engvik et al., 2005). If a crack is accelerated to the terminal velocity, theoretically limited by the Raleigh wave speed (e.g. Lawn, 1975; Atkinson, 1987; Anderson, 1995; Bertram and Kalthoff, 2003), a further increase in the energy release rate cannot be attained by further acceleration. Instead, cracks branch to increase the area of new surface and the volume of the related damage zone per growth increment. This type of fracture branching is symmetric in isotropic and homogeneous material, with a characteristic apex angle of 30° (Kalthoff, 1973).

From the general law of effective stress (Rice and Cleary, 1976), the normal stress σ_n acting on the wall of a fluid filled crack is reduced to an effective value σ'_n by the pore fluid pressure P_f:

$$\sigma'_n = \sigma_n - P_f \qquad (2)$$

Crack opening is only possible, when σ'_n gets negative due to a sufficient magnitude of P_f (Sibson, 1981; Atkinson and Cook, 1993). The pore fluid pressure P_f in the deeper crust, beneath the brittle ductile transition, is assumed to be approximately lithostatic, i.e. to correspond to the overburden pressure of the rock mass $\sigma_v = \rho_r gz$, with ρ_r denoting the average rock density, g the gravitational acceleration, and z the depth (Bradley, 1975; Walder and Nur, 1984; Nur and Walder, 1990; Manning and Ingebritsen, 1999).

In a natural rock, pore fluid is distributed as fluid inclusions or channels along grain edges and as fluid inclusions on grain boundaries or within crystals (Watson and Brenan, 1987; Spear 1993). For a dihedral angle above 60°, the pore fluid will be confined into isolated pockets at grain corners and grain edges, and for a dihedral angle below 60°, an interconnected network of channels along the grain edges will form that results in a high permeability (Watson and Brenan, 1987). Transient network permeabilities may also form in response to loading, when (micro-)fractures start to propagate along grain and interphase boundaries (Etheridge, 1983; Etheridge et al., 1984). In the following discussion, the pressure of fluid distributed in interconnected intergranular interstices is referred to as pore fluid pressure P_f^p. Apart from fluids in this interconnected pore space, fluids are also entrapped in isolated voids, like fluid inclusions within crystals. At temperatures sufficient to allow creep deformation of the host mineral, the fluid pressure inside such isolated voids is expected to correspond to the mean stress, $(\sigma_1 + \sigma_2 + \sigma_3) / 3$ (Etheridge et al., 1984). The pore fluid pressure in isolated voids is referred to as void fluid pressure P_f^v.

Based on these concepts, the veins analyzed in the present study are interpreted to result from cracks which propagated driven by high remote stress, i.e. at a high stress intensity factor K_I. This interpretation is based on two principal observations: First, the veins crosscut pre-existing planes of low tensile strength in the host rock, e.g. schistosity, at a variable and in places acute angle (Figs. 3, 4 a, b). The structures show that pre-existing anisotropy and planes of weakness did not affect the crack path. If so, the crack path was exclusively controlled by the orientation of the principal stresses. In contrast, when tensile cracks propagate in an environment of low remote stress, as expected for hydraulic fractures (Secor, 1965; Secor and Pollard, 1975; Sibson, 1981), the crack path is strongly influenced by the anisotropy of tensile strength (e.g. Henderson et al. 1990). Second, symmetrical branching of the cracks (Fig. 4c) is indicative for unstable crack propagation at the terminal velocity (Kalthoff, 1973; Lawn, 1975; Atkinson, 1987; Anderson, 1995; Bertram and Kalthoff, 2003). Crack propagation with terminal velocity is achieved by converting excessive crack extension force into kinetic energy (Kalthoff, 1973; Atkinson, 1987; Anderson, 1995). For a crack to propagate with a speed close to the terminal velocity, the crack extension force must be very high. Crack branching is therefore indicative of a very high remote differential stress (Kalthoff, 1973; Lawn, 1975).

In structural geology, it is a widely accepted paradigm that veins developing from tensile cracks can only form in an environment of high pore fluid pressure and low remote differential stress (e.g. Secor, 1965; Secor and Pollard, 1975; Sibson, 1981). Based on the Griffith failure criterion and illustrated in the Mohr diagram, formation of tensile cracks is proposed to be restricted to a differential stress not exceeding $4T_0$, with T_0 denoting tensile strength (e.g. Secor, 1965; Secor and Pollard, 1975; Sibson, 1981). Furthermore, it is anticipated that hydraulic fractures advance and arrest in a cyclic process, controlled by the changing fluid pressure in the crack (Atkinson and Cook, 1993; Renshaw and Harvey, 1994). The pressure change arises

from the volume increase related to crack propagation (Atkinson and Cook, 1993; Renshaw and Harvey, 1994; Olson, 2003). If the rate of fluid flow into the crack cannot keep up with the dilatation rate, the crack gets arrested. Crack propagation is re-initiated, when the internal fluid pressure has sufficiently recovered so that $K_I = K_{IC}$. As such, the propagation rate is limited by the rate of fluid flow into the crack, which in turn is governed by the permeability of the host rock (Atkinson and Cook, 1993; Renshaw and Harvey, 1994). As a consequence, for hydraulic fractures, the crack extention force must remain low. In rocks of low permeability, particularly under metamorphic conditions (Brace, 1980, 1984; Nur and Walder, 1990; Oliver, 1996; Manning and Ingebritsen, 1999), hydraulic fractures are prevented from unstable runaway crack propagation (Atkinson and Cook, 1993; Renshaw and Harvey, 1994). Instead, they grow in a cyclic process with repeated initiation and arrest after a small increment of growth (Atkinson and Cook, 1993; Renshaw and Harvey, 1994). Crack propagation gets quasi-static at an approximately constant, slightly fluctuating, stress intensity factor ($K_I \approx K_{IC}$). For a comprehensive poroelastic treatment of fluid flow in porous media affecting the crack propagation rate the reader is referred to Renshaw and Harvey (1994).

Based on the above considerations, the structural record of the veins investigated in the present study is in conflict with an origin by hydraulic fracturing as described above. The structures indicate that tensile cracks propagated in an environment of high remote stress. At the stage of crack propagation, the crack extention force must have been very high, as indicated by the symmetrical branching observed for some of the veins. Loading of the middle crust, which behaves in a viscous manner on the long term, to high differential stress must necessarily be achieved in a very short time, most probably by stress redistribution during a major seismogenic faulting event in the overlying upper crust (Sibson, 1980; Tse and Rice, 1986; Scholz, 1990; Ellis and Stöckhert, 2004a, 2004b; Ellis et al., 2006). On the local scale, coseismic loading is expected to correspond to a fixed grip mode deformation, a volume element in the middle crust being distorted elastically within seconds to less than a few percent strain.

A high stress cannot be built up while pore fluid pressure remains near-lithostatic (Secor, 1965; Secor and Pollard, 1975; Sibson, 1981; Etheridge, 1983; Etheridge et al. 1984; Nur and Walder, 1990; Kohlstedt et al., 1995; Küster and Stöckhert, 1999). During coseismic loading, the pressure of the fluid in the pore space along grain and interphase boundaries P_f^p has to drop within seconds. This is probably achieved by the initiation of cracks propagating from the fluid-filled pockets (e.g. Etheridge, 1983; Etheridge et al. 1984). The length of such hydraulic fractures will be restricted, when the loading rate is high (Atkinson and Cook, 1993) for the following reason. During crack propagation, the crack volume increases and causes a drop in P_f^p, if the rate of fluid flow into the crack is lower than the rate of volume increase (Atkinson and Cook, 1993; Renshaw and Harvey, 1994; Olson 2003). It is generally presumed that the rate of fluid flow into cracks developing in the course rapid coseismic loading is too low to maintain an effective tensile stress (Brace, 1980, 1984; Nur and Walder, 1990; Oliver, 1996;

Manning and Ingebritsen, 1999), and that the cracks get arrested after a very short time. Rapid loading therefore results in a high density of intergranular micro-cracks with restricted length (Atkinson and Cook, 1993).

The initiation of mesoscopic cracks, on a larger length scale, does not necessarily coincide with the loading stage. It is not certain if all voids in the rock failed immediately, and there may be some delay between loading and failure. While sharp intergranular flaws are commonly found in rocks situated in the cool upper crust, voids in a warm and viscous rock volume are predicted to heal and blunt rapidly (e.g. Smith and Evans, 1984; Hickman and Evans, 1987). Healing of such flaws leads to strength recovery of the material, a well known process in technical ceramics and metals (Evans and Charles, 1977; Rödel and Glaeser, 1990). The processes active during flaw healing (Evans and Charles, 1977; Rödel and Glaeser, 1990) are also described for natural rocks (Smith and Evans, 1984; Hickman and Evans, 1987). The healing process is described to take place in two steps (Evans and Charles, 1977; Smith and Evans, 1984; Hickman and Evans, 1987; Rödel and Glaeser, 1990): (1) Generation of arrays of cylindrical voids in the immediate crack tip vicinity, and (2) dissociation of the cylindrical voids to arrays of spherical voids (in geology commonly referred to as fluid inclusion planes or trails) (Evans and Charles, 1977; Smith and Evans, 1984; Hickman and Evans, 1987; Rödel and Glaeser, 1990). This process results in the transformation of originally sharp flaws into discrete blunt residual voids, which are small compared to the preceding flaw.

Such blunt voids, at which the fracture toughness K^*_{IC} exceeds K_{IC} at sharp crack tips (e.g. Anderson, 1995; Bertram and Kalthoff, 2003), are expected to be capable to endure the stage of coseismic loading without initiation of hydraulic microfractures. Therefore, mesoscopic fractures may be initiated from such originally blunt voids after some delay. The following sequence of processes is proposed: First, the stress intensification rises as the length of the void increases by subcritical crack growth, driven by the strong remote stress and the fluid pressure inside the void P_f^v (Broek, 1987; Meredith and Atkinson, 1985; Atkinson and Meredith, 1987a). If the associated decrease in the internal fluid pressure is overcompensated by the stress intensification, K_I may eventually reach K^*_{IC} at the blunt tips of the evolving cracks, and unstable crack propagation is intitiated. The higher fracture toughness K^*_{IC} at blunt voids (e.g. Anderson, 1995; Bertram and Kalthoff, 2003), permits that unstable crack propagation gets initiated at $K_I = K^*_{IC} > K_{IC}$. After initiation, the crack tip sharpens immediately and propagates driven by excess energy, given by $K^*_{IC} - K_{IC}$. This excess energy is then available to accelerate the crack, leading to an unstable runaway crack propagation. During incipient unstable crack propagation, P_f^v may still exceed σ_n (eq. 1) and contribute to crack acceleration to very high speed. At this condition, symmetrical crack branching gets possible.

The length of such delayed runaway cracks is taken to correspond to the length of the veins, which ranges between a few decimetres and several meters. For high-speed crack propagation (the terminal velocity being on the order of 10^3 m s^{-1}, depending on the material), crack initiation and arrest must have taken place within a few milliseconds. Crack arrest is the consequence of a drop in the extension force K_I to $K_{IA} < K_{IC}$. K_I is expected to drop as a consequence of (1) the release of stored elastic strain energy by fracturing and (2) of an almost instantaneous drop in fluid pressure inside the crack $\dot{P}_f^v$, caused by an increase in crack volume. If so, crack propagation is a fast process compared to the rate of fluid infiltration (Atkinson and Cook, 1993; Renshaw and Harvey, 1994).

2.5.3. The stage of vein formation

2.5.3.1. Vein geometry

At the stage of crack arrest, the remote stress has dropped but is not completely relaxed. As a consequence, deformation of the host rock continues by viscous creep, driven by the residual stress. The maximum principal stress parallels the crack plane, and this corresponds to the direction of shortening during subsequent creep. At this stage, with $K_I<K_{IC}$, crack propagation is not more possible. Instead, buckling of the crack walls by viscous creep of the host rock commences and leads to opening of the crack.

Prerequisite for vein formation is a divergent displacement normal to the crack walls, providing space for mineral precipitation. Opening of a crack by purely elastic distortion of the host rock would be restricted to veins with a high aspect ratio ($AR = L/w_0$; L: length, w_0: maximum aperture), limited by the elastic properties and the fracture toughness K_{IC} of the rock (e.g. Sneddon and Elliott, 1946; Pollard and Segall, 1987; Vermilye and Scholz, 1994). During elastic distortion, the stress intensity factor (eq. 1) rises until K_{IC} is reached. At this point, the aspect ratio of the crack would increase by re-initiation of crack propagation.

Linear elastic fracture mechanics (LEFM) predicts that the crack aperture w correlates with the crack length L and the wall normal effective stress σ'_n (Sneddon and Elliot, 1946; Pollard and Segall, 1987):

$$w = -\sigma'_n \frac{2\left(1-\nu^2\right)}{E} L \qquad (3)$$

where ν denotes Poissons ratio, and E Youngs modulus. This relation holds for non-interacting mode I cracks and a two-dimensional plane strain geometry. The maximum possible elastic

opening is limited by material yield according to eq. 1, when $K_I = K_{IC}$. Inserting eq. 1 into eq. 3, with $K_I = K_{IC}$, yields the theoretical upper limit to the maximum aperture w_0 of an open crack (vein) for purely elastic deformation (Olson, 2003):

$$w_0 = \frac{K_{IC}\left(1-\nu^2\right)}{E\sqrt{\pi/8}}\sqrt{L} \qquad (4)$$

Eq. 4, solved for K_{IC} (eq. 5), can be used to estimate rock K_{IC} from the length and aperture data of mineralized veins:

$$K_{IC} = \frac{w_0}{\sqrt{L}}\frac{E\sqrt{\pi/8}}{(1-\nu^2)} \qquad (5)$$

The aspect ratio of a crack may be decreased by processes not addressed by LEFM, especially plastic or viscous deformation of the host rock (e.g. Vermilye and Scholz, 1994; Bürgmann et al., 1994) or crack tip blunting (e.g. Pollard and Aydin, 1988). Therefore, the K_{IC} derived by eq. 5 for an individual vein is referred to as apparent fracture toughness.

In Fig. 11, the apparent K_{IC} calculated for the geometry of the lense shaped veins in Southern Evia is compared to published K_{IC} values for rocks (Atkinson and Meredith, 1987b), to published data for mineralized veins interpreted to have formed in the upper crust (Vermilye and Scholz, 1994; Olson 2003) and to the data for a magmatic dyke (Delaney and Pollard, 1981; Olson 2003). The objective of this comparison is to figure out whether the geometry of the lense shaped veins is compatible with host rock distortion obeying a LEFM model, or whether the geometry requires non-elastic deformation to attain the obsereved length to aperture ratio (Fig. 11).

The geometry of magmatic dykes is strongly influenced by thermally activated deformation enabled by heat transfer from the intruding magma (e.g. Delaney and Pollard, 1981; DeGraff and Aydin, 1993). Such effects include thermal erosion at the dyke walls (e.g. Delaney and Pollard, 1981; DeGraff and Aydin, 1993) and enhanced plasticity at the dyke tips (e.g. DeGraff and Aydin, 1993). Therefore, the final shape of the Ship Rock Dykes (Delaney and Pollard, 1981) is probably not adequate to estimate K_{IC} of the host rock, but represents a situation with significant inelastic deformation of the host rock.

To calculate the apparent K_{IC} of the host rock of the lense shaped veins in southern Evia, E was set to 50 GPa and ν to 0,25, which seems to be justified for the given temperatures (Turcotte and Schubert, 2002). The resulting values of the apparent K_{IC} range between 3 x 10^2 and 3 x 10^3 MPa $m^{1/2}$ (Fig. 11) and clearly exceed typical laboratory values of rocks, where K_{IC} is found to range between 1 and 4 MPa $m^{1/2}$, and in exceptional cases up to 10 MPa $m^{1/2}$ (Atkinson and Meredith, 1987b) (Fig. 11). Published data of single-segment mineralized veins of Culpepper Quarry / Virginia USA and Florence Lake / California USA, which are interpreted to have formed in the upper crust (Vermilye and Scholz, 1994), typically point to magnitudes of about 8-25 MPa $m^{1/2}$ for K_{IC} of the host rock (Olson 2003) (Fig. 11). In contrast, length and aperture data of the magmatic Ship Rock Dyke / New Mexico USA (Delaney and Pollard, 1981) result in excessive values of apparent K_{IC} of 8 to 800 MPa $m^{1/2}$ (Olson, 2003) (Fig. 11). For a comprehensive discussion of the length to aperture ratio of veins and dykes the reader is referred to Delaney and Pollard (1981), Vermilye and Scholz (1994), and Olson (2003).

The magnitude of apparent K_{IC} derived for the lense shaped veins in southern Evia exceeds that of the laboratory values of K_{IC} found for rocks by 1 - 3 orders of magnitude (Fig. 11) and that of Culpepper Mine and Florence Lake veins by 1 - 2 orders of magnitude (Fig. 11). Even the data of the Ship Rock Dyke, despite the presumably high contribution of inelastic deformation enabled by magmatic heat, is exceeded by 70 % of the lense shaped veins in southern Evia (Fig. 11).

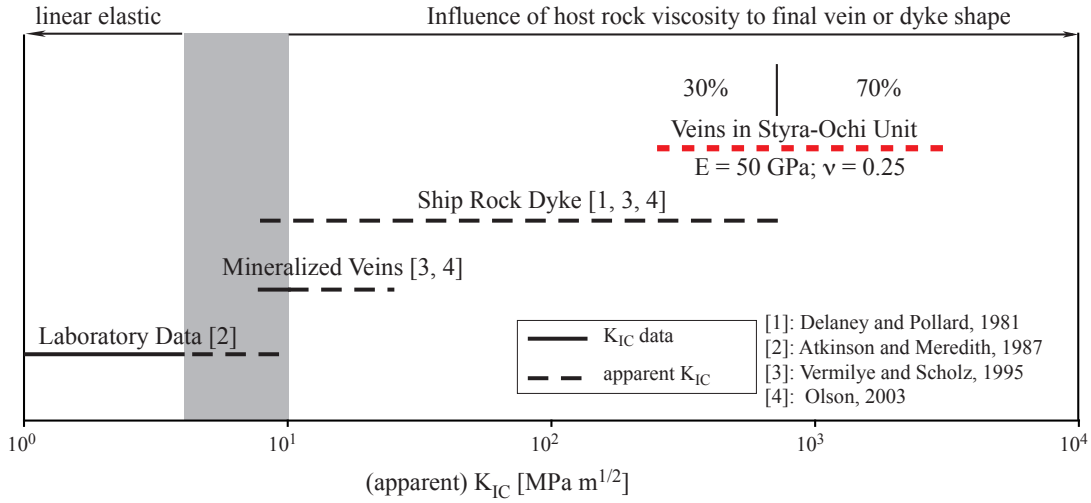

Fig. 11: Comparison of the apparent K_{IC} data derived for the discordant lens-shaped veins in the Styra-Ochi Unit (eq. 5) with published data for the magmatic Ship Rock Dyke (Delaney and Pollard, 1981), for Culpepper Quarry and Florence Lake mineralized veins (Vermilye and Scholz, 1995) and with published laboratory data for K_{IC} of rocks (Atkinson and Meredith, 1987).

Fig. 12 shows the correlation between length and aspect ratio of the lense shaped veins. This ratio is compared to other data sets obtained for mineralized veins (Vermilye and Scholz, 1994), for the Ship Rock Dyke (Delaney and Pollard, 1981), and to the limiting length / aspect ratio data calculated by eq. 4 for a typical laboratory value of K_{IC} = 10 MPa $m^{1/2}$ (Atkinson and Meredith, 1987b). The ratio length / aspect ratio of the lense-shaped veins is low compared to all other data sets (Fig. 12). Also, the aspect ratios of the lense shaped veins of South Evia are below those observed for the reference veins and dykes (Vermilye and Scholz, 1995; Delaney and Pollard, 1981) and well below those predicted based on the laboratory data (Atkinson and Meredith, 1987b).

Based on the above considerations, the length to aperture ratio found for all lense shaped veins in southern Evia is in conflict with an origin by deformation of the host rock obeying a LEFM-model. Instead, the geometry of the veins requires irreversible viscous deformation of the host rock. The amount of inelastic crack-parallel shortening can be obtained from the vein aspect ratio.

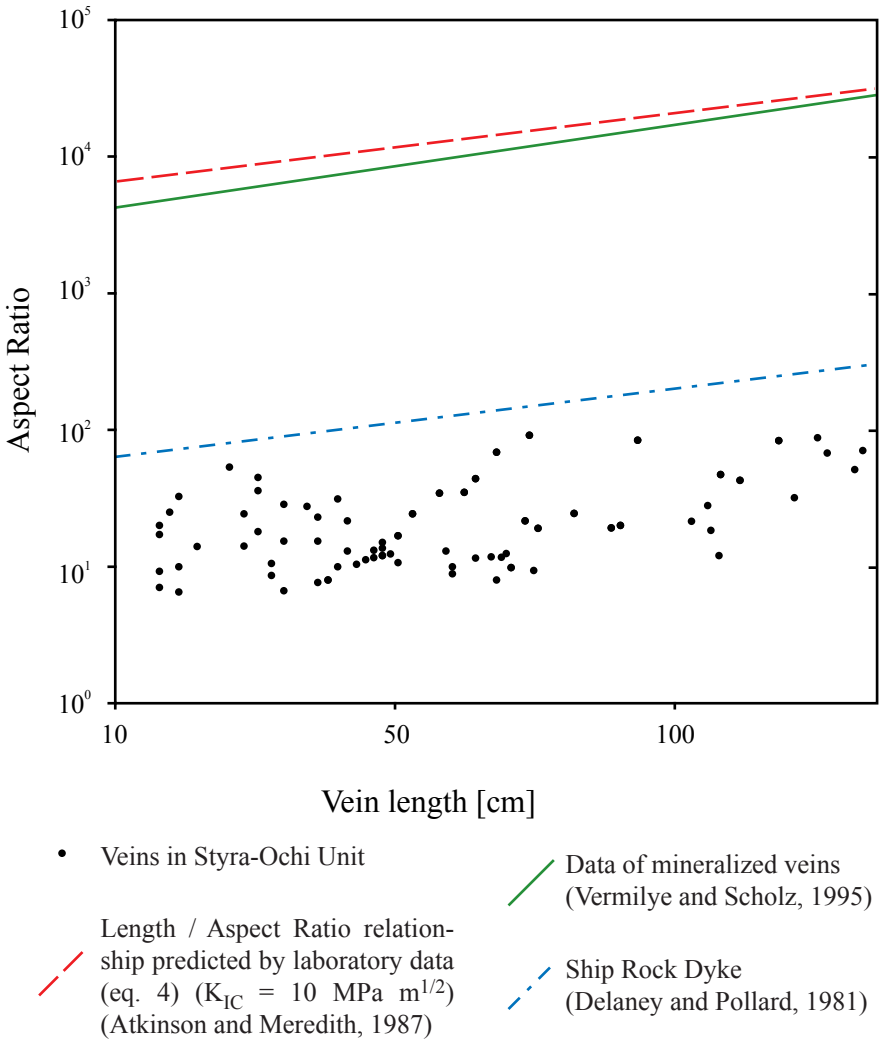

Fig. 12: Plot of the length and aspect ratio of veins. The data obtained for lens-shaped veins in the Styra-Ochi Unit are compared to the data for Culpepper Quarry and Florence Lake mineralized veins, for the magmatic Ship Rock Dyke, and to the (eq. 5) length / aspect ratio calculated from laboratory KIC data for rocks.

2.5.3.2. Shortening parallel to the opening crack

To derive the finite strain accumulated during inelastic deformation, the length of the buckled vein wall of lens-shaped veins is taken to correspond to the length of the initial crack (L_0). Comparison of L_0 with the distance between both tips of the vein (L) yields the amount of crack parallel shortening. For analysis, the shape of the buckled vein wall is approximated by the segment of a circle (Fig. 13). Using the relation $\overline{AS}\cdot\overline{SC}=\overline{BS}\cdot\overline{SD}$ (Fig. 13), the radius r of the circle is calculated:

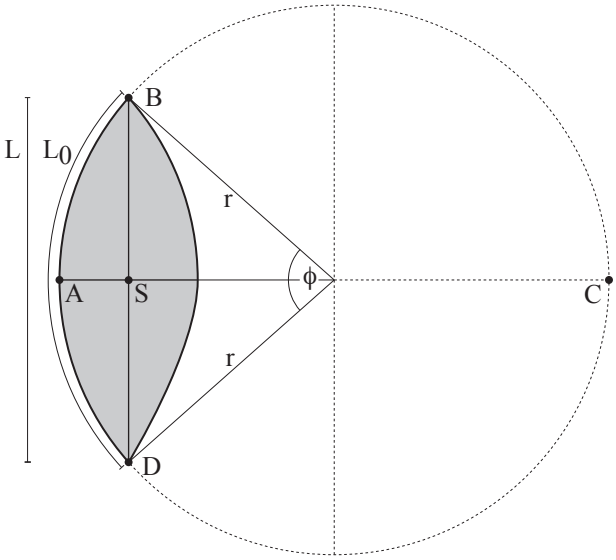

Fig. 13: Definition of the symbols used in the strain calculation. The grey shaded area represents the geometry of an ideal lens-shaped vein.

$$\frac{w}{2}\cdot\left(2r-\frac{w}{2}\right)=\left(\frac{L}{2}\right)^2 \Leftrightarrow r=\frac{L^2}{4w}+\frac{w}{4} \qquad (6)$$

The apex angle defining the segment of the circle, ϕ, is given by:

$$\phi=2\cdot\left(\sin^{-1}\frac{L/2}{r}\right) \qquad (7)$$

The initial crack length, L_0, is represented by the length of the segment of the circle:

$$L_0=\frac{\phi}{360}\cdot 2\pi r \qquad (8)$$

The finite elongation ε [%] can now be calculated by implementing eqs. 6 to 8 into eq. 9:

$$\varepsilon=\left(\frac{L-L_0}{L_0}\right)\cdot 100 \qquad (9)$$

The resulting non-linear function ε = f(L, w) (Fig. 14a) indicates that the aspect ratio (AR) is very sensitive to strain in the early stage of vein opening (starting at an AR ≤ ∞) and remains so to an aspect ratio of about 30. When the AR drops to below about 30, the gradient of this function increases rapidly over a narrow transition zone (grey shaded field in Fig. 14 a, b) and the aspect ratio becomes much less sensitive on the amount of crack parallel shortening. With other words, from this stage a significant lowering of the aspect ratio requires high additional strain. The aspect ratio of the majority of the veins (54 %) in the present study, shown as a histogram in Fig. 14b, plots within the transition zone (grey shaded field in Figs. 14 a, b). 24 % of the veins show a somewhat higher aspect ratio, and 22 % a somewhat lower one. The data set

reveals that the amount of vein-parallel shortening does not exceed 1,6 %, most values being in the range of 0.1 % to 0.7 % (Fig. 14b).

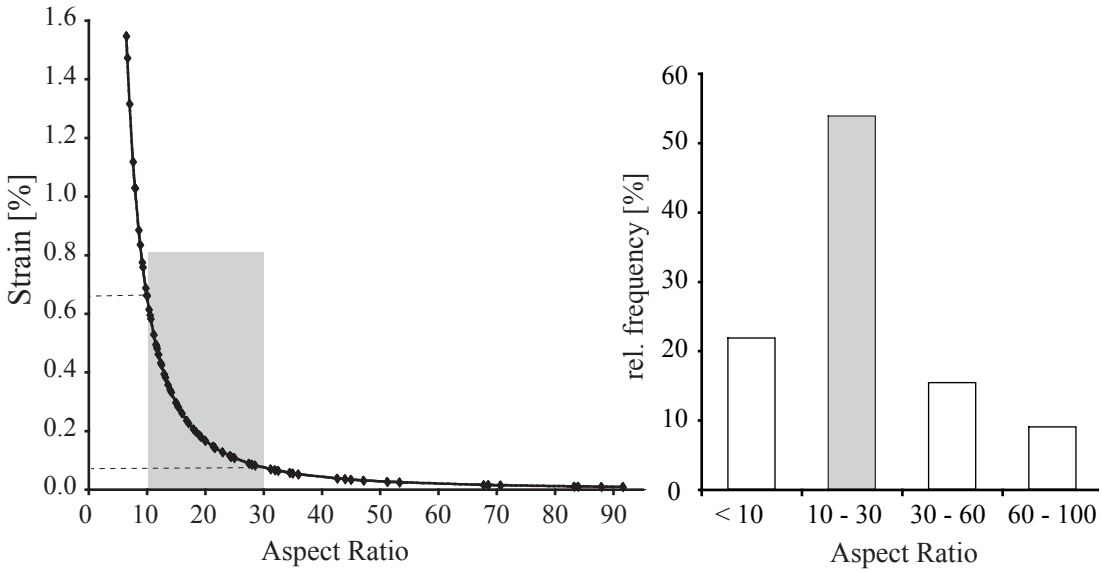

Fig. 14: a) Plot of the function ε = f(L, w); see text. The limit of AR ≈ 30 defines the transition from strain sensitive to strain insensitive behaviour of an evolving cavity (grey shaded field). b) Histogram of aspect ratios. Most veins reveal an aspect ratio within the transition zone (grey shaded). The typical strain is between 0.1% and 0.7%.

2.5.4. Cavity sealing

The microstructure of vein-filling material provides information on the opening and sealing history of the vein (e.g. Durney and Ramsay, 1973; Ramsay, 1980; Cox and Etheridge, 1983; Urai et al. 1991; Fisher and Brantley, 1992; Hilgers and Urai, 2002). Two types of microstructures are diagnostic for the relation between the opening rate and the sealing rate:

1) If the sealing rate exceeds the opening rate, vein formation gets cyclic. Incremental widening is followed by complete sealing. The process is called the crack-seal mechanism (Durney and Ramsay, 1973; Ramsay, 1980; Cox and Etheridge, 1983; Fisher and Bryne, 1990; Fisher and Brantley, 1992; Fisher et al., 1995). The indicative microfabrics comprise fibrous crystals, generally without lattice preferred orientation, and narrowly spaced inclusion trails parallel to the vein walls (Durney and Ramsay, 1973; Ramsay, 1980; Cox and Etheridge, 1983; Fisher and Bryne, 1990; Fisher and Brantley, 1992; Fisher et al., 1995). These inclusion trails mark healed cracks; each trail represents a single increment of opening. Urai et al. (1991) proposed that the grain fibres are detained from development of crystallographic controlled facets by pinning at asperities on the opposite vein wall.

2) If the opening rate exceeds the sealing rate, crystals grow into an open fluid filled cavity. In this case, the crystals may attain crystal facets (e.g. Fisher and Bryne, 1990; Fisher and Brantley, 1992; Fisher et al., 1995; Ague, 1995). The growth of crystals is restricted only by growth competition between adjacent grains. This leads to a selection of those grains, for which the fastest growth direction is oriented about normal to the vein wall, the growth of others grains becoming eventually terminated by impingement (e.g. Hilgers and Urai, 2002). For quartz, the direction of fastest growth is parallel to the c-axis (Iler, 1979; Fisher and Brantley, 1992). Consequently, growth competition between adjacent crystals leads to a selection of quartz crystals with a c-axis orientation about normal to the vein wall. Due to progressive elimination of grains in less favourable orientation, the grain size increases towards the center of the vein and a crystallographic preferred orientation of c-axes normal to the vein walls develops (e.g. Fisher and Brantley, 1992; Fisher et al., 1995; Hilgers and Urai, 2002).

The microfabrics of the lense-shaped veins in southern Evia show no discontinuities indicative of episodic or cyclic processes of opening and sealing. In particular, the microstructures characteristic for the crack-seal vein growth mechanism (Durney and Ramsay, 1973; Ramsay, 1980; Cox and Etheridge, 1983; Urai et al., 1991) are systematically absent. Instead, the coarse-grained microfabric with elongate or blocky crystals suggests crystallization from a free fluid phase in an open cavity. This is indicated (1) by the occurrence of euhedral growth faces (Fig. 6), (2) by residual voids between euhedral crystals (Fig. 10c) (e.g. Ague, 1995), (3) by microstructures resulting from growth competition, which leads to impingement and inward coarsening of the grain size (Figs. 7a, b; 8a, b) (e.g. Fisher and Bryne, 1990; Fisher

and Brantley, 1992; Fisher et al., 1995; Hilgers and Urai, 2002), and (4) by the development of an increasingly pronounced crystallographic preferred orientation with increasing distance to the vein wall (Fig. 8a, b) (Fisher and Brantley, 1992; Hilgers and Urai, 2002). All these features demonstrate that the cracks were opened in a single stage. During the early history, the opening rate was high compared to the sealing rate, leaving the cracks as open cavities and pathways for focused fluid flow. Local crustal permeability must have been high at that stage.

The combination of high stress in the initial stage of crack propagation with low finite strain accumulated in the subsequent creep stage precludes that the vein geometry results from long term steady state deformation. Fracturing and cavity formation rather reflect a cycle of instantaneous loading followed by stress relaxation within a geologically very short time. Eventually, the veins got largely or completely sealed, when the rate of opening decayed. The reasons for that are twofold: (1) The coseismically induced stress relaxes and the driving force for crack opening vanishes. (2) The opening rate of the lense-shaped veins becomes low for geometrical reasons at an aspect ratio of about 30 (Fig. 14). As internal discontinuities are absent, cavity evolution in incremental steps can be precluded and the veins are interpreted to record a single stress cycle.

2.6. Summary and conceptual model

In the following, at first, the fundamental properties and inferred processes are summarized, and then an integrated model is presented. The discordant lense-shaped veins in southern Evia show evidence for brittle failure immediately followed by ductile deformation of the host rock to low finite ductile strain. This happened in a horizon just beneath the crustal scale brittle ductile transition, referred to as uppermost level of the plastosphere sensu Scholz (1990), where the crust otherwise deforms in a viscous manner on a long term. The structural and microstructural record of the veins yields the following characteristic features:

1) The veins crosscut all syn-metamorphic structures related to pervasive deformation of the Styra-Ochi Unit during HP / LT metamorphism. Brittle failure and vein formation must postdate high pressure metamorphism and concomitant deformation at depth. The cracks and veins have formed during exhumation.

2) The vein quartz reveals a broad spectrum of microfabrics typically developed at temperatures of about 300°C or slightly above, indicating brittle failure, progressive sealing and crystal plastic deformation to have occurred at similar temperatures, hence at a crustal level just beneath the long term crustal scale brittle ductile transition.

3) The veins are discordant to pre-existing planes of low tensile strength and the crack path was exclusively controlled by the orientation of the principal remote stresses. Branching veins indicate unstable crack propagation with a speed near to the terminal velocity. Rapid

crack propagation of relative short cracks requires a high extension force and high remote stress (eq. 1).

4) Opening and cavity formation commenced immediately after crack arrest, controlled by viscous deformation of the host rock driven by the decaying remote stress, with concomitant recovery of P_f (eq. 2). The veins formed in a single stage; inelastic strain is mostly less than 1 %.

From the structural record summarized above, the following model of vein formation is derived (Fig. 15):

1. Stage: Coseismic loading

Rapid coseismic loading leads to distortion in the middle crust near the tip of a seismogenic fault; local deformation can be approximated as being in a fixed grip mode. The high imposed strain rate causes a downward deflection of the brittle ductile transition (Küster and Stöckhert 1999; Ellis and Stöckhert 2004a; Rolandone et al., 2004). The characteristic time scale of coseismic loading is a few seconds (e.g. Scholz, 1990; Wald and Heaton, 1994), determined by the duration of slip on the overlying fault segment. During rapid coseismic loading, the pore fluid pressure drops by the formation of distributed microcracks.

2. Stage: Subcritical crack growth and unstable crack initiation

The initiation of mesoscopic cracks is proposed to start with some delay from blunt voids, which are capable to endure the stage of coseismic loading due to higher fracture toughness at blunt crack tips, $K^*_{IC} > K_{IC}$ (e.g. Anderson, 1995; Bertram and Kalthoff, 2003). The initiation of unstable cracks from such blunt voids is expected to be a two step process: First, the embryonic cracks are likely to grow subcritically by stress corrosion from the blunt voids, increasing the effective void length (Broek, 1987; Meredith and Atkinson, 1985; Atkinson and Meredith, 1987a). As a consequence, the stress intensification rises in a constant remote stress field (Broek, 1987). When the fracture toughness K^*_{IC} is met, unstable crack propagation is initiated in a framework of excess energy available to drive and accelerate the crack. The timescale of crack initiation by subcritical crack growth is not well constrained, as the growth rate depends on several physical and chemical factors (Meredith and Atkinson, 1985; Atkinson and Meredith, 1987a) and experimental studies are scarce. For instance, Meredith and Atkinson (1985) found subcritical crack growth rates on the order of 10^{-6} to 10^{-4} ms^{-1} in Westerly Granite. The timescale for unstable crack initiation is therefore estimated to be between a few seconds and maybe some days. It may be supposed that the time-scale of the crack initiation stage may be similar to that of typical aftershock activity.

3. Stage: Unstable crack growth

After initiation, the crack tips sharpen immediately and K_I escalates in response to increasing crack length at high remote stress. The higher stored strain energy in materials with blunt voids, compared to materials with initially sharp flaws, may cause a comparatively higher acceleration. The crack tip propagation rate eventually reaches the terminal velocity and forms symmetrical branches. Cracks get arrested when the stable K_I drops to K_{IA}, as a consequence of strain energy release. Given the length of the cracks and the inferred terminal propagation rate on the order of 10^3 ms^{-1}, the cracks must have arrested a few milliseconds after initiation.

4. Stage: Ductile deformation and vein formation

After crack arrest, the residual stress drives viscous deformation of the host rock. Creep deformation and concomitant recovery of the pore fluid pressure in the stage of postseismic stress relaxation causes progressive opening of the cracks, which become cavities and develop into veins by sealing (Fig. 15 Stage 4). The orientation of the stress field remains constant, with σ_1 parallel to the crack and σ_3 normal to the crack. Progressive shortening of the host rock parallel to the crack, which is parallel to the maximum principal stress, results in buckling of the crack walls. This leads to the typical lense shape of the veins.

Development of the open cavity into a vein is the consequence of aqueous solutions flowing through the cavity (e.g. Yardley, 1984; Ague, 1995). Large amounts of solution are required to seal a cavity, as the solubility of quartz in aqueous fluids is similar to 0.1 % by weight at the inferred pressure and temperature conditions (e.g. Fournier and Potter, 1982; Manning, 1994). The volume of solution required to transport the material precipitated in the vein by far exceeds the volume of the cavity. The respective quantity of aqueous solution needs to enter and to leave the cavity by passing through the vein-wall rock interface. The permeability of the host rock must have been accordingly high. The high permeability is probably achieved as a consequence of distributed damage, as required for the drop in pore fluid pressure during coseismic loading.

Finally, the quartz crystals grown early during the opening stage, with a position near to the vein walls, are expected to undergo deformation due to distortion of the vein walls during progressive opening, while grains positioned in the vein centre have grown lately and are little deformed. This prediction is supported by the microfabrics of the vein quartz (Nüchter and Stöckhert, submitted).

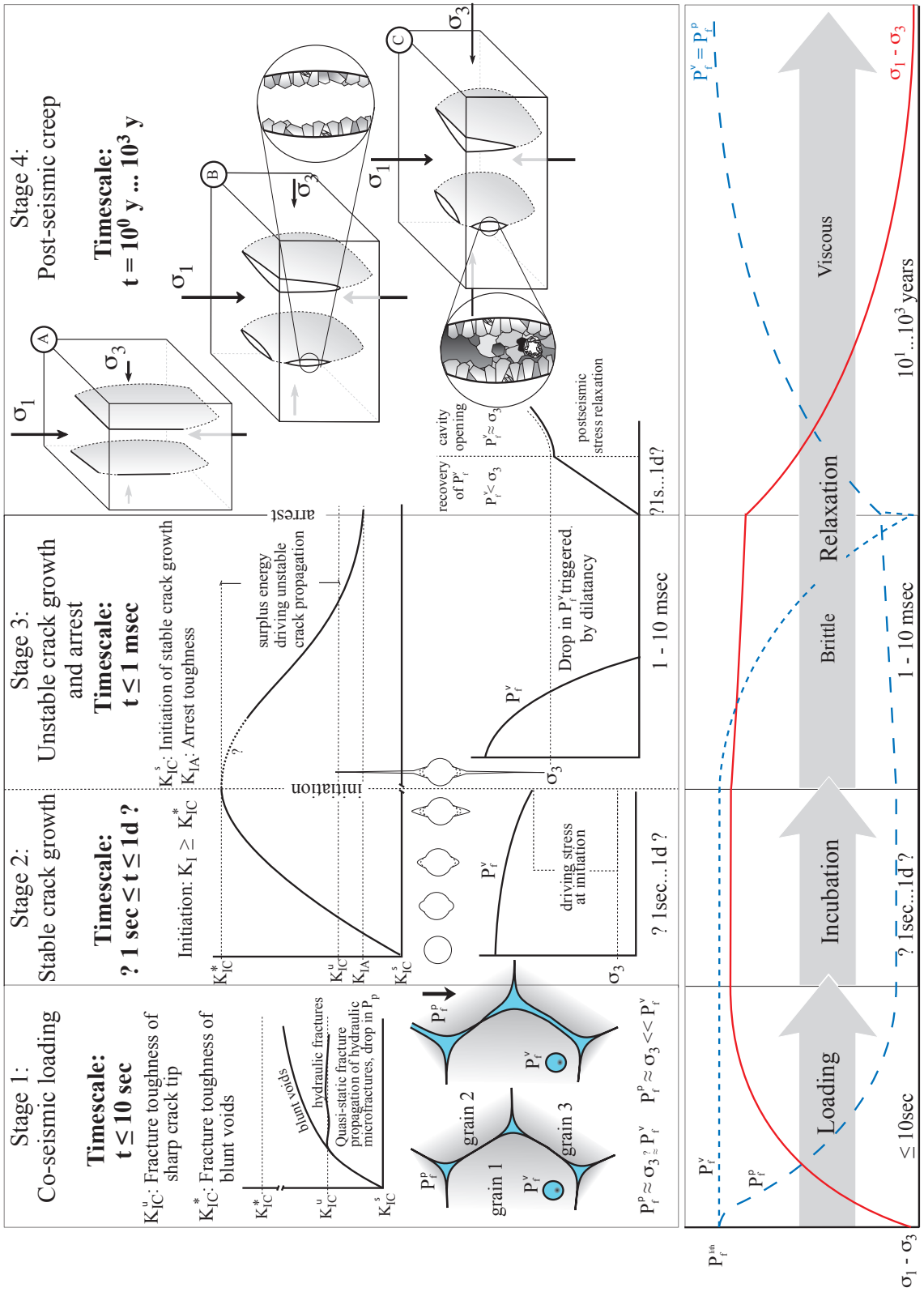

Fig. 15: Synoptic diagram showing the stages of coseismic loading and fracture initiation followed up by the stages of postseismic stress relaxation and vein formation. See text for discussion.

2.7. Conclusions

The structural and microstructural record of lense-shaped discordant veins in the HP / LT - metamorphic Styra-Ochi unit of southern Evia yield insight into earthquake-related brittle / ductile processes at a depth level just below the crustal scale brittle ductile transition, hence in the uppermost plastosphere. The following features are characteristic:

1) The crack path is controlled by the orientation of the principle stress components and not by preexisting planes of weakness in the host rock. Some veins branch symmetrically. Therefore, the original cracks propagated driven by high remote stress.

2) The length to aperture ratio of the veins is inconsistent with host rock distortion obeying a linear elastic fracture mechanics model. Distributed ductile deformation of the host rock has controlled the geometry of the veins.

3) The vein sealing quartz crystals grew into an open cavity. At an early stage, the crack opening rate must have exceeded the sealing rate.

4) At a later stage, the veins got sealed when the crack opening rate diminished, probably due to a combination of progressive relaxation of the coseismically imposed stress and the geometrical constraints. Overall finite shortening parallel to the cracks is found to be less than 1.6 % throughout, and mostly between 0.6 and 0.1 %.

The features indicate the characteristics of high stress – low strain deformation events in a crustal volume beneath the crustal scale brittle ductile transition. According to my analysis, the record is readily explained by nearly instantaneous coseismic loading to high stress, related to an earthquake in the formerly overlying and now eroded ancient schizosphere, followed up by a stage of creep deformation during postseismic stress relaxation. The discordant veins are interpreted to represent mesoscopic features of damage in the middle crust, introduced by seismic activity in the overlying schizosphere. Such distributed brittle failure is anticipated to cause a drop of pore fluid pressure to significantly sub-lithostatic values, and to create a transient high permeability. Restoration to near-lithostatic pore fluid pressures is indicated by the opening of the cracks during progressive stress relaxation. Notably, each vein records a single seismic cycle and multiple overprinting has not been observed. Following the principle of uniformitarianism, the structural record of such discordant monogenetic veins provides valuable insight into processes and conditions relevant for the understanding of present day earthquakes and the interpretation of related surface deformation recorded by geodesy.

References:

Ague, J.J. (1995): Deep crustal growth of quartz, kyanite and garnet into large-aperture, fluid filled fractures, north-eastern Connecticut, USA.- J. metamorphic Geol., 13: 299-314.

Anderson, T.L. (1995): Fracture mechanics - Fundamentals and Application, second edition.- CRC Press.

Arnadottir, T., Segal, P. (1994): The 1989 Loma-Prieta earthquake imaged from inversion of geodetic data.- J. Geophys. Res., 99: 21,835-21,855.

Atkinson, B.K. (1987): Introduction to fracture mechanics and its geophysical applications.- In: Atkinson, B.K. [ed.]: Fracture mechanics of rock (pp. 1-26). Academic Press Limited.

Atkinson, C., Cook, J.M. (1993): Effect of loading rate on crack propagation under compressive stress in a saturated porous material.- J. Geophys. Res., 98(B4): 6383-6395.

Atkinson, B.K., Meredith, P.G. (1987a): The theory of subcritical crack growth with applications to minerals and rocks.- In: Atkinson, B.K. [ed.]: Fracture mechanics of rock (pp. 111-166). Academic Press Limited.

Atkinson, B.K., Meredith, P.G. (1987b): Experimental fracture mechanics data.- In: Atkinson, B.K. [ed.]: Fracture mechanics of rock (pp. 477-525). Academic Press Limited.

Bertram, A., Kalthoff, J.F. (2003). Crack propagation toughness of rock for the range from low to very high crack speeds.- Paper presented at the third international conference on fracture and damage mechanics, FDM 2003.

Bradley, J.S. (1975): Abnormal formation pressure.- AAPG Bulletin, 59: 957-973.

Brace, W.F. (1980): Permeability of crystalline and argillaceous rocks.- Int. J. Rock Mech. Min. Sci., 17: 241-251.

Brace, W.F. (1984): Permeability of crystaline rocks: new in situ measurements.- J. Geophys. Res., 89(B6): 4327-4330.

Brace, W.F., Bombolakis, E.G. (1963): A note on brittle crack growth in compression.- J. Geophys. Res., 68(12): 3709-3713.

Brix, M.R., Stöckhert, B., Seidel, E., Theye, T., Thomson, S.N., Küster, M. (2002): Thermobarometric data from a fossil zircon partial annealing zone in high pressure - low temperature rocks of eastern and central Crete, Greece.- Tectonophysics, 349: 309-326.

Broek, D. (1987): Elementary engineering fracture mechanics.- Martinus Nijhoff Publishers.

Bürgmann, R., Pollard, D.D., Martel, S.J. (1994): Slip distributions on faults: effects of stress gradients, inelastic deformation, heterogeneous host-rock stiffness, and fault interaction.- J. Struct. Geol., 16(12): 1675-1690.

Cox, S.F., Etheridge, M.A. (1983): Crack-seal fibre growth mechanisms and their significance in the development of oriented layer silicate microstructures.- Tectonophysics, 92: 147-170.

Crager, M., Paris, P.C. (1967): Elastic field equations for blunt cracks with reference to stress corrosion cracking.- Int. J. Frac. Mech., 3: 247-252.

DeGraff, J.M., Aydin, A. (1993): Effect of thermal regime on growth increment and spacing of contraction joints in basaltic lava.- J. Geophys. Res., 98: 6411-6430.

Delaney, P.T., Pollard, D.D. (1981): Deformation of host rocks and flow of magma during growth of minette dikes and breccia-bearing intrusions near Ship Rock, New Mexico.- U.S. Geol. Sur. Prof. Pap., 1202: 1-61.

Dunlap, W.J., Hirth, G., Teyssies, C. (1997): Thermomechanical evolution of a ductile duplex.- Tectonics, 16: 983-1000.

Durney, D.W., Ramsay, J.G. (1973): Incremental strains measured by syntectonic crystal growth.- In: De Jong, K.A., Scholten, R. (Eds.), Gravity and Tectonics. (pp. 67-96). New York: John Wiley.

Ellis, S., Stöckhert, B. (2004a): Imposed strain localization in the lower crust on seismic timescales. Earth Planets Space, 56(12): 1103-1109.

Ellis, S., Stöckhert, B. (2004b): Elevated stresses and creep rates beneath the brittle-ductile transition caused by seismic faulting in the upper crust.- J. Geophys. Res., 109(5), B05407.

Ellis, S., Beavan, J., Eberhart-Phillips, D., Stöckhert, B. (2006): Simplified models of the Alpine Fault seismic cycle: stress transfer in the mid-crust.- Geophys. J. Int., 166(1): 386-402.

Engvik, A., Bertram, A., Kalthoff, J.F., Stöckhert, B., Austrheim, H., Elvevold, S. (2005): Magma-driven hydraulic fracturing and infiltration of fluids into the damaged host rock, an example from Dronning Maud Land, Antarctica.- J. Struct. Geol., 27: 839-854.

Evans, A.G., Charles, E.A. (1977): Strength recovery by diffusive crack healing.- Acta Metal., 25, 919-27.

Etheridge, M.A. (1983): Differential stress magnitudes during regional deformation and metamorphism: upper bound imposed by tensile fracturing.- Geology, 11: 231-234.

Etheridge, M.A., Wall, V.J., Cox, S.F., Vernon, R.H. (1984): High fluid pressures during regional metamorphism and deformation: implications for mass transport and deformation mechanisms.- J. Geophys. Res., 89: 4344-4358.

Faure, M., Bonneau, M., Pons, J. (1991): Ductile deformation and syntectonic granite emplacement during the late Miocene extension of the Aegea (Greece).- Neues Jahrb. Mineral. Monatsh., 4: 145-162.

Fisher, D.M., Bryne, T. (1990): The character and distribution of mineralized fractures in the Kodiak Formation, Alaska: implications for the fluid flow in an underthrust sequence.- J. Geophys. Res., 95(B6): 9069-9080.

Fisher, D.M., Brantley, S.L. (1992): Models for quartz overgrowth and vein formation: deformation and episodic fluid flow in an ancient subduction zone.- J. Geophys. Res., 97(B13): 20043-20061.

Fisher, D.M., Brantley, S.L., Everett, M., Dzvonik, J. (1995): Cyclic fluid flow through a regionally extensive fracture network within the Kodiak accretionary prism.- J. Geophys. Res., 100(B7), 12,881-12,894.

Fournir, R.O., Potter II, R.W. (1982): An equation correlating the solubility of quartz in water from 25° to 900°C at pressures up to 10,000 bars.- Geochim. Cosmochim. Acta, 46: 1969-1973.

Freed, A.M., Bürgmann, R. (2004): Evidence of powerlaw flow in the Mojave desert mantle.- Nature, 430: 548-551.

Freed, A. M., Bürgmann, R., Calais, E., Freymueller, J., Hreinsdóttir, S. (2006): Implications of deformation following the 2002 Denali, Alaska, earthquake for postseismic relaxation processes and lithospheric rheology.- J. Geophys. Res., 111(B1), doi: 10.1029.

Gautier, P., Brun, J.-P. (1994): Crustal-scale geometry and kinematics of late-orogenic extension in the central Aegean (Cyclades and Evvia Island).- Tectonophysics, 238: 399-424.

Griffith, A.A. (1920): The Phenomena of rupture and flow in solids.- Philosophical Transactions, Series A, 221: 163-198.

Hauksson, E. (2000): Crustal structure and seismicity distribution adjacent to the Pacific and North America plate boundary in southern California.- J. Geophys. Res., 105: 13875-13903.

Henderson, J.R., Henderson, M.N., Wright, T.O. (1990): Water-sill hypothesis for the origin of certain veins in the Megum Group, Nova Scotia, Canada.- Geology, 18: 654-657.

Hickman, S.H., Evans, B. (1987): Influence of geometry upon crack healing rate in calcite.- Phys. Chem. Minerals, 15: 91-102.

Hilgers, C., Urai, J. (2002): Experimental study of syntaxial vein growth during lateral fluid flow in transmitted light: first results.- J. Struct. Geol., 24: 1029-1043.

Hirth, G., Teyssier, C., Dunlap, W.J. (2001): An evaluation of quartzite flow laws based on comparisons between experimentally and naturally deformed rocks.- Int. J. Earth. Sci., 90(1): 77-87.

Iler, R. (1979): The chemistry of silica.- Wiley-Interscience, New York.

Irwin, G.R. (1948): Fracture dynamics.- Fracturing of metals, American society for metals, Cleveland: 147-166.

Irwin, G.R. (1956): Onset of fast crack propagation in high strength steel and aluminium alloys.- Sagamore research conference proceedings, 2: 289-305.

Irwin, G.R. (1957): Analysis of stresses and strains near the end of a crack traversing a plate.- J. Appl. Mech., 24: 361-364.

Irwin, G.R. (1961): Plastic zone near a crack and fracture toughness.- Sagamore research conference proceedings, 4.

Jolivet, L., Faccenna, C. (2000): Mediterranean extension and the Africa-Eurasia collision.- Tectonics, 19: 1095-1106.

Kalthoff, J.F. (1973): On the propagation direction of bifurcated cracks.- In: Sih, G.C. (ed.): Proc. Int. Conf. on Dynamic Crack Propagation, Bethlehem, Pa., Nordhoff Int. Publ.: 449-458.

Küster, M., Stöckhert, B. (1999): High differential stress and sublithostatic pore fluid pressure in the ductile regime - microstructural evidence for short-term post-seismic creep in the Sesia Zone, Western Alps.- Tectonophysics, 303: 263-277.

Klein-Helmkamp, U. (1996): Metamorphose und Exhumierung der niedrigtemperierten Hochdruckmetamorphite der Styra-Ochi-Einheit in Süd-Euböa, Attisch-Kykladisches Kristallin, Griechenland.- Ruhr University Bochum, Germany.

Kohlstedt, D.L., Evans, B., Mackwell, S.J. (1995): Strength of the lithosphere: constraints imposed by laboratory experiments.- J. Geophys. Res., 100(B9): 17,587-17,602.

Lawn, B. (1975): Fracture of brittle solids.- second edition. Cambridge University Press.

Le Pichon, X., Angelier, J. (1981): The Aegean Sea.- Philos. Trans. R. Soc. Lond., Ser. A, 300: 357-372.

Lister, G.S., Banga, G., Feenstra, A. (1984): Metamorphic core complexes of Cordilleran type in the Cyclades, Aegean Sea, Greece.- Geology, 12: 221-225.

Manning, C.E. (1994): The solubility of quartz in H_2O in the lower crust and upper mantle.- Geochim. Cosmochim. Acta, 58(22): 4831-4839.

Manning, C.E., Ingebritsen, S.E. (1999): Permeability of the continental crust: implications of geothermal data and metamorphic systems.- Rev. Geophys., 37: 127-150.

Meredith, P.G., Atkinson, B.K. (1985): Fracture toughness and subcritical crack growth during high-temperature tensile deformation of Westerly Granite and Black Gabbro.- Phys. Earth Planet. Int., 39: 33-51.

Meulenkamp, J.E., Wortel, M.J.R., Van Wamel, W.A., Spakman, W., Hoogerduyn Strating, E. (1988): On the Hellenic subduction zone and the geodynamic evolution of Crete since the late Middle Eocene.- Tectonophysics, 146: 203-215.

Nüchter, J.-A., Stöckhert, B. (submitted): Gradients in Quartz Vein Micofabrics - Progressive Cavity Formation in the Ductile Field.- J. Struct. Geol.

Nur, A., Walder, J. (1990): Time-dependent hydraulics of the earth´s crust.-. In: Bredehoeft, J.D., Norton, D. (Eds.): The role of fluids in crustal processes. (pp. 113-127).

Oliver, N.H.S. (1996): Review and classification of structural controls on fluid flow during regional metamorphism.- J. Metamorph. Geol., 14: 447-492.

Olson, J. E. (2003): Sublinear scaling of fracture aperture versus length: An exception or the rule?- J. Geophys. Res., 108(B9).

Peltzer, G., Rosen, P., Rogez, F., Hudnut, K. (1996): Postseismic rebound in fault step-overs caused by pore fluid flow.- Science, 273: 1202-1204.

Pollard, D.D., Aydin, A. (1988): Progress in understanding jointing over the past century.- The Geological Society of America: Bulletin, 100: 1181-1204.

Pollard, D.D., Segall, P. (1987): Theoretical displacements and stresses near fractures in rock: With applications to faults, joints, veins, dikes and solution surfaces.- In: Atkinson, B.K. [ed.]: Fracture mechanics of rock (pp. 277-350), Academic Press Limited.

Pollitz, F.F., Wicks, C., Thatcher, W. (2001): Mantle flow beneath a continental strike-slip fault: postseismic deformation after the 1999 Hector Mine earthquake.- Science, 293: 1814-1818.

Ramsay, J.G. (1980): The crack-seal mechanism of rock deformation.- Nature, 284: 135-139.

Ranalli, G., Murphy, D.C. (1987): Rheological stratification of the lithosphere.- Tectonophysics, 132: 281-295.

Renshaw, C.E., Harvey, C.F. (1994): Propagation velocity of a natural hydraulic fracture in a poroelastic medium.- J. Geophys. Res., 99(B11): 21,667-21,677.

Rice, J.R., Cleary, M.P. (1976). Some basic stress diffusion solutions for fluid-saturated elastic porous media with compressible constituents.- Rev. Geoph. Space Phys., 14(2): 227-241.

Rödel, J, Glaeser, A.M. (1990): High-temperature healing of lithographically introduced cracks in sapphire.- J. Amer. Ceram. Soc., 73: 592-602.

Rolandone, F., Bürgmann, R., Nadeau, R.M. (2004): The evolution of the seismic-aseismic transition during the earthquake cycle; constraints from the time-dependent depth distribution of aftershocks.- Geophys. Res. Lett., 31(23).

Scholz, C.H. (1990): The mechanics of earthquake and faulting.- Cambridge University press.

Secor, D.T. (1965): Role of fluid pressure in jointing.- Am. J. Sci., 263: 633-646.

Secor, D.T., Pollard, D.D. (1975): On the stability of open hydraulic fractures in the earth´s crust.- Geophys. Res. Lett., 2(11): 510-513.

Sibson, R.H. (1980): Transient discontinuities in ductile shear zones.- J. Struct. Geol., 2: 165-171.

Sibson, R.H. (1981): Fluid flow accompanying faulting: Field evidence and models.- In Simpson, D.W., Richards, P.G. (Eds.), Earthquake Prediction: An international review. (pp. 593-603). American Geophysical Union.

Smith, D., Evans, B. (1984): Diffusional crack healing in quartz.- J. Geophys. Res., 89(B6): 4125-4135.

Sneddon, I.N., Elliott, H.A. (1946): The opening of a griffith crack under internal pressure.- Q. Appl. Math., 4: 262-267.

Spear, F.S. (1993): Metamorphic phase equilibria and pressure-temperature-time paths.- Min. Soc. Am. Monograph (799 pp).

Stöckhert, B., Brix, M.R., Kleinschrodt, R., Hurford, A.J., Wirth, R. (1999): Thermochronometry and microstructures of quartz: a comparison with experimental flow laws and predictions on the temperature of the brittle-plastic transition.- J. Struct. Geol., 21: 351-369.

Strehlau, J., Meissner, R. (1987): Estimation of crustal viscosities and shear stresses from an extrapolation of experimental steady state flow data.- Geodynamic series, 16: 69-87.

Trepmann, C.A., Stöckhert, B. (2001): Mechanical twinning of jadeite: an indication of synseismic loading beneath the brittle-plastic transition.- Int. J. Earth Sci., 90(1): 4-13.

Trepmann, C.A., Stöckhert, B. (2002): Cataclastic deformation of garnet; a record of synseismic loading and postseismic creep.- J. Struct. Geol., 24(11): 1845-1856.

Trepmann, C.A., Stöckhert, B. (2003): Quartz microstructures developed during non-steady state plastic flow at rapidly decaying stress and strain rate.- J. Struct. Geol., 25(12): 2035-2051.

Tse, S.T., Rice, J.R. (1986): Crustal earthquake instability in relation to the depth variation of frictional slip properties.- J. Geophys. Res., 91(9): 9452-9472.

Turcotte, P.L., Schubert, G. (2002): Geodynamics.- Cambridge University Press (456 pp.).

Urai, J., Williams, P.F., Roermund, v. H.L.M. (1991): Kinematics of crystal growth in syntectonic fibrous veins.- J. Struct. Geol., 13(7): 823-836.

Vermilye, J.M., Scholz, C.H. (1994): Relations between vein length and aperture.- J. Struct. Geol., 238: 423-434.

Voll, G. (1976): Recrystallization of quartz, biotite and feldspars from Erstfeld to the Leventina Nappe, Swiss Alps, and its geological significance.- Schweizerische Miner. Petrog., 56: 541-647.

Wald, D.J., Heaton, T.H. (1994): Spatial and temporal distribution of slip for the 1992 Landers, California, earthquake.- Bull. Seismol. Soc. Amer., 84: 668-691.

Walder, J., Nur, A. (1984): Porosity reduction and crustal pore pressure developement.- J. Geophys. Res., 89: 11,539-11,548.

Watson, E.B., Brenan, J.M. (1987): Fluids in the lithosphere, 1. experimentally-determined wetting characteristics of CO_2-H_2O fluids and their implications for fluid transport, host-rock physical properties, and fluid inclusion formation.- Earth Planet Sci. Lett., 85: 496-515.

Yardley, B. (1984): Fluid migration and veining in the Connemara Schists, Ireland.- In: Walther, J.V., Wood, B.J. [eds.]: Fluid-rock interactions during metamorphism, pp. 109-131, Springer-Verlag, New York.

3. Gradients in Quartz Vein Microfabrics - Progressive Cavity Formation in the Ductile Field

Abstract

The length to aperture ratio of a set of low aspect ratio veins in the high pressure / low temperature metamorphic Styra-Ochi Unit in southern Evia systematically exceeds the maximum aperture predicted by linear elastic fracture mechanic analysis. Non-elastic ductile deformation in the host rock must have contributed to widening of an arrested crack. As the microfabrics in the polyphase host rock are generally too complex and strain related to cavity formation is too low, the microstructural record related to this stage of deformation cannot be isolated in the host rock. Information is obtained from the microfabrics of the vein sealing quartz. The microfabrics show a decrease in the intensity of inhomogeneous crystal plastic deformation from the vein walls towards the vein centre. As a measure, the gradient in the density of geometrically necessary dislocations is quantified in orientation maps created by EBSD. The gradient results from progressive crack-parallel shortening during cavity formation and mineral precipitation. Early grown crystals, positioned at the vein margins, got deformed with progressive buckling of the vein walls, and record a prolonged deformation history compared to lately grown grains in the centre of the vein. It is anticipated that formation of the veins took place during postseismic stress relaxation by creep, after cracks had formed as a consequence of rapid coseismic loading. If so, the early grown crystals also experienced a higher differential stress compared to the crystals grown lately after significant stress relaxation.

3.1. Introduction

Veins form from cracks. Space for mineral precipitation from the crack-filling fluid is provided by divergent displacement normal to the crack walls. For cracks of limited length, widening of the crack and cavity formation imply crack parallel shortening of the host rock (Nüchter and Stöckhert, submitted). Elastic distortion is limited by the elastic properties and the strength of the host rock. Crack opening by purely elastic deformation is therefore restricted to high crack aspect ratios (AR = L/w; L: length, w: aperture). In the case of veins with a low aspect ratio, there must be a contribution of non-elastic deformation of the host rock, as predicted by a linear elastic fracture mechanic (LEFM) approach (e.g. Delaney and Pollard, 1981; Vermilye and Scholz, 1994; Olson, 2003; Nüchter and Stöckhert, submitted). At elevated temperatures, this non-elastic deformation is expected to be time-dependent and concomitant to stress relaxation.

The geometry of veins in metamorphic rocks of the Styra-Ochi Unit in southern Evia (Greece) indicates that tensile failure at a high loading rate (Nüchter and Stöckhert, submitted) was followed by a stage of ductile deformation, with crack parallel shortening of the host rock. The microstructural record of this stage of ductile deformation cannot be isolated in the host rock, the microstructure of the polyphase material being too complex and strain too low. Information can be obtained from the vein material, however. On principle, the precipitation of quartz in the cavity could have occurred in a static environment, after formation of the cavity, or dur-

ing progressive time-dependent opening. Here I investigate the microfabrics of the vein quartz as a function of position in the vein.

At first, I show that the apertures of the veins in southern Evia systematically exceed the maximum value predicted by LEFM analysis for the given vein length (Nüchter and Stöckhert, submitted). Then, the microfabrics of the vein quartz are investigated to test whether crystallization took place in a static environment or during progressive widening of the cavity, controlled by viscous creep of the host rock. While elastic distortion of the host rock is instantaneous in response to loading by remote stress, ductile creep is time-dependent and slow compared to elastic distortion. It depends on host rock rheology and ambient conditions. This means that cracks, which opened by purely elastic distortion of the host rock get sealed after opening in a static environment, whereas cracks opening by viscous creep of the host rock get sealed during progressive opening. In the latter case, early grown crystals positioned at the vein walls get progressively deformed due to concomitant shortening and buckling of the vein walls. If so, early grown grains at the vein walls record a prolonged deformation history compared to lately grown grains. Also, if crack opening takes place by creep during stress relaxation after an event of rapid loading, the early grown crystals were subjected to higher stresses compared to those grown lately in the centre of the vein. A gradient in the style and intensity of crystal plastic deformation, decreasing inwards from the vein walls and reflecting a history, is expected. The objective of the present paper is to test the hypothesis, that the veins record an event of rapid loading, presumably driven by stress redistribution during a nearby seismic event, and subsequent stress relaxation by creep of the host rock with precipitation of minerals from the pore fluid in the progressively widening cavity.

3.2. Geological setting

The Styra-Ochi Unit in southern Evia Island, Greece, is part of the high pressure / low temperature (HP / LT) metamorphic internal Cyclades belt, situated in the backarc region of the active Hellenic subduction zone. The structure of the Cyclades is governed by extensional tectonics and crustal thinning since the Early Miocene (Le Pichon and Angelier, 1981; Jolivet and Faccenna, 2000), driven by continuing roll back of the Hellenic subduction zone (Meulenkamp et al., 1988). The extension is localized in a single major (Lister et al., 1984; Faure et al., 1991) or several (Gautier and Brun, 1994) detachment faults. For the major part, the hanging wall block is eroded on the Cyclades with the exception of remnants on the islands of Tinos, Kea, and Paros (Gautier and Brun, 1994).

The HP / LT metamorphic Styra-Ochi Unit in southern Evia is derived from a variety of siliciclastic and carbonate-rich marine sediments, with intercalated basaltic to rhyolitic volcanic and intrusive rocks. During its earlier history, the Styra-Ochi Unit underwent pervasive deformation and HP / LT metamorphic overprint at a maximum temperature of about 400°C and a pressure similar to 1 GPa (Klein-Helmkamp, 1996), indicating maximum burial to a depth

of about 30 to 35 km. It was exhumed as a coherent unit, interpreted to represent the footwall block of a metamorphic core complex. The structures developed during that stage reflect a continuous evolution from ductile to brittle extensional deformation within a uniform kinematic framework (Gautier and Brun, 1994; Klein-Helmkamp, 1996). The veins investigated in the present study formed during exhumation and postdate HP-LT metamorphism.

3.3. Methods

The length and the aperture of 79 discordant quartz veins was measured. A correction was applied in those cases, where the angle between the outcrop surface and the vein wall deviates significantly from 90°. Oriented samples were taken from 33 veins. Additionally, 3 veins were sampled along profiles normal to the vein walls (a vein similar to EN 4, see Fig. 1a; EN 38, see Fig. 1b; EN 45, see Fig. 1c). The samples were cut normal to the host rock foliation and normal to the vein wall. The microstructures were examined in thin section (30 µm thick) with a polarizing microscope. The scanning electron microscope (SEM)-based technique of electron backscatter diffraction (EBSD), using polished thin sections, yields microstructural information with a resolution on the µm scale and provides information on the spatial distribution of the full crystallographic orientation in a thin section. EBSD-investigations were carried out using an SEM (LEO 1530) equipped with a field emission gun and a forescatter detector. Thin sections used for the EBSD technique were chemically polished using a silica suspension (SYTON®) to minimise surface damage, and then coated with carbon to limit charging effects. For EBSD analysis, the SEM was operated at an accelerating voltage of 20 kV and a working distance of 25 mm, with the thin section tilted at an angle of 70° with respect to the beam.

3.4. Structural setting and geometry of the discordant low aspect-ratio quartz veins

3.4.1. Structural setting

The veins of interest crosscut the foliation and all former syn-metamorphic structures and fabrics, including schistosity (Fig. 1a-c) shearband foliation, and pre-existing earlier veins parallel to the foliation (Fig. 1b). The orientation of the vein walls, hence of the original cracks, is more or less uniform all over the Styra-Ochi Unit in southern Evia, an area of more than 500 km^2. The veins trend about SE to SSE and are nearly vertical. This orientation is consistent with a stress field characterized by $\sigma_1 = \sigma_v$ and σ_3 at about NE to ENE at the stages of fracturing and vein formation (Fig. 2). Most veins show a symmetric lens shape (Fig. 1a, b), while some veins are more irregular in shape, showing minor swelling and pinching (Fig. 1c). The geometry suggests tensile failure (mode I) and opening normal to the least principal stress, σ_3. The length of most veins ranges between 10^{-1} m and 10^{1} m, which is taken to reflect the characteristic length scale of the parental cracks. The spectrum of vein aspect ratios ranges between 7 and 100 (Fig. 3). 62% of the veins show aspect ratios < 20 (Fig. 3).

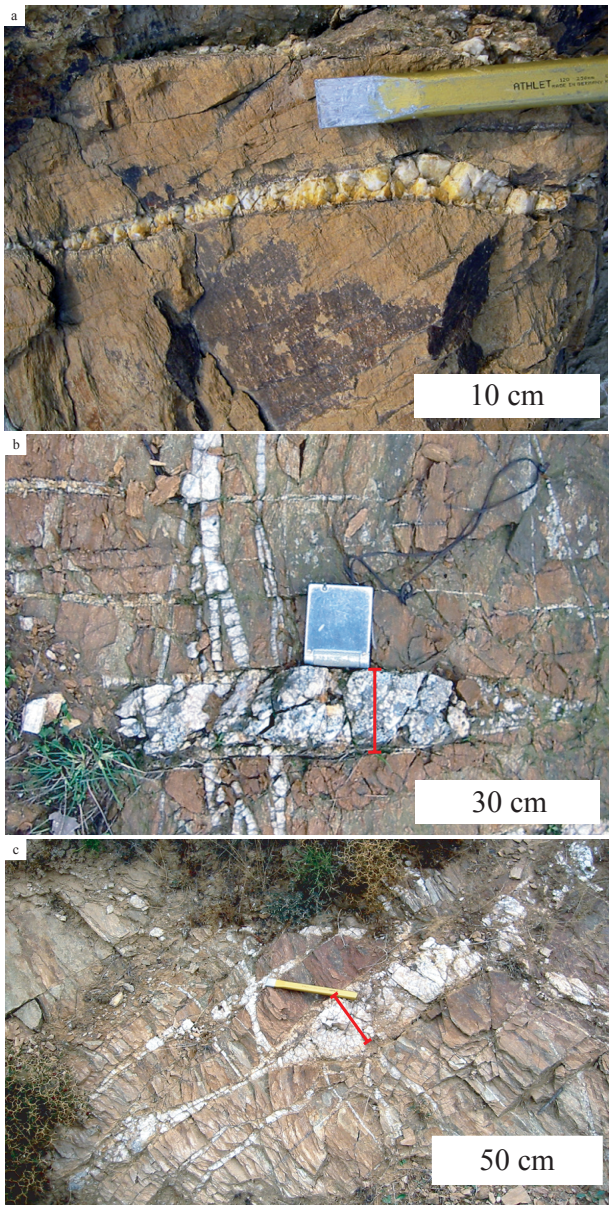

Fig. 1: Discordant quartz veins in the Styra-Ochi Unit selected for analysis. The red bars show the sampled profile lines. a) A lens-shaped vein very similar to vein EN 4 and from the same outcrop. Vein EN 4 got damaged during sampling, before a photograph was taken. b) The lens-shaped vein EN 38 with a low aspect ratio of about 12 crosscuts pre-existing concordant veins. c) The irregular shaped vein EN 45 shows swelling and pinching.

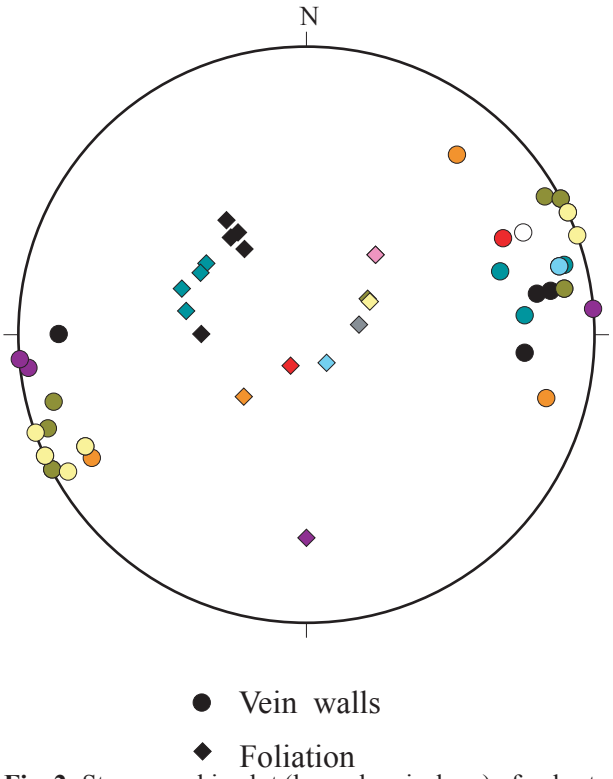

Fig. 2: Stereographic plot (lower hemisphere) of poles to the foliation and to the vein walls at different locations in the Styra-Ochi Unit of southern Evia (Greece). The data cover an area of more than 500 km2.

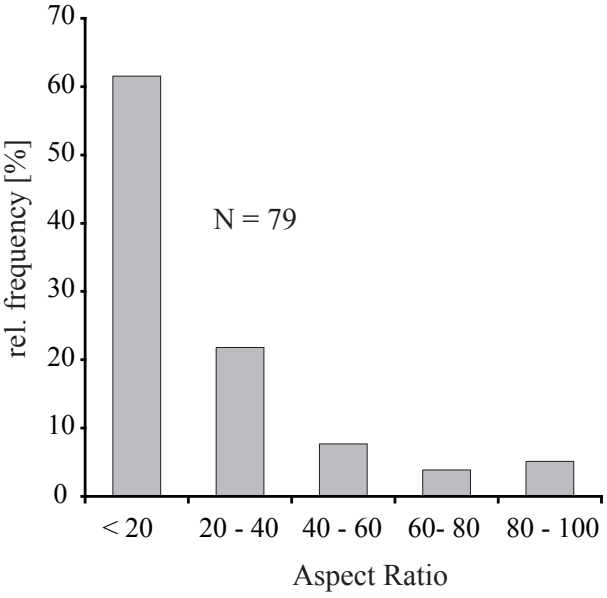

Fig. 3: Histogram showing the frequency distribution of vein aspect ratios. Most veins reveal an aspect ratio of 20 or below.

3.4.2 Vein Geometry in the context of linear elastic fracture mechanics

In response to linear elastic deformation of the host rock, opening of an arrested crack is controlled by the elastic properties of the host rock (e.g. Sneddon and Elliott, 1946; Pollard and Segall, 1987; Vermilye and Scholz, 1994; Olson, 2003) and the effective stress acting normal to the crack wall, $\sigma'_n = \sigma_n - P_f$ (1) (Rice and Cleary, 1976). σ_n denotes the remote stress component acting normal to the crack wall, in this case the least principal compressive stress σ_3, and P_f denotes the fluid pressure inside the crack.

Linear elastic fracture mechanics (LEFM) predicts that the aperture w of an arrested crack correlates with the crack length L and with the wall normal effective tensile stress σ'_n. The following relation holds for non-interacting, opening mode cracks under two-dimensional plane strain conditions (Sneddon and Elliott, 1946; Pollard and Segall, 1987):

$$w = -\sigma'_n \frac{2(1-\nu^2)}{E} L \qquad (2)$$

E denotes the Youngs modulus and ν the Poissons ratio. The state of stress in the material close to the tip of a crack at a distance r under tensile load is proportional to the stress intensity factor K_I and to $r^{-1/2}$ (Irwin, 1948, 1956, 1957). The stress intensity factor K_I depends on σ'_n and on L (Irwin, 1948, 1956, 1957):

$$K_I = -\sigma'_n \sqrt{\pi L/2} \qquad (3)$$

If K_I reaches a certain material constant, the fracture toughness K_{IC} (Irwin, 1961), the matter fails by initiation of unstable crack propagation:

$$K_{IC} = -\sigma'_{nc} \sqrt{\pi L/2} \qquad (4)$$

where σ'_{nc} denotes the critical tensile stress. According to eq. 2 and eq. 4, crack opening by linear elastic distortion of the host rock is limited by $\sigma'_n < \sigma'_{nc}$. Implementation of eq. 4 into eq. 2 yields a criterion for the maximum possible crack width w_0, sustained by the host rock (Olson, 2003):

$$w_0 = K_{IC} \frac{(1-\nu^2)}{E\sqrt{\pi/8}} \sqrt{L} \qquad (5)$$

Eq. 5, solved for K_{IC} (eq. 6), can be used to estimate K_{IC} holding for the rock, using the length and aperture data of mineralized veins (Olson, 2003). This approach presumes that the veins

formed in response to purely elastic distortion of the host rock and, hence, under LEFM-conditions:

$$K_{IC} = \frac{w_0}{\sqrt{L}} \frac{E\sqrt{\pi/8}}{(1-\nu^2)} \qquad (6)$$

Eq. 6 is used to compare the geometry of the discordant veins in the Styra-Ochi Unit to laboratory data for K_{IC} (Atkinson and Meredith, 1987) and to the geometry of single-segment veins at Culpepper Quarry / Virginia USA and Florence Lake / California USA (Vermilye and Scholz, 1994), as well as the geometry of multi-segment dykes at Ship Rock (Delaney and Pollard, 1981) (Fig. 4). The geometry of the Culpepper Quarry and Florence Lake veins is interpreted to result from elastic distortion of the vein walls during cavity formation (Vermilye and Scholz, 1994; Olson, 2003). In contrast, the geometry of magmatic dykes is expected to be strongly influenced by thermal effects due to magmatic heat transfer (e.g. Delaney and Pollard, 1981; DeGraff and Aydin, 1993). Such effects include thermal erosion at the dyke walls (e.g. Delaney and Pollard, 1981) and enhanced plasticity at the dyke tips (e.g. DeGraff and Aydin, 1993), resulting in a marked increase in the fracture toughness due to crack tip blunting (e.g. Anderson, 1995). The geometry of magmatic dykes is expected to be influenced by a number of processes and does by no means reflect a purely elastic deformation of the host rock (e.g. Delaney and Pollard, 1981; Vermilye and Scholz, 1994; Olson, 2003). As K_{IC} is exclusively defined for sharp crack tips stressed at LEFM conditions, the results of eq. 6 are referred to apparent fracture toughness, K^*_{IC}, wherever the values exceed the values for K_{IC} determined in the laboratory (Atkinson and Meredith, 1987).

Equation 5 is solved for the length and aperture data of the discordant veins in the Styra-Ochi

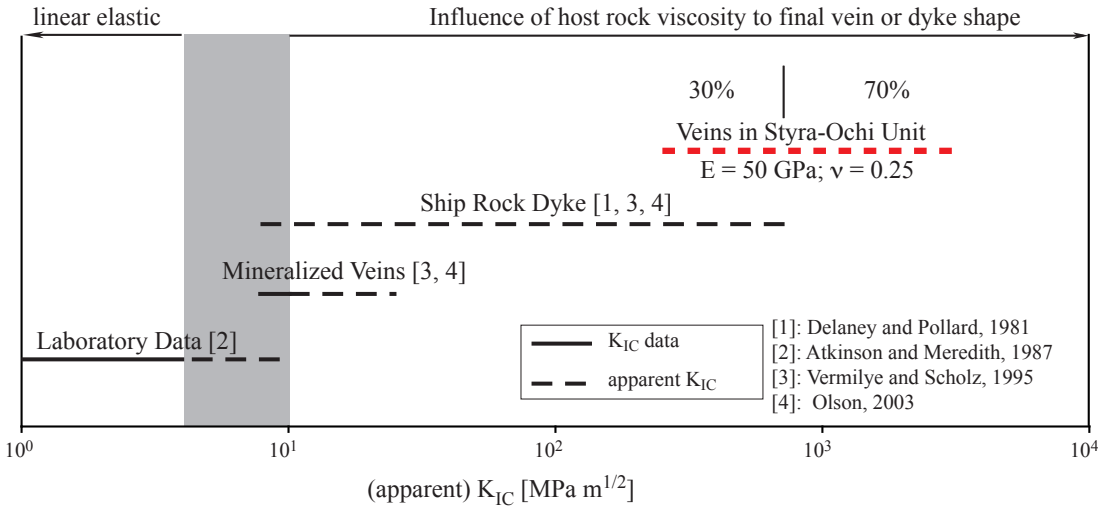

Fig. 4: Comparison of the apparent K_{IC} data derived for the discordant lens-shaped veins in the Styra-Ochi Unit (eq. 5) with published data for the magmatic Ship Rock Dyke (Delaney and Pollard, 1981), for Culpepper Quarry and Florence Lake mineralized veins (Vermilye and Scholz, 1995) and with published laboratory data for K_{IC} of rocks (Atkinson and Meredith, 1987).

Unit using moderate values of E = 50 GPa and ν = 0.25 for metamorphic rocks (Turcotte and Schubert, 2002), resulting in values of K^*_{IC} between 3 x 10^2 and 3 x 10^3 MPa $m^{1/2}$ (Fig. 4). The K^*_{IC} values derived for the Culpepper Quarry and Florence Lake veins and for the Ship Rock Dyke range between 8 and 25 MPa $m^{1/2}$, and 8 and 800 MPa $m^{1/2}$, respectively (Olson, 2003) (Fig. 4). Typical laboratory values of K_{IC} range between 1 and 4 MPa $m^{1/2}$, and in exceptional cases up to 10 MPa $m^{1/2}$ (Atkinson and Meredith, 1987). The calculated apparent fracture toughness, K^*_{IC}, for the discordant veins in the Styra-Ochi Unit exceeds the laboratory K_{IC} data (Atkinson and Meredith, 1987) and the K^*_{IC} of the reference veins (Vermilye and Scholz, 1994; Olson, 2003) by 1 to 3 orders of magnitudes. The maximum K^*_{IC} of Ship Rock Dyke (Olson, 2003) is exceedet by 70 % of the veins. Therefore, the geometry of the lens-shaped veins in southern Evia is in conflict with an origin by purely elastic deformation of the host rock, and is interpreted to reflect a significant contribution of viscous deformation of the host rock during the period of cavity formation.

3.5. Microfabrics of vein quartz

The quartz microfabrics of 33 discordant veins in the Styra-Ochi Unit of South Evia were investigated by optical microscopy. Three veins, EN 4, EN 38 and EN 45, were selected for a more detailed quantitative analysis. The dimensions of veins EN 4, EN 38 and EN 45 are L = 42 cm, w = 4,1 cm; L = 120 cm, w = 10 cm; and L = 192 cm, w = 21 cm, respectively. L denotes the vein length and w the maximum aperture. These veins were chosen for the following reasons:

The veins are sealed by quartz, while other minerals are subordinate and, if present, restricted to a narrow zone close to the vein walls. The microfabrics developed during sealing in EN 4 and EN 45 are representative for the fabrics observed in the vast majority of the 33 microscopically inspected veins. The microfabrics of vein EN 38 show some peculiarities, but are interpreted to reflect the same principal mechanisms of vein sealing as in the other veins.

The veins EN 38 and EN 45 show the largest aperture of all investigated veins and hence, provide the best spatial resolution along the profiles. While EN 4 and EN 38 represent the most common lens-shape geometry (Fig. 1a, b), EN 45 represents the group of irregular shaped veins, showing some swelling and pinching (Fig. 1c). The comparably short and thin vein EN 4 was chosen in order to explore whether the evolution of the deformation related microfabrics in the vein quartz depends on the size of the vein.

3.5.1. Vein quartz microfabrics related to sealing

The veins EN 4 and EN 38 are almost exclusively sealed by quartz. In vein EN 45, subordinate amounts of albite and zoisite are restricted to a narrow zone at the vein margin. The present study focuses on the quartz microstructures. First of all, inclusion trails parallel to the vein walls (Durney and Ramsay, 1973; Ramsay, 1980; Cox and Etheridge, 1983; Fisher and Byrne, 1990; Fisher and Brantley, 1992; Fisher et al., 1995) are systematically absent in all veins. At the vein margin, the quartz microstructure of EN 4 and EN 45 is characterized by elongate grains with an aspect ratio of 1.5 to 2 (Figs. 5a, 7a). In contrast, the quartz microstructure at the margins of vein EN 38 is characterized by elongate grains with an aspect ratio of about 3 to 3.5 (Fig. 6a). In this vein, the majority of these elongate grains at both vein walls appear bent (Fig. 6a, c). The long axis of the elongate grains at both vein margins are inclined in the opposite direction. The curvature of the grains coincides with a curvature in the crystallographic orientation (Fig. 6a - c).

In all veins, the sealing quartz shows a crystallographic preferred orientation (CPO) of the c-axes. In the veins EN 4 and EN 45, the c-axes are preferentially oriented normal to the vein walls (Figs. 5b, 7b), and in vein EN 38, the c-axes are oriented at a high angle to the vein walls (Fig. 6b). The CPO of the quartz c-axes gets more pronounced over a narrow interval form the vein margin towards the vein centre. Close to the vein margins, the CPO is diffuse with multiple weak maxima (Figs. 5b, 6b, 7b). With increasing distance to the vein walls, the number of maxima decreases and a uniform preferred orientation of the quartz c-axes develops (Figs. 5b, 6b, 7b). The grains generally display a pronounced shape preferred orientation (SPO), the long axes being oriented parallel to the c-axes (Figs. 5c, 6c, 7c). The grain size increases towards the vein centre, resulting in a decrease in the number of grains per cross sectional area (Figs. 5-7 a, d). At the vein margins, the grain size ranges between 10 and 100 μm in the veins EN 4 and EN 45 (Figs. 5, 7, 9a, 10d), while it is on the millimetre scale in vein EN 38 (Fig. 7 a, d). Close to the centres of the veins, the grains reach several centimetres in diameter (Figs. 6a, d, 8). Residual open vugs bound by crystallographically controlled faces are common and most frequently found close to the vein centres (Figs. 9d, 10c).

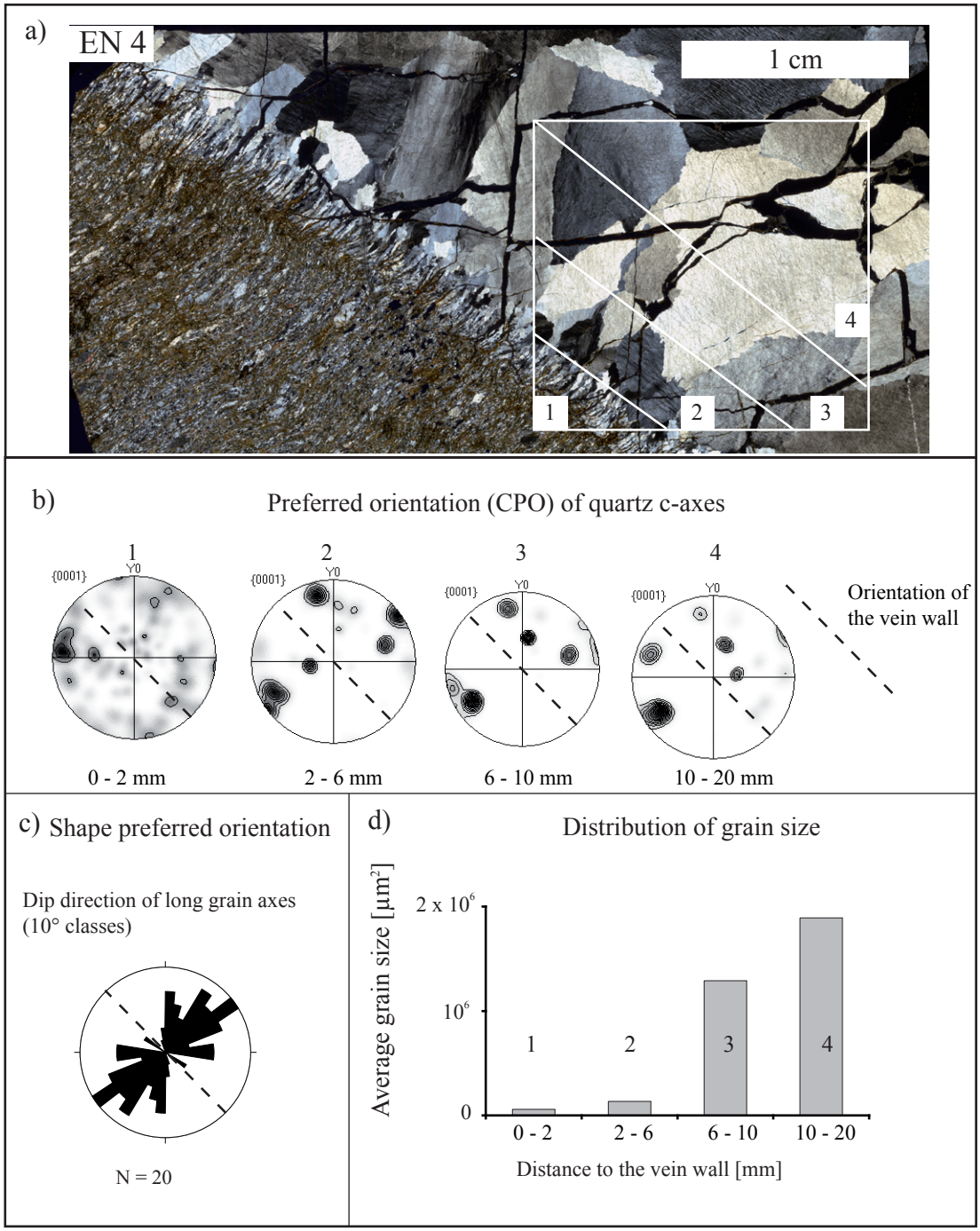

Fig. 5: Quartz microfabrics of vein EN 4, grain shape and orientation data acquired by EBSD: a) Optical microstructure (thin sections scanned with crossed polarizers). b) Development of a more pronounced quartz c-axes preferred orientation with increasing distance to the vein walls. c) Shape preferred orientation of the quartz crystals. d) Increase in quartz grain size with increasing distance to the vein walls.

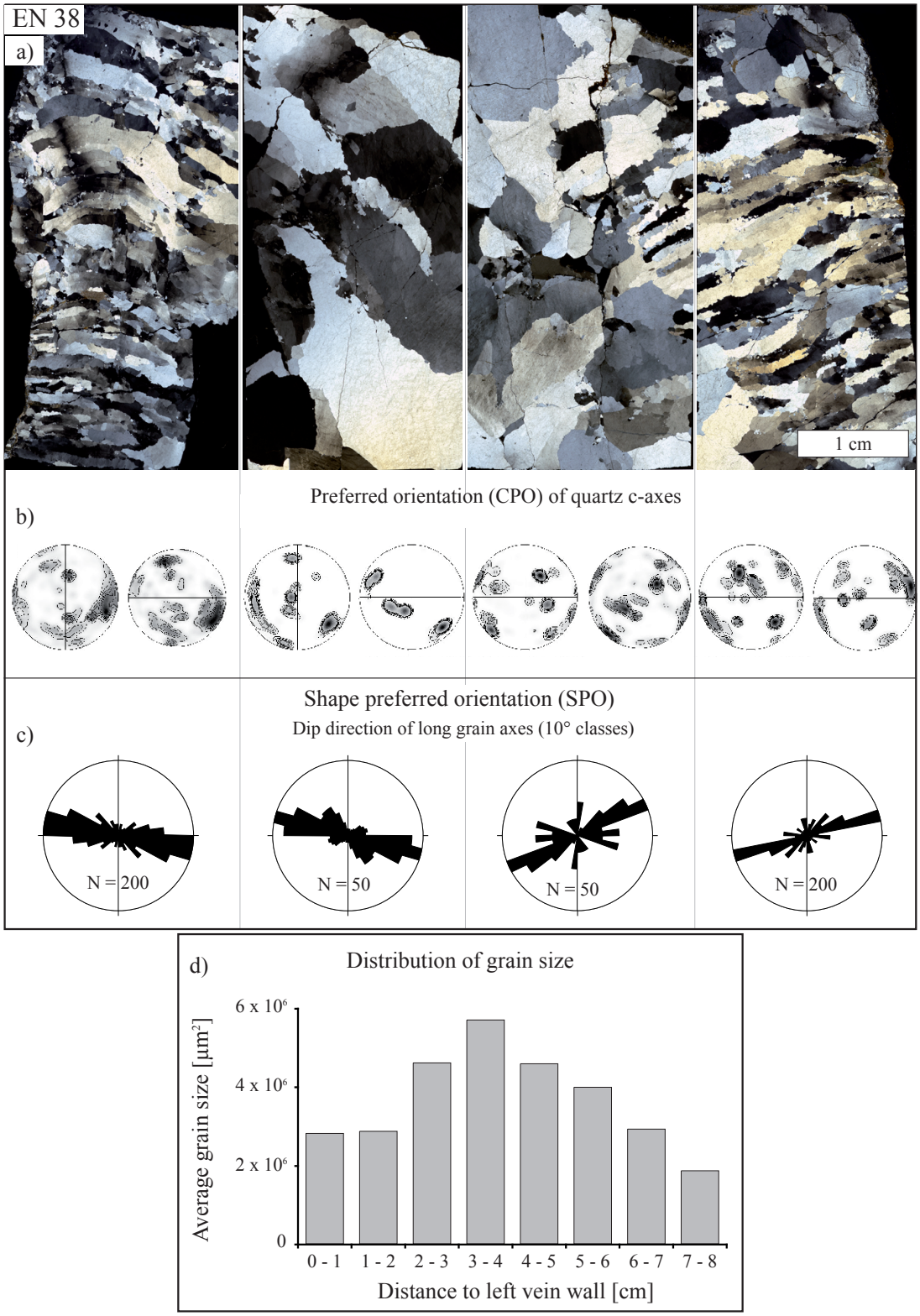

Fig. 6: Quartz microfabrics of vein EN 38, grain shape and orientation data acquired by EBSD: a) Optical microstructure (thin sections scanned with crossed polarizers). b) Development of a more pronounced quartz c-axes preferred orientation with increasing distance to the vein walls. c) Shape preferred orientation of the quartz crystals. d) Increase in quartz grain size with increasing distance to the vein walls.

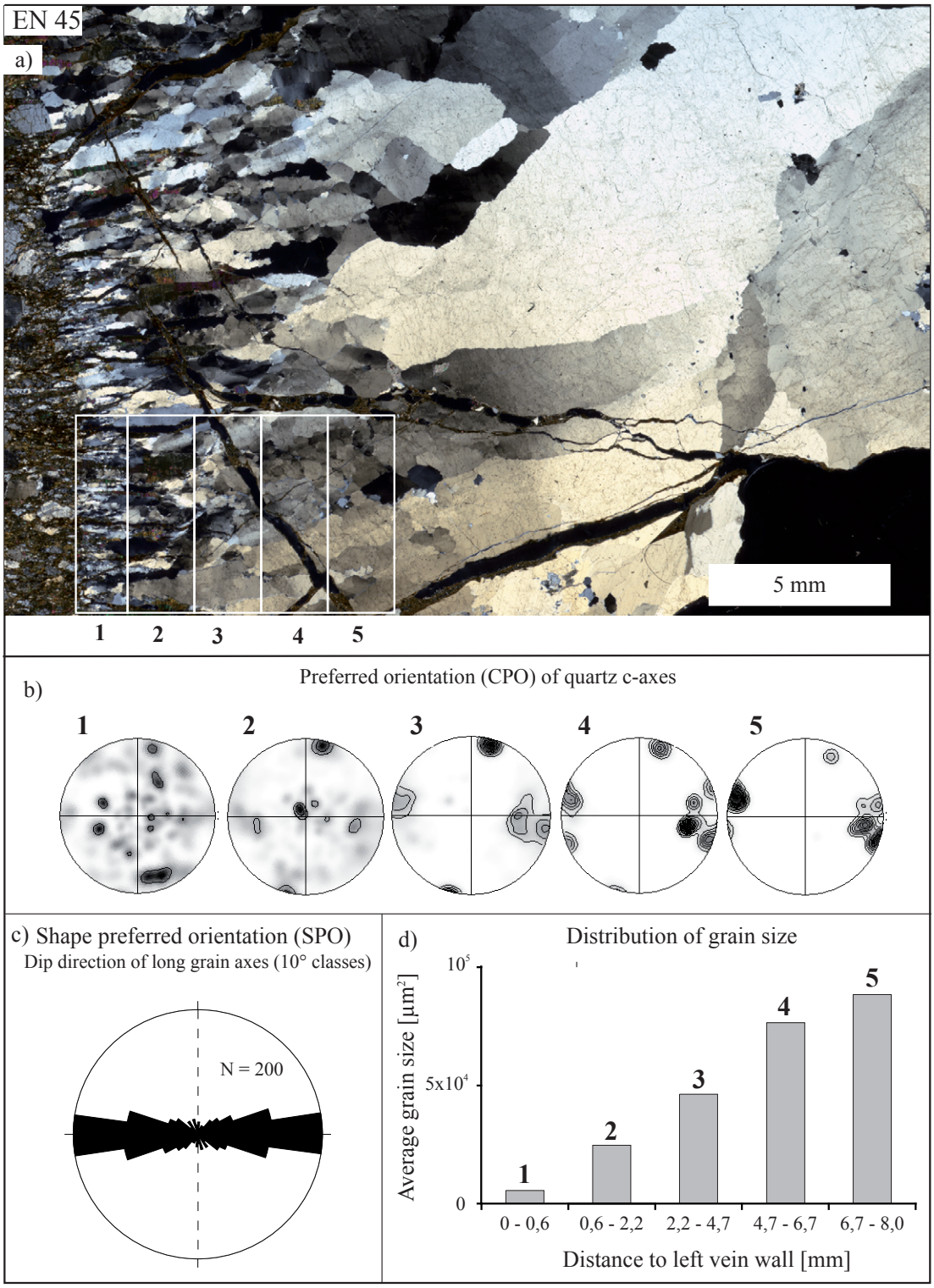

Fig. 7: Quartz microfabrics of vein EN 45, grain shape and orientation data acquired by EBSD: a) Optical microstructure (thin sections scanned with crossed polarizers). b) Development of a more pronounced quartz c-axes preferred orientation with increasing distance to the vein walls. c) Shape preferred orientation of the quartz crystals. d) Increase in quartz grain size with increasing distance to the vein walls.

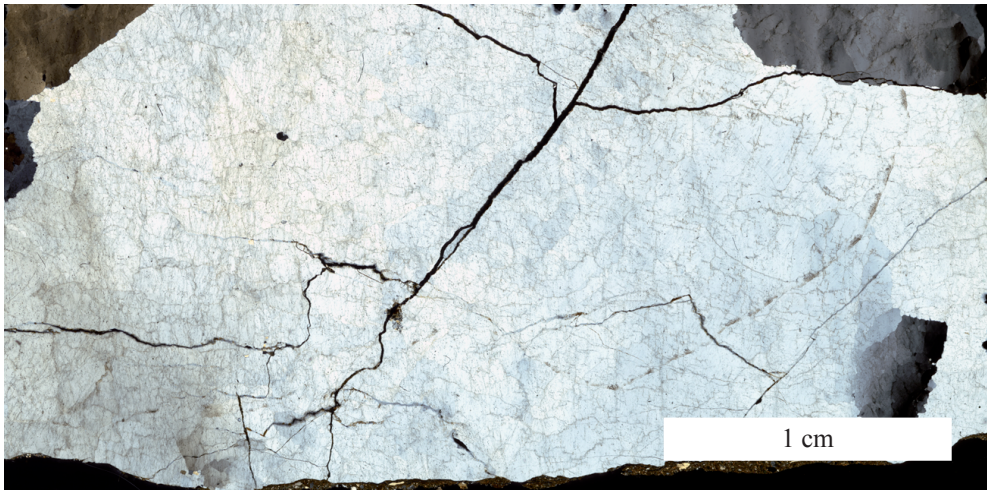

Fig. 8: Centimetre-sized quartz crystals at the centre of vein EN 45. The grains show undulatory extinction. Scanned thin section with crossed polarizers.

3.5.2. Vein quartz microfabrics related to deformation

The quartz grains in the veins show microstructures indicative of crystal plastic deformation by dislocation glide, least so in the vicinity of open vugs (Figs. 9d, 10c). Inhomogeneous deformation is revealed by marked undulatory extinction, deformation bands and deformation lamellae (Figs. 5a, 6a, 7a, 8, 9, 10). Microstructures indicating thermally activated annealing processes comprise subgrains and sutured high-angle grain boundaries resulting from strain-induced grain boundary migration (migration recrystallization) (Figs. 9, 10). However, the distortion of the majority of the grains is minor and the original grain shape is largely preserved.

3.5.2.1. Gradients in crystal plastic deformation observed in the optical microscope

According to the predominant microfabrics related to deformation, the veins are subdivided into zones parallel to the vein walls. First, the general characteristics of the microfabrics in each zone are presented. Then, the position of these zones and deviations from the standard model are described for each vein.

Zone A is restricted to the outermost part of the veins. Here, recrystallized grains have formed around deformed large grains, a fabric commonly referred to as core and mantle structures (e.g. Hirth and Tullis, 1992) (Figs. 9a, 10d). With increasing distance to the vein walls, the disappearance of recrystallized grains defines the transition from zone A to zone B. In zone B, preserved original grains are intensely polygonized, with small subgrains and high misorientation angles at the subgrain boundaries. The high angle grain boundaries are strongly sutured (Fig. 9b). Towards the vein centre, the misorientation across the subgrain boundaries decreases and the subgrains increase in size. The transition to Zone C is defined by the onset of a SPO of the subgrains parallel to the c-axis. In zone C, the high angle grain boundaries are gently sutured (Fig. 9c, 10b). The innermost zone D is characterized by the absence of subgrains. Instead, the grains show at best a slight undulatory extinction and weakly sutured high angle grain boundaries. Open vugs bound by euhedral facets are common (Figs. 9d, 10c).

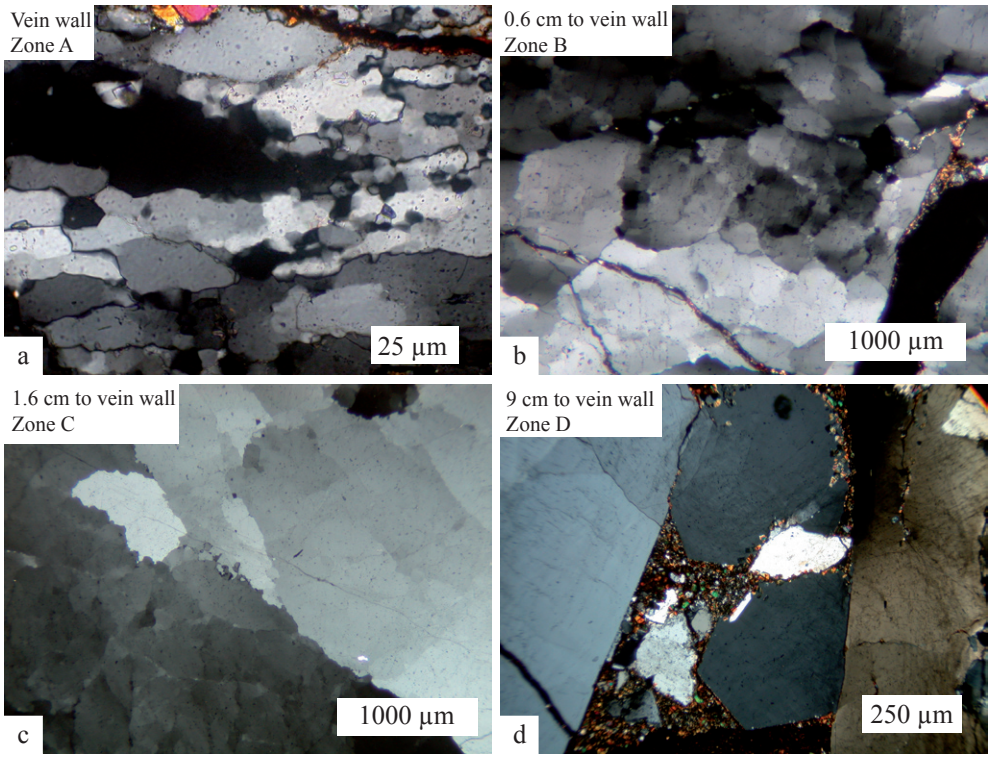

Fig. 9: The quartz microfabrics in vein EN 45 show a decrease in the intensity of crystal plastic deformation with increasing distance to the vein wall. A) Recrystallized grains close to the vein wall (zone A). B) Original grain with small subgrains and high misorientation angles at the subgrain boundaries (Zone B). C) Large subgrains with shape preferred orientation. The misorientation angle at the subgrain boundaries is low. D) Open vug bound by euhedral facets embedded quartz grains with undulatory extinction. Photomicrographs with crossed polarizers.

Vein EN 45 comprises the zones A-D. In zone A, the diameter of the recrystallized grains ranges between 2.5 and 30 µm (Fig. 9a). The transition to zone B occurs at a distance of about 6 mm to the vein wall. Here, the size of the isometric subgrains ranges between 500 and 600 µm (Fig. 9b). The border to zone C is located at approximately 1.6 cm from the vein wall. Here, the elongate subgrains reach a diameter of up to 2 mm parallel and 0.6 mm normal to the c-axis (Fig. 9c). The transition to zone D is poorly defined due to the gradual disappearance of the subgrains between 4.8 and 7.7 cm from the vein wall. The first open vugs occur at a distance of 9 cm from the vein wall (Fig. 9d).

In vein EN 38 zone A is not discernible. At the vein margin the microfabrics correspond to zone B. Zones C and D are well developed. In the outermost part of zone B a few isolated recrystallized grains occur with a diameter between 10 and 30 µm (Fig. 10a). The microstructure of the original grains is dominated by intense undulatory extinction, small isometric subgrains 15 to 50 µm in diameter, and strongly sutured high angle grain boundaries (Fig. 10a). The transition to zone C is located at about 1 to 1.3 cm from the vein wall. The anisometric subgrains measure up to 1 mm in diameter parallel and up to 0.6 mm normal to the c-axis (Fig. 10b). The high angle grain boundaries are less sutured compared to zone B (Fig. 10a). The transition into zone D is at approximately 3 cm distance from the vein wall. Open vugs occur close to the vein centre (Fig. 10c).

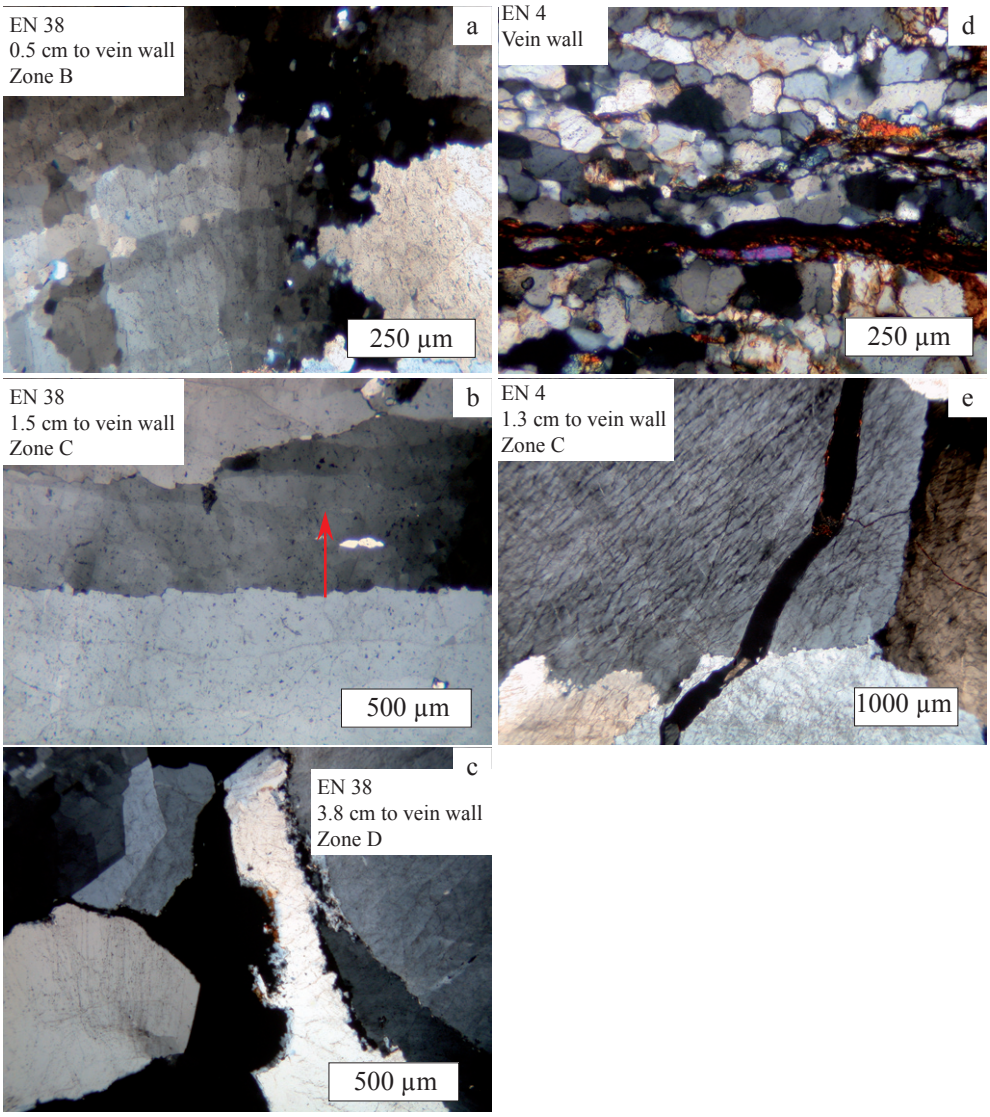

Fig. 10: Microfabrics of quartz in veins EN 38 (a-c) and EN 4 (d, e) a) Original grains with intense undulatory extinction, small subgrains, and highly sutured high angle boundaries close to the vein wall. Small isometric recrystallized grains are sparse (Zone B). B) Large anisometric subgrains with shape preferred orientation (arrow) (Zone C). C) Open vug bound by euhedral facets embedded in large quartz grains with undulatory extinction. d) Recrystallized grains at the margin of vein EN 4 (Zone A). E) Large grains in the centre show undulatory extinction and deformation bands. The grain boundaries are sutured. Photomicrographs with crossed polarizers.

In vein EN 4, the zones A through C are identified, though their appearance deviates somewhat from the standard model. Zone D is missing. In zone A, the size of the recrystallized grains ranges between 50 and 100 µm (Fig. 10d). The transition to zone B is at about 2 mm distance to the vein wall. Subgrains, comparable to those in EN 38 and EN 45, are absent. Instead, the grains show diffuse deformation bands and elongate subgrains parallel to the c-axis. The transition to zone C is located at approximately 5 mm distance to the vein wall. Within zone C, the microstructure is dominated by deformation bands parallel to the c-axis and subbasal deformation lamellae (Fig. 10e).

3.5.2.2. Assessment of gradients in crystal plastic deformation using EBSD maps

EBSD–generated maps provide information on the spatial distribution of the complete crystallographic orientation of the vein quartz. In the following, such maps are used to derive the intracrystalline misorientation gradients, as a function of position within the vein. The misorientation gradients reflect the density of geometrically necessary dislocations (Nicolas and Poirier, 1976) introduced during inhomogeneous crystal plastic deformation.

When crystal plastic deformation is exclusively governed by dislocation glide, the activation of less than five independent glide systems in a single crystal leads to inhomogeneous deformation and distortion of the crystal (Nicolas and Poirier, 1976; Poirier, 1985). This means that the orientation of the indicatrix depends on the position, causing undulatory extinction observed in the polarizing microscope. At moderate temperature and stress conditions, quartz preferentially deforms by glide in the system (0001)<11.0> (basal a-glide) (Hobbs, 1985). Using EBSD maps, the intracrystalline misorientation gradients reflecting the density of geometrically necessary dislocations are quantified as follows:

Colour gradients in the EBSD map in Fig. 11a reflect the degree of misorientation within a single large quartz grain from EN 38 with respect to an arbitrarily chosen reference point. Close to the vein wall, the stereographic plot of the c-axis orientations shows considerable dispersion (Fig. 11a), while at some distance to the vein wall the spread of the c-axis orientation within the same grain is much less (Fig. 11a). The degree of inhomogeneous crystal plastic deformation, i.e. the density of geometrically necessary dislocations, decreases inwards from the vein wall. Here, the steepest gradient in intracrystalline misorientation is used as a measure. The angle of misorientation with respect to a reference point is measured along the steepest gradient on EBSD maps (Fig. 11a, b). The misorientation profiles are approximated by a line of best fit (Fig. 11b). The gradient of the line of best fit provides a measure for the intensity of inhomogeneous crystal plastic deformation, and is referred to as the gradient of the misorientation profile, GMP [°/μm] (Fig. 11b).

To assess the GMP as a function of position within the veins, EBSD mapping with 10 μm step size was performed on thin sections along a profile normal to the vein walls. The maps were subdivided into subsets. In each subset, several GMPs parallel to the steepest gradient in misorientation were collected. Then, the average GMP is plotted for each subset position within the vein (Fig. 11c). The procedure of GMP determination and creation of a GMP-position plot is illustrated in Fig. 11.

The GMP as a function of position is plotted in Fig. 12 for the three investigated veins. At the vein walls, the GMP is highest and decreases non-linearly by about one order of magnitude towards the vein centre. For the vein EN 38, the pattern is symmetric.

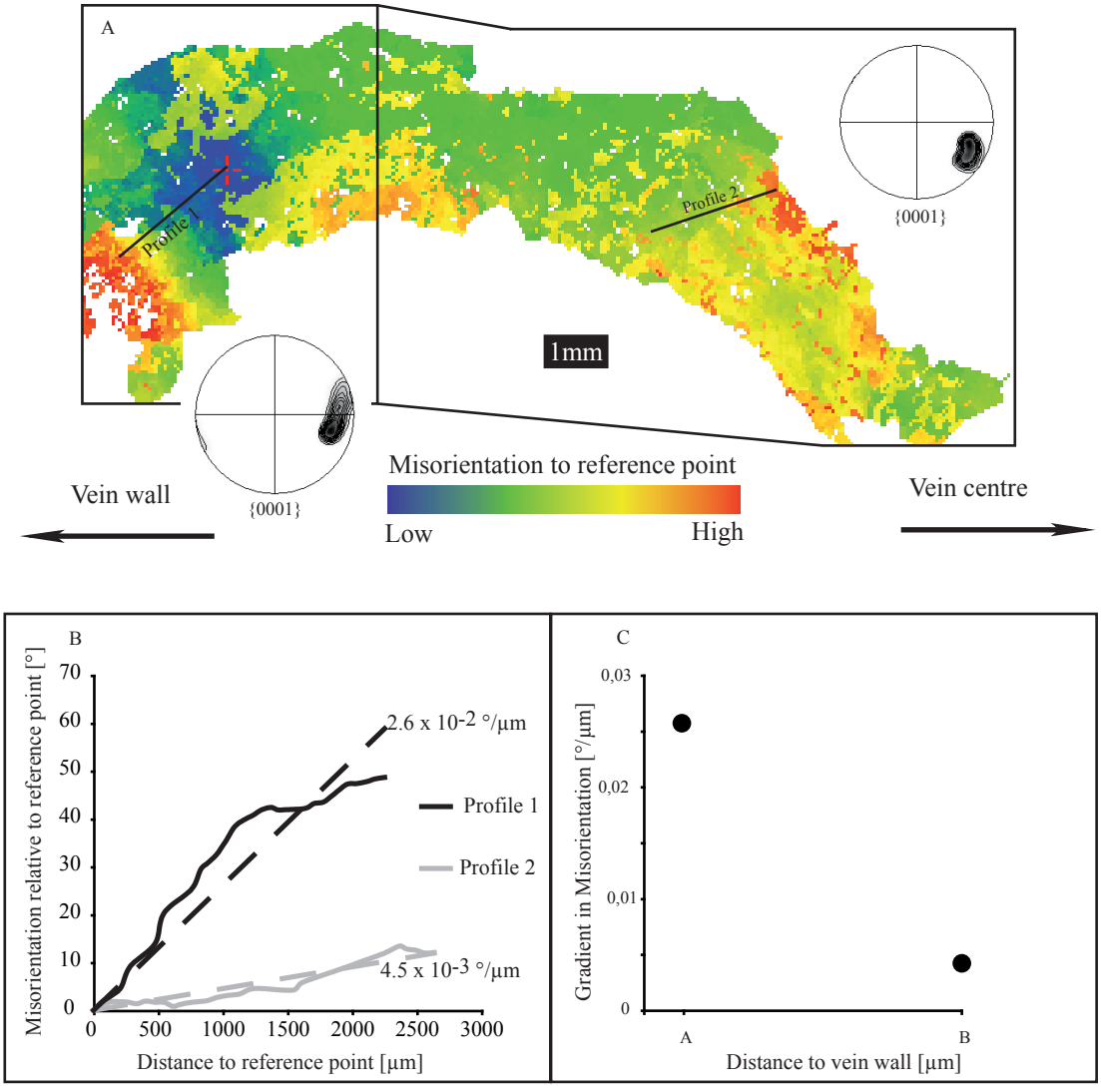

Fig. 11: Principles of the assessment of gradients in crystal plastic deformation: a) The angle of misorientation with respect to a reference point is measured along the steepest gradient on EBSD maps. b) The gradient is approximated by a line of best fit, and is referred to as the gradient of the misorientation profile, GMP [°/µm]. c) The GMP is plotted as a function of the position within the vein.

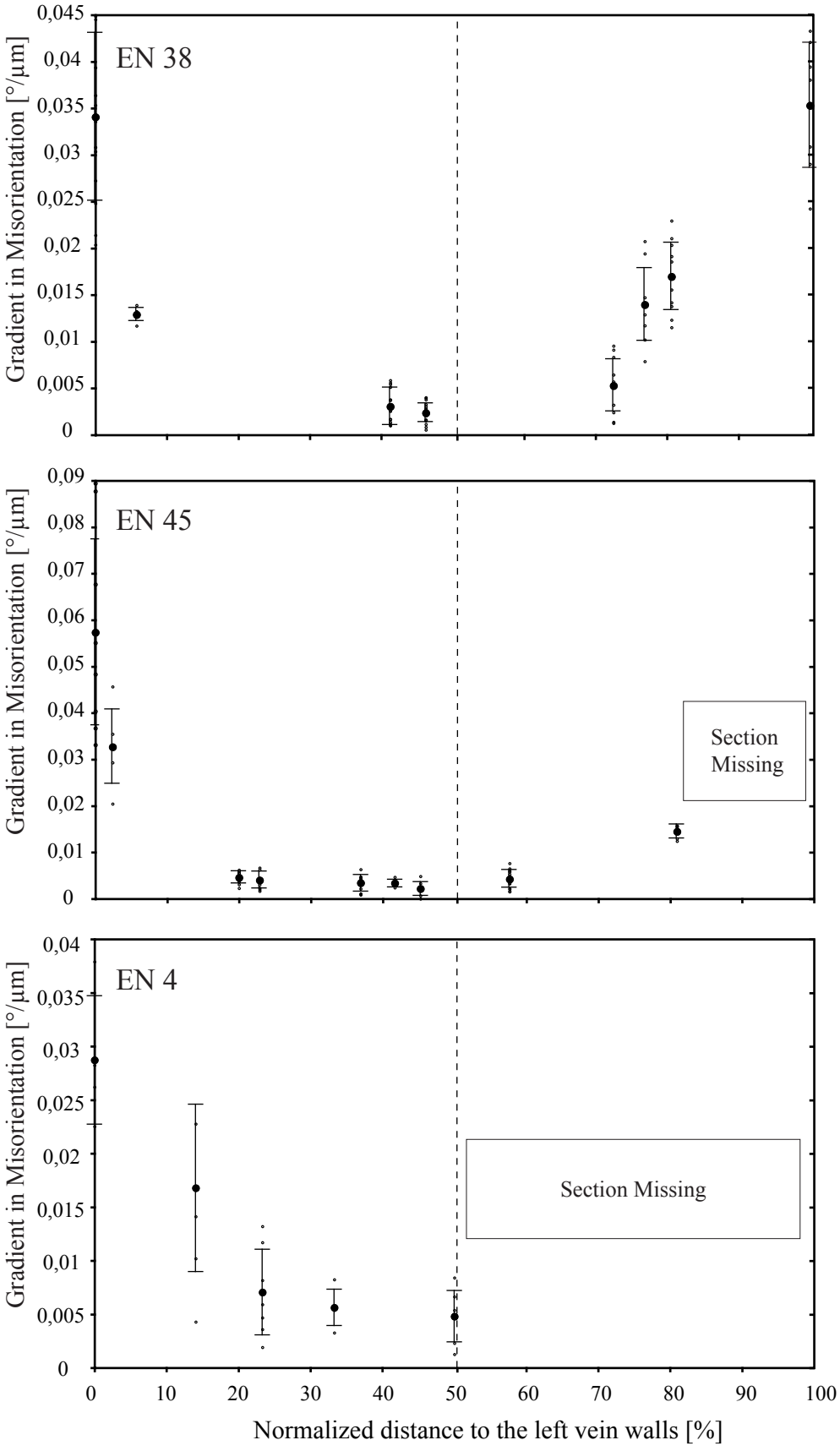

Fig. 12: Plots of the gradients of the misorientation profile (GMP) as a function of the position within the veins. At the vein walls, the GMP is highest and decreases non-linearly by about one order of magnitude towards the vein centres. a) Vein EN 38; b) vein EN 45; c) vein EN 4.

3.6. Discussion

3.6.1. Crustal level of fracturing and vein formation

The cracks and the resulting veins postdate the pervasive ductile deformation during HP / LT metamorphism, as the veins crosscut all syn-metamorphic structures of the host rock and the original vein shapes appear to be at best little modified by later deformation. The orientation of the veins indicates tensile fracturing and vein formation during crustal extension. This structural record indicates that the veins do not represent deep-seated syn-metamorphic structures, but must have formed during exhumation and cooling.

The vein quartz microstructure records thermally activated annealing processes, which indicates deformation at elevated temperatures. The correlation between thermochronometry and natural quartz microstructures (e.g. Voll, 1976; Dunlap et al., 1997; Stöckhert et al., 1999; Brix et al., 2002), supported by the extrapolation of experimental flow laws to slow geological strain rates (e.g. Hirth et al., 2001) allows to estimate the syn-kinematic temperature. Based on these comparisons, the microfabrics point to deformation at temperatures similar to or slightly above 300°C, hence at a depth just below the crustal scale long-term brittle-ductile transition. As there is no evidence for a complex thermal history (Klein-Helmkamp, 1996) and uniform cooling during exhumation can be assumed, formation of the parent cracks and veins must have taken place at a minimum temperature near to or somewhat above 300°C. This temperature is sufficient for viscous deformation of the host rock, contributing to crack opening and cavity formation.

3.6.2. Cavity sealing

The microstructure of the veins provides information on the opening and sealing history (e.g. Durney and Ramsay, 1973; Ramsay, 1980; Cox and Etheridge, 1983; Urai et al. 1991; Fisher and Brantley, 1992; Hilgers and Urai, 2002). Two microstructural endmembers are diagnostic for the relation between the rates of opening and of sealing:

1) If the sealing rate exceeds the opening rate, vein formation gets cyclic. Incremental widening is followed by complete sealing. The process is called the crack-seal mechanism (Durney and Ramsay, 1973; Ramsay, 1980; Cox and Etheridge 1983; Fisher and Bryne, 1990; Fisher and Brantley, 1992; Fisher et al. 1995). The indicative microfabrics show fibrous crystals, generally without CPO, and narrowly spaced inclusion trails parallel to the vein walls (Durney and Ramsay, 1973; Ramsay 1980; Cox and Etheridge 1983; Fisher and Bryne, 1990; Fisher and Brantley, 1992; Fisher et al. 1995). These inclusion trails mark healed cracks. Each trail represents a single increment of opening. Urai et al. (1991) proposed that the grain fibres are detained from development of crystallographic controlled facets by pinning at asperities on the opposite vein wall. Such fibres are capable to track the

displacement path during vein widening (Durney and Ramsay, 1973; Ramsay and Huber, 1983; Urai et al., 1991), which may be non-linear. In this case, fibrous crystals can attain a markedly curved shape without a corresponding curvature in the crystallographic orientation (Urai et al., 1991). Veins are called syntaxial when the crystals grow inwards from the vein wall.

2) If the opening rate exceeds the sealing rate, crystals grow into an open fluid filled cavity. In this case, the crystals may form crystal facets (e.g. Fisher and Bryne, 1990; Fisher and Brantley, 1992; Fisher et al., 1995; Ague, 1994; Ague, 1995; Hilgers et al., 2003). The growth of crystals is inhibited by growth competition between adjacent grains (Hilgers and Urai, 2002; Hilgers et al., 2003). This leads to a selection of those grains, for which the fastest growth direction is oriented normal to the vein wall (Fisher and Brantley, 1992; Hilgers and Urai, 2002; Hilgers et al., 2003). For quartz, this is the direction parallel to the c-axis (Iler, 1979; Fisher and Brantley, 1992). As a consequence of growth competition the number of grains per area is reduced and the grain size increases towards the centre of the vein. Also, a marked preferred orientation of the c-axes at a high angle to the vein walls develops (Fisher and Brantley, 1992; Fisher et al., 1995; Hilgers and Urai, 2002; Nollet et al., 2005). Open vugs bound by euhedral crystals represent remnants of the open cavity (Augue, 1995). Crystallization in such veins is always syntaxial.

The microfabrics of the lens-shaped veins of southern Evia show no discontinuities indicative of a multi-stage or cyclic processes of opening and sealing. Instead, the coarse-grained microfabric with elongate or blocky crystals suggests crystallization from a fluid phase in a wide open cavity (Yardley, 1984). This is indicated (1) by the inward increasing grain size and increasing sharpness of a c-axis preferred orientation at a high angle to the vein wall (Figs. 5-7 b, e), (2) by an SPO with the orientation of the larges diameter of the grains parallel to their c-axes (Figs. 5-7 b, c), and (3) by residual open vugs bound by crystal faces of large quartz grains at the vein centre (Figs. 9d, 10c) (e.g. Ague, 1995).

An apparent deviation from this simple pattern is observed at the margins of vein EN 38 (Fig. 6). There, the curved grains with a high aspect ratio suggest on the first glance that the microstructure may be the result of cyclic crack-seal vein growth (e.g. Oliver and Bons, 2001). However, some characteristic features indicate that the microfabric at the margins of vein EN 38 did also originate by crystallization in a fluid filled cavity. These features are: First, a marked inward increase in grain size accompanied by the inward development of a c-axis preferred orientation (Fig. 6), with the c-axes parallel to the long axes of the grains (Fig. 6b, c), indicates growth competition. Second, the inclusion trails which are characteristic for the crack-seal mechanism (Durney and Ramsay, 1973; Ramsay, 1980) are systematically absent. Third, the curved shape of the grains is accompanied by a corresponding curvature in the crystallographic orientation (Fig. 6b, c). Finally, the long axes of the grains on both vein walls are inclined in opposite directions (Fig. 6a, c). This geometry and the curvature in the crystallographic orientation are not

consistent with an origin by displacement-controlled fibrous crystallization (e.g. Urai, 1991). Instead, the curvature of the crystals may result from crystal plastic deformation, though the process that lead to this pattern is not evident. The coarse anisometric grains close to the vein centre show the same SPO as the grains close to the margins (Fig. 6), but their features indicative of crystal plastic deformation appear much less pronounced (Figs 10b, c, 12). This means that the deformation of the elongate grains at the vein margins must have taken place prior to the growth of the grains at the vein centre.

Based on these observations, the sealing quartz of the three veins investigated in detail (and of all other inspected veins) crystallized syntaxially from the vein walls towards the centre, with some grains becoming selected due to impingment. This process is commonly referred to as growth competition and is indicative for sealing of a wide open cavity (e.g. Fisher and Brantley, 1992; Fisher et al., 1995; Hilgers and Urai, 2002). Sealing took place in a single stage, with early grown crystals situated at the vein margins, and lately grown crystals at the vein centre.

3.6.3. Gradients in crystal plastic deformation indicated by optical microstructure and GMP – position plots

Undulatory extinction of a crystal observed in the polarizing microscope results from the presence of geometrically necessary dislocations (Nicolas and Poirier, 1976). Geometrically necessary dislocations are introduced during inhomogeneous crystal plastic deformation. Their re-arrangement into low-angle grain boundaries indicates syn- or post-kinematic recovery. The size of the subgrains and the misorientation at the subgrain boundaries depends on the density of geometrically necessary dislocations (e.g. Nicolas and Poirier, 1976).

Recrystallization is commonly characterized as either rotation or migration recrystallization (Guillopé and Poirier, 1979; Poirier, 1985). Rotation recrystallization implies the progressive transformation of low-angle grain boundaries into high angle grain boundaries. The increase in misorientation is achieved by progressive incorporation of further geometrically necessary dislocations in the grain boundary (Guillopé and Poirier, 1979). On the optical scale, an indication of migration recrystallization are sutured high angle grain boundaries. Migration recrystallization is also referred to as strain induced grain boundary migration. Depending on whether recrystallization takes place during or after deformation it is referred to as dynamic or static, respectively (Nicolas and Poirier, 1976; Gottstein and Mecking, 1985).

The three selected veins show gradients in the quartz microfabrics related to deformation (Figs. 9, 10, 12), on the optical as well as on the SEM scale. The quartz microstructure of the veins EN 4 and EN 45 reveals abundant small recrystallized grains at the vein margin, and large grains with slight undulatory extinction close to the vein centre (Figs. 8, 9, 10d, e). In vein EN 38, the vein quartz shows strong undulatory extinction and abundant small subgrains at the vein margins (Fig. 10a), as well as large grains with slight undulatory extinction near the

vein centre (Figs. 6a, 10c). These microstructural gradients are interpreted to reflect a decreasing concentration of geometrically necessary dislocations introduced during inhomogeneous crystal plastic deformation, from the vein margins towards the vein centre, i.e. from early grown to lately grown crystals.

The plots of GMP versus position within the veins show a non-linear decrease in the slope of the gradients. This reflects an inward decrease in the concentration of geometrically necessary dislocations, correlated with a decrease in the degree of inhomogeneous crystal plastic deformation (Fig. 12). The GMP gradients are in accordance with the differences in the microstructure observed in the polarizing microscope.

For syntaxial veins sealed by crystallization into a fluid filled cavity, the displacement rate between the fracture walls must have exceeded the sealing rate (Hilgers and Urai, 2002). Two scenarios are possible: (1) Vein sealing commences after instantaneous opening of the cavity, with an aperture corresponding to the width of the final vein. In this case, the crystals grow into a stationary cavity. Distortion of the host rock can be purely elastic. Any crystal plastic deformation of the vein quartz postdates the stage of sealing. (2) Sealing is concomitant with slow opening of the cavity accompanied by crack parallel shortening, controlled by viscous deformation of the host rock.

In the second case, single stage syntaxial vein sealing is expected to be a short episode compared to geological timescales. As a first approximation, the sealing process and the concomitant deformation can be considered to be isothermal. The finite strain accumulated during a stage of deformation in a given rheological regime is then controlled by the temperature and the stress history.

In the first scenario, the deformation postdates the sealing stage. All crystals in the vein sealing experience the same stress history at the same temperature. For such a scenario, gradients in the intensity of crystal plastic deformation would require stress concentration due to an inhomogeneous distribution of other minerals, or systematic differences in the in the crystallographic orientation yielding a variable Schmid factor (Nicolas and Poirier, 1976), depending on the position within the vein.

First, in vein EN 45, minor occurrence of zoisite and albite at the vein margin may have acted as a stress concentrator. Comparison with vein EN 4, a pure quartz vein, does not show any contrast in the deformation related microfabrics. Also, the GMP decreases systematically towards the vein centre beyond the zone with a subordinate occurrence of other minerals. This rules out an effect of second phase crystals acting as stress concentrators. Second, there is a marked CPO of quartz in all veins, with the c-axis oriented perpendicular to the vein wall. This rules out an effect related to crystallographic orientation. Therefore, the systematic decrease in GMP from the vein margins towards the vein centre and the associated changes in the microstructure cannot result from a later stage of deformation affecting the completely sealed vein.

In the second scenario, the gradients in the intensity of crystal plastic deformation are interpreted to result from progressive growth of quartz crystals into a cavity widening by slow viscous creep, while the host rock is getting shortened parallel to the crack. In this scenario, the crystals get deformed immediately after their crystallization and the early grown grains have a longer deformation history compared to the lately grown grains. The time span of deformation, t_d, and hence the accumulated finite strain are reflected by the differing microstructures and in particular the gradient in the concentration of geometrically necessary dislocations. The difference in t_d between two crystals located at the positions x_1 and x_2 along the profiles and crystallized at the time t_1 and t_2, respectively, equals the time interval $\Delta t_d = t_2 - t_1$. The gradients in the intensity of crystal plastic deformation reflect the decrease in t_d with increasing distance to the vein walls. Furthermore, progressive widening of the cavity is attributed to creep of the host rock during postseismic stress relaxation (Nüchter and Stöckhert, submitted). According to this model, the crystals grown early at the vein margins must have been subject to higher differential stress and been deformed at higher strain rate compared to those in the centre of the vein, which have grown at a stage when deformation had come to a rest and coseismically imposed stress were relaxed. The high stresses and strain rates at the initial stage of crack opening by postseismic creep are recorded at the vein margins, and the inward decrease in the intensity of crystal plastic deformation reflects the history of stress relaxation.

3.7. Conclusions

Systematic gradients in the microstructural record of quartz in monogenetic veins indicate that the vein quartz crystallized during progressive widening of the cavity and shortening parallel to the crack. The deformation was controlled by creep of the host rock. Within the host rock, the record of this deformation cannot be isolated due to the complex microstructure and the very low finite strain. The formation of the cracks is attributed to coseismic loading, the deformation, opening and sealing to postseismic creep at decreasing stress. The early grown crystals at the vein margins record a longer history of deformation and the higher intial stresses compared to crystals grown lately at the vein centre, when stresses were relaxed and deformation had come to rest. The results corroborate the conclusion drawn from linear elasticity and fracture mechanics considerations that the aperture of the lens shaped veins cannot result from purely elastic distortion of the host rock.

References

Ague, J.J. (1994): Mass transfer during Barrovian metamorphism of pelites, south-central Connecticut, II, channelized fluid flow and the growth of staurolithe and kyanite.- Am. J. Sci., 294: 1061-1134.

Ague, J.J. (1995): Deep crustal growth of quartz, kyanite and garnet into large-aperture, fluid filled fractures, north-eastern Connecticut, USA.- J. metamorphic Geol., 13: 299-314.

Anderson, T.L. (1995): Fracture mechanics - fundamentals and application, second edition.- CRC Press.

Atkinson, B.K., Meredith, P.G. (1987): Experimental fracture mechanics data.- In: Atkinson, B.K. [ed.]: Fracture mechanics of rock (pp. 477-525). Academic Press Limited.

Brix, M.R., Stöckhert, B., Seidel, E., Theye, T., Thomson, S.N., Küster, M. (2002): Thermobarometric data from a fossil zircon partial annealing zone in high pressure-low temperature rocks of eastern and central Crete, Greece.- Tectonophysics, 349: 309-326.

Cox, S.F., Etheridge, M.A. (1983): Crack-seal fibre growth mechanisms and their significance in the development of oriented layer silicate microstructures.- Tectonophysics, 92:147-170.

DeGraff, J.M., Aydin, A. (1993): Effect of thermal regime on growth increment and spacing of contraction joints in basaltic lava.- J. Geophys. Res., 98: 6411-6430.

Delaney, P.T., Pollard, D.D. (1981): Deformation of host rocks and flow of magma during growth of minette dikes and breccia-bearing intrusions near Ship Rock, New Mexico.- U.S. Geol. Sur. Prof. Pap., 1202: 1-61.

Dunlap, W.J., Hirth, G., Teyssies, C. (1997): Thermomechanical evolution of a ductile duplex.- Tectonics, 16: 983-1000.

Durney, D.W., Ramsay, J.G. (1973): Incremental strains measured by syntectonic crystal growth. In De Jong, K.A., Scholten R. [Eds.], Gravity and Tectonics. (pp. 67-96). New York: John Wiley.

Faure, M., Bonneau, M., Pons, J. (1991): Ductile deformation and syntectonic granite emplacement during the late Miocene extension of the Aegea (Greece).- Neues Jahrb. Mineral. Monatsh., 4: 145-162.

Fisher, D.M., Bryne, T. (1990): The character and distribution of mineralized fractures in the Kodiak Formation, Alaska: Implications for the fluid flow in an underthrust sequence.- J. Geophys. Res., 95(B6): 9069-9080.

Fisher, D.M., Brantley, S.L. (1992): Models for quartz overgrowth and vein formation: Deformation and episodic fluid flow in an ancient subduction zone.- J. Geophys. Res., 97(B13): 20043-20061.

Fisher, D. M., Brantley, S. L., Everett, M., Dzvonik, J. (1995): Cyclic fluid flow through a regionally extensive fracture network within the Kodiak accretionary prism. J. Geophys. Res., 100(B7): 12881-12894.

Gautier, P., Brun, J.-P. (1994): Crustal-scale geometry and kinematics of late-orogenic extension in the central Aegean (Cyclades and Evvia Island).- Tectonophysics, 238: 399-424.

Gottstein, G., Mecking, H. (1985): Rerystallization.- In: Wenk, H.R. [ed.]: Preferred orientation in deformed metals and rocks; an introduction to modern texture analysis (183-218 pp.).- Acad. Press: Orlando, Fl, United States.

Guillope, M., Poirier, J.P. (1979): Dynamic recrystallization during creep of single-crystalline halite; an experimental study.- J. Geophys. Res., 84(10): 5557-5567.

Hilgers, C., Dilg-Gruschinski, K., Urai, J. (2003): Microstructures grown experimentally from advective supersaturated solution and their implication for natural vein systems.- Journal of geochemical Exploration, 78: 221-225.

Hilgers, C., Urai, J. (2002): Experimental study of syntaxial vein growth during lateral fluid flow in transmitted light: first results.- J. Struct. Geol, 24: 1029-1043.

Hirth, G., Teyssier, C., Dunlap, W.J. (2001): An evaluation of quartzite flow laws based on comparisons between experimentally and naturally deformed rocks.- Int. J. Earth. Sci., 90(1), 77-87.

Hirth, G., Tullis, J. (1992): Dislocation creep regime in quartz aggregates.- J. Struct. Geol., 14(2): 145-159.

Hobbs, B.E. (1985): The geological significance of microfabric analysis.- In: Wenk, H.R. [ed.]: Preferred orientation in deformed metals and rocks; an introduction to modern texture analysis (463-479 pp.).- Acad. Press: Orlando, Fl, United States.

Iler, R. (1979): The chemistry of silica.- Wiley-Interscience, New York.

Irwin, G.R. (1948): Fracture dynamics.- Fracturing of metals, American society for metals, Cleveland: 147-166.

Irwin, G.R. (1956): Onset of fast crack propagation in high strength steel and aluminium alloys.- Sagamore research conference proceedings, 2: 289-305.

Irwin, G.R. (1957): Analysis of stresses and strains near the end of a crack traversing a plate.- J. Appl. Mech., 24: 361-364.

Irwin, G.R. (1961): Plastic zone near a crack and fracture toughness.- Sagamore research conference proceedings, 4.

Jolivet, L., Faccenna, C. (2000): Mediterranean extension and the Africa-Eurasia collision.- Tectonics, 19: 1095-1106.

Klein-Helmkamp, U. (1996): Metamorphose und Exhumierung der niedrigtemperierten Hochdruckmetamorphite der Styra-Ochi-Einheit in Süd-Euböa, Attisch-Kykladisches Kristallin, Griechenland.- Ruhr University Bochum, Germany.

Le Pichon, X., Angelier, J. (1981): The Aegean Sea.- Philos. Trans. R. Soc. Lond., Ser. A, 300: 357-372.

Lister, G.S., Banga, G., Feenstra, A. (1984): Metamorphic core complexes of Cordilleran type in the Cyclades, Aegean Sea, Greece.- Geology, 12: 221-225.

Meulenkamp, J.E., Wortel, M.J.R., Van Wamel, W.A., Spakman, W., Hoogerduyn Strating, E. (1988): On the Hellenic subduction zone and the geodynamic evolution of Crete since the late Middle Eocene.- Tectonophysics, 146: 203-215.

Nicolas, A., Poirier, J.P. (1976): Crystalline Plasticity and Solid State Flow in Metamorphic Rocks.- Wiley-Interscience, (444 pp).

Nollet, S., Urai, J., Bons, P. D., Hilgers, C. (2005): Numerical simulations of polycrystal growth in veins.- J. Struct. Geol., *27*: 217-230.

Nüchter, J-A., Stöckhert, B. (submitted): Fracturing and single-event vein formation in the middle crust – the record of coseismic loading and postseismic creep.- J. Geophys. Res.

Oliver, N.H.S., Bons, P.D. (2001): Mechanisms of fluid flow and fluid–rock interaction in fossil metamorphic hydrothermal systems inferred from vein–wallrock patterns, geometry and microstructure.- Geofluids, 1: 137-162.

Olson, J.E. (2003): Sublinear scaling of fracture aperture versus length: An exception or the rule?- J. Geophys. Res., 108(B9).

Poirier J.-P. (1985): Creep of crystals – High temperature deformation processes in metals, ceramics and minerals.- Cambridge University press.

Pollard, D.D., Segall, P. (1987): Theoretical displacements and stresses near fractures in rock: With applications to faults, joints, veins, dikes and solution surfaces.- In: Atkinson, B.K. [ed.]: Fracture mechanics of rock (pp. 277-350), Academic Press Limited.

Ramsay, J.G. (1980): The crack-seal mechanism of rock deformation. Nature, 284: 135-39.

Ramsay, J.G., Huber, M.I. (1983): The techniques of modern structural geology, Volume 1: Strain analysis.- Academic Press. London.

Rice, J.R., Cleary, M.P. (1976). Some basic stress diffusion solutions for fluid-saturated elastic porous media with compressible constituents.- Rev. Geoph. Space Phys, 14(2): 227-241.

Sneddon, I.N., Elliott, H.A. (1946): The opening of a griffith crack under internal pressure.- Q. Appl. Math., 4: 262-267.

Stöckhert, B., Brix, M.R., Kleinschrodt, R., Hurford, A.J., Wirth, R. (1999): Thermochronometry and microstructures of quartz; a comparison with experimental flow laws and predictions on the temperature of the brittle-plastic transition.- J. Struct. Geol, 21: 351-369.

Trucotte, P.L. and Schubert, G. (2002): Geodynamics.- Cambridge University Press (456 pp.).

Urai, J., Williams, P.F., Roermund, v. H.L.M. (1991): Kinematics of crystal growth in syntectonic fibrous veins.- J. Struct. Geol., 13(7): 823-836.

Vermilye, J.M., Scholz, C.H. (1994): Relations between vein length and aperture.- J. Struct. Geol., *238*: 423-434.

Voll, G. (1976): Recrystallization of quartz, biotite and feldspars from Erstfeld to the Leventina Nappe, Swiss Alps, and ist geological significance.- Schweizerische Miner. Petrog., 56: 541-647.

Yardley, B. (1984): Fluid migration and veining in the Connemara Schists, Ireland.- In: Walther, J.V., Wood, B.J. [eds.]: Fluid-rock interactions during metamorphism (pp. 109-131), Springer-Verlag, New York.

4. Pore fluid pressure in the earthquake cycle – the record of fluid inclusions

Abstract

The fluid inclusions of vein quartz in monogenetic discordant veins of the HP / LT – metamorphic Styra-Ochi Unit of southern Evia are analyzed. The parental cracks formed in the middle crust at temperatures similar to 300°C in response to coseismic loading to high stress; they were opened and sealed during subsequent time-dependent deformation of the host rock. Syntaxial growth of the quartz crystals implies early grown crystals to be situated at the vein margins, and lately grown crystals in the centre. The primary fluid inclusions as a function of position therefore record the history of the pore fluid during progressive opening and sealing. The composition of the inclusions is uniform: An aqueous solution of low salinity. In contrast, the density of the inclusions is a function of position. It increases from the rim towards the centre. For a short-term and nearly isothermal process, the change in density reflects a change in pore fluid pressure. It is markedly sublithostatic at an early stage of sealing, and quasi-lithostatic in the final stage. A linear elastic fracture mechanics approach suggests that the fluid pressure in the open fissures approximately equals the least principal stress, $P_{fluid} \approx \sigma_3$. For a given depth and lithostatic load, $\sigma_1 = \sigma_v$, in an extensional tectonic regime, the change in pore fluid pressure can then be translated into a change in differential stress. The fluid inclusion record therefore reflects the history of pore fluid pressure and differential stress for the stage of opening and sealing of the crack in the middle crust, attributed to the earthquake cycle. High differential stress and markedly sub-lithostatic fluid pressure are attained at coseismic loading. Afterwards, the differential stress decreases and the pore fluid pressure increases during a stage of thermally activated postseismic creep. Each monogenetic discordant vein records a single stress and fluid pressure cycle at a depth level just below the crustal scale brittle ductile transition, related to a major earthquake.

4.1. Introduction

Major earthquakes generally nucleate at the base of the schizosphere, where rock strength is maximum (Scholz, 1990; Kohlstedt et al., 1995) and cause a stress redistribution in the crust surrounding the fault plane (e.g. Sibson, 1980; Tse and Rice, 1986; Scholz, 1990; Wald and Heaton, 1994; Bouchon, 1997; Bouchon et al. 1998; Küster and Stöckhert, 1999; Trepmann and Stöckhert, 2001, 2002, 2003; Ellis and Stöckhert, 2004a, 2004b; Ellis et al. 2006). While the stress in the surrounding crust is reduced in consequence to seismic slip, very high differential stress may built up locally at and below the termination of the fault in the uppermost part of the plastosphere (Scholz, 1990). Numerical models show how the crust near the tip of a fault is rapidly loaded to high stress (Ellis and Stöckhert, 2004a; Ellis and Stöckhert, 2004b; Ellis et al. 2006), and that this loading causes a downward deflection of the brittle ductile transition in consequence to the high imposed strain rate (e.g. Sibson, 1980; Scholz, 1990; Küster and Stöckhert 1999; Ellis and Stöckhert 2004a; Rolandone et al. 2004). The uppermost horizon of the plastosphere (Scholz, 1990) beneath the fault tip, capable of viscous flow on the long term, will undergo brittle failure in consequence to coseismic loading (Sibson, 1980; Baisch and Bokelmann, 2001; Miller et al., 2004). During postseismic stress relaxation, the brittle ductile transition recovers to its long term depth level (e.g. Scholz, 1990; Küster and Stöckhert, 1999; Trepmann and Stöckhert, 2001, 2002, 2003; Ellis and Stöckhert, 2004a; Rolandone et al.,

2004). Indirect evidence for coseismic loading and related brittle damage in the middle crust, followed by slow deformation during postseismic stress relaxation is derived from a variety of sources, including geodesy, seismology, and structural geology. Here are some examples:

- Transient postseismic surface displacement patterns, observed by modern geodetic techniques, are interpreted to reflect viscous deformation in the half space below the brittle ductile transition (e.g. Rice and Gu, 1983; Ivins, 1996; Bosl and Nur, 2002; Freed and Bürgmann, 2004; Freed et al., 2006).
- Baisch and Bokelmann (2001) observed an increase in the scatter of seismic waves in consequence to the 1989 M 6.9 Loma Prieta main shock, followed by gradual recovery within a few years. The authors propose that the scatter of seismic waves is caused by coseismically opened cracks, which heal or seal during the stage of postseismic stress relaxation.
- In consequence to the 1992 M 7.3 Landers earthquake, an almost instantaneous coseismic downward shift of the vertical distribution of hypocentres is followed by recovery to the long term depth distribution within a period on the order of 10^1 years (Rolandone et al., 2004).
- Miller et al. (2004) described a series of aftershocks following two M 5.7 mainshocks, triggered by CO_2 degassing from a ruptured high pressure reservoir at depth. The decay of aftershock activity occurred on a timescale of about 10^3 days and is interpreted to reflect sealing of the CO_2 reservoir.
- Episodic mineral precipitation on fault planes is interpreted to reflect coseismic rupture of supra-hydrostatic fluid reservoirs at depth, followed by subsequent sealing and restoration of the long term fluid pressure (e.g. Sibson, 1981).

Direct evidence for coseismic loading to high stress and postseismic stress relaxation by viscous creep is reported from the structural and microstructural record of exhumed metamorphic rocks, albeit for a fossil, inactive system with the once overlying fault being removed by erosion (Küster and Stöckhert, 1999; Trepmann and Stöckhert, 2001, 2002, 2003; Nüchter and Stöckhert, submitted).

Due to the low permeability of metamorphic rocks, the fluid pressure below the brittle ductile transition transition (BDT) is generally presumed to be close to the mean stress with $P_f \approx (\sigma_1 + \sigma_2 + \sigma_3) / 3$. For a low differential stress, it can be taken as approximately lithostatic (Brace, 1980, 1984; Etheridge et al., 1983; Nur and Walder, 1990; Oliver, 1996; Manning and Ingebritsen, 1999). A near-lithostatic pore fluid pressure is not compatible with a high differential stress due to the limited rock strength (Secor, 1965; Secor and Pollard, 1975; Sibson, 1981; Etheridge et al., 1983; Kohlstedt et al., 1995). Therefore, P_f has to drop to markedly sublithostatic values during coseismic loading to high stress (Mullis, 1975, 1976; Küster and Stöckhert, 1999; Nüchter and Stöckhert, submitted). Fluid inclusion evidence for a low pore fluid pressure during ductile deformation at high differential stress has been reported from the Sesia Zone in the Italian Western Alps (Küster and Stöckhert, 1999). Moreover, fluid inclusions

trapped in the quartz sealing veins in the Val d´Illez in the Swiss Alps show a cyclic drop and recovery of the pore fluid pressure during the sealing stage, attributed to earthquakes (Mullis, 1975, 1976). Trepmann and Stöckhert (2002) derived indirect evidence for the recovery of a near-lithostatic pore fluid pressure during a stage of postseismic deformation and stress relaxation from the microstructural record of coseismically shattered garnet crystals in rocks of the Sesia Zone.

In the present study, the density of fluid inclusions as a function of position in monogenetic syntaxial quartz veins formed from earthquake related fractures in the middle crust (Nüchter and Stöckhert, submitted) is used to derive the history of pore fluid pressure during progressive sealing. It is then shown that, based on principles of fracture mechanics, the fluid pressure in an open cavity represents a gauge to measure the magnitude of the remote stress. The history of pore fluid pressure, derived from the fluid inclusion densities as a function of position in the sealed vein, can therefore be translated into a stress history.

The objective of the present study is to gain insight into the history of pore fluid pressure and differential stress in a horizon just beneath the crustal scale brittle ductile transition in consequence to seismic activity in the overlying schizosphere (Scholz, 1990), with switches between brittle failure and viscous creep depending on the imposed strain rate.

4.2. Geological setting

The Styra-Ochi Unit in southern Evia Island, Greece, is part of the high pressure / low temperature (HP / LT) metamorphic internal Cyclades belt, situated in the backarc region of the active Hellenic subduction zone. The structure of the Cyclades is governed by extensional tectonics and crustal thinning since the Early Miocene (Le Pichon and Angelier, 1981; Jolivet and Faccenna, 2000), driven by continuing roll back of the Hellenic subduction zone (Meulenkamp et al. 1988). The extension is localized in a single major (e.g. Lister et al., 1984; Faure et al., 1991) or several (e.g. Gautier and Brun, 1994) detachment faults. For the major part, the hanging wall block is eroded on the Cyclades (e.g. Gautier and Brun, 1994). The Styra-Ochi Unit in South Evia is composed of a variety of siliciclastic and carbonate-rich marine sediments, with metamorphosed basaltic to rhyolitic volcanic and intrusive rocks. During its earlier history, the Styra-Ochi Unit underwent pervasive deformation and HP-LT metamorphic overprint at about 400°C and 1 GPa (Klein-Helmkamp, 1996), indicating maximum burial to a depth of about 30 to 35 km. It was exhumed as a coherent unit, interpreted to represent the footwall block of a metamorphic core complex. The structures developed during that stage reflect a continuous evolution from ductile to brittle extensional deformation within a uniform kinematic framework (Gautier and Brun, 1994; Klein-Helmkamp, 1996). The veins investigated in the present study formed during exhumation and postdate HP-LT metamorphism.

4.3. Methods

The density of fluid inclusions trapped in the vein quartz is determined by microthermometric analysis as a function of the distance to the vein walls. The results are compared to the microstructural record of the vein quartz. Oriented samples were taken along profiles normal to the vein walls of two representative veins (EN 38: Fig. 1a; EN 45: Fig. 1b). The samples were cut normal to the host rock foliation and normal to the vein wall. The microstructures were examined in thin section (30 µm thick) with a polarizing microscope. The scanning electron microscope-based technique of electron backscatter diffraction (EBSD) yields microstructural information with a resolution on the µm scale and provides information on the spatial distribution of the full crystallographic orientation. Thin sections used for the EBSD technique were chemically polished using a silica suspension (SYTON®) to minimise surface damage, then coated with carbon to limit charging effects. EBSD-investigations were carried out using a SEM (LEO 1530) equipped with a field emission gun and a forescatter detector. For EBSD analysis, the SEM was operated at an accelerating voltage of 20 kV and a working distance of 25 mm, with the thin section tilted at an angle of 70° with respect to the beam.

For fluid inclusion analysis, polished thick sections (250 – 300 µm thickness), were prepared and cover the entire profile length. Microthermometry was performed on small fragments of the thick sections, using a Linkham 600 heating / cooling stage. To exclude an effect of additional volatile components on the density derived by microthermometry, a representative number of sample fragments was analysed by Quadrupol Mass Spectrometry (QMS) (Röller et al., 2001).

4.4. Discordant monogenetic quartz veins with low aspect ratio

Veins originate as fractures. As such, the stage of brittle failure and crack propagation is to be set apart from the stage of opening and sealing, i.e. vein formation. Information on the length of the original fracture, its orientation and shape, and its relation to pre-existing structures is readily obtained from the geometry of the vein walls, with the filling material virtually removed. The processes of opening of the fracture and sealing with material crystallizing from the pore fluid (e.g. Yardley, 1984) are recorded by the shape of the vein and the microstructures of the sealing minerals.

The veins of interest crosscut the foliation and all former syn-metamorphic structures and fabrics, including schistosity (Fig. 1, 3), shearband foliation, and pre-existing earlier veins parallel to the foliation (Fig. 1a). Some veins branch symmetrically at an aperture angle of about 30° (Fig. 2). The branches are straight and are not influenced by pre-existing structures of the host rock. The geometry suggests tensile failure (mode I) and opening normal to the least principal stress, σ_3. The orientation of the vein walls, hence of the original fractures, is more or less uniform all over the Styra-Ochi Unit in southern Evia, an area of more than 500 km^2. They trend about NW to NNW and are nearly vertical (Fig. 3). The orientation is consistent with a

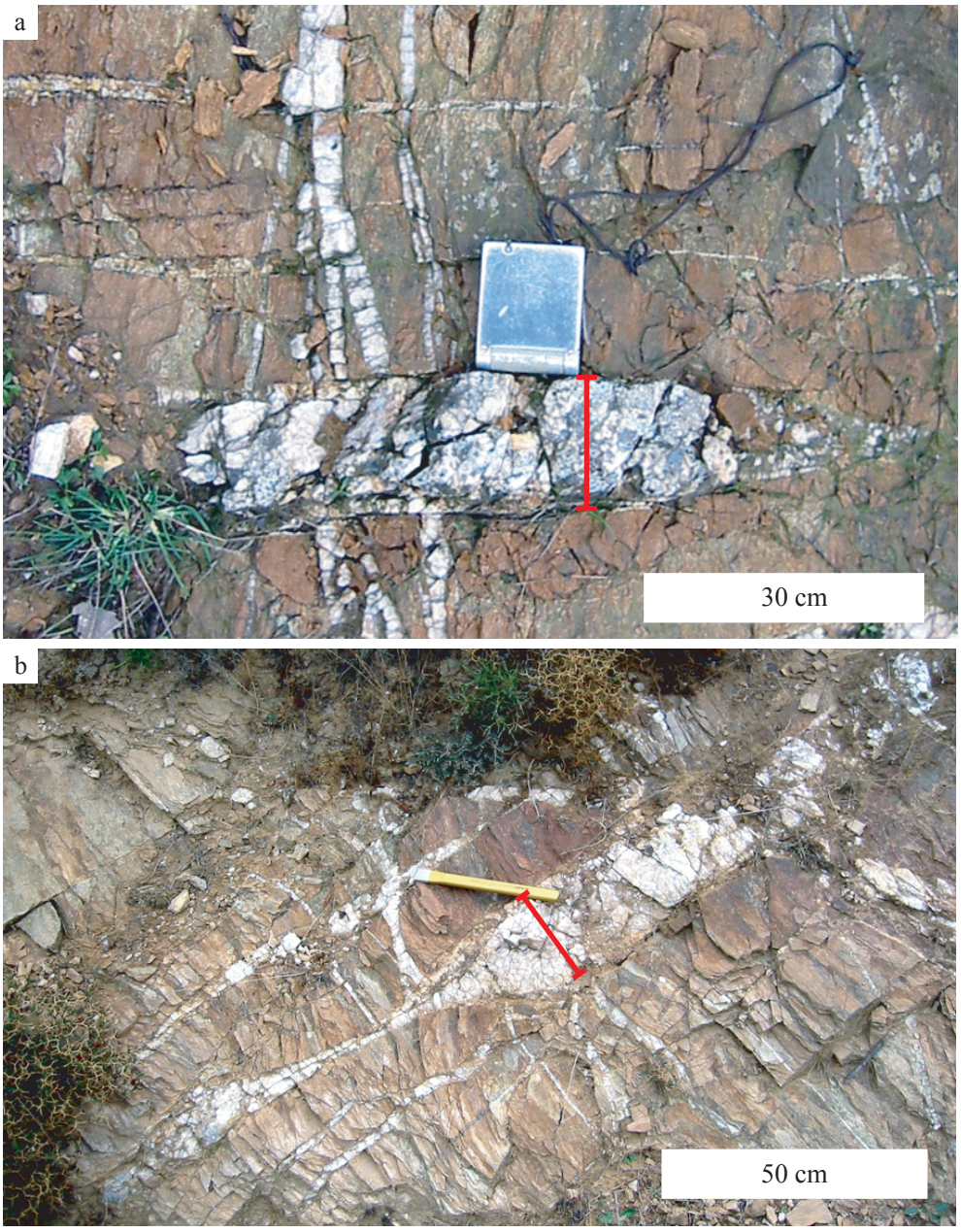

Fig. 1: Discordant quartz veins in the Styra-Ochi Unit selected for analysis. The red bars show the sampled profile lines. a) The lens-shaped vein EN 38 with a low aspect ratio of about 12 crosscuts pre-existing concordant veins. b) The irregularly shaped vein EN 45 shows swelling and pinching.

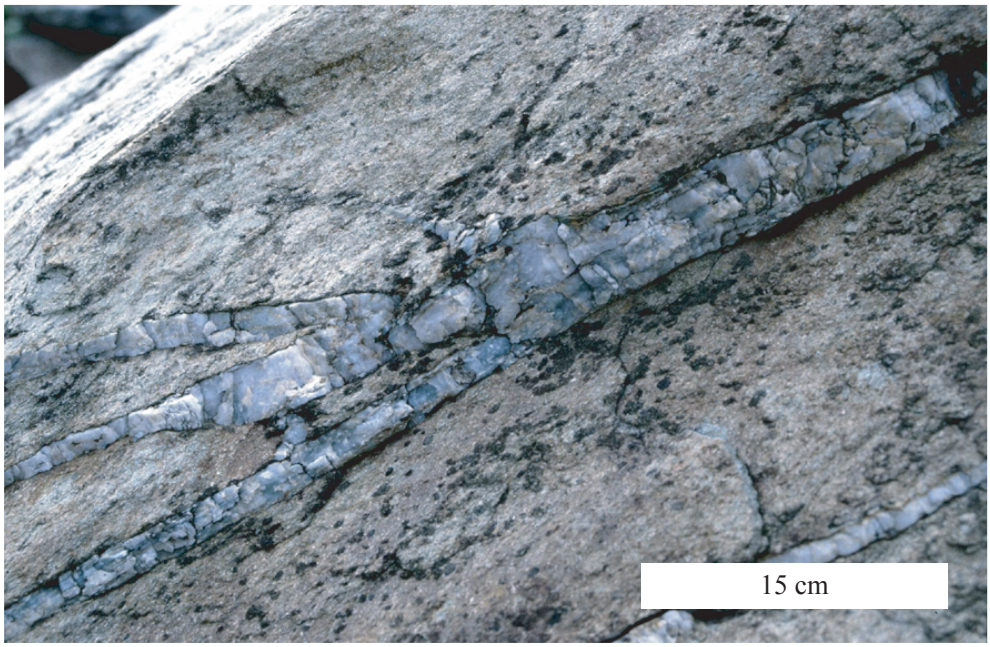

Fig 2: Symmetrically branching vein with the characteristic aperture angle of about 30°.

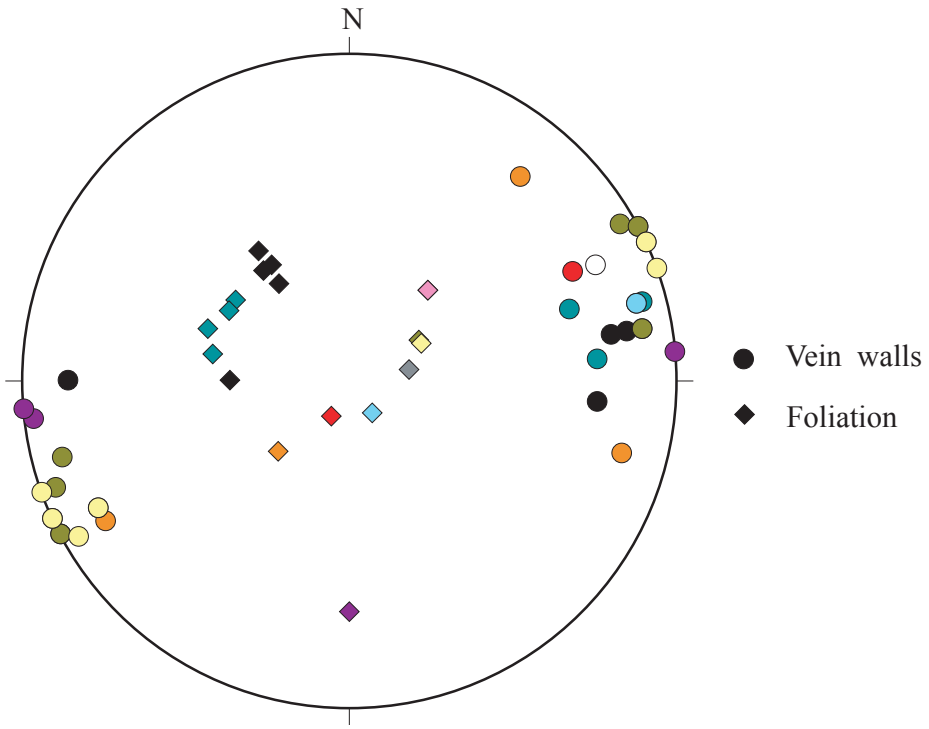

Fig. 3: Stereographic plot (lower hemisphere) of poles to the foliation and to the vein walls at different locations in the Styra-Ochi Unit of southern Evia (Greece). The data set covers an area of more than 500 km^2.

stress field characterized by $\sigma_1 = \sigma_v$ and σ_3 at about NE to ENE at the stages of fracturing and vein formation (Fig. 3). The length of most veins ranges between 10^{-1} m and 10^{1} m, which is taken to reflect the characteristic length scale of the fractures. Most veins show a symmetric lense shape with a low aspect ratio between 10 and 30 (Fig. 1a). Some veins are more irregular in shape, showing swelling and pinching (Fig. 1b). Based on linear elastic fracture mechanics (LEFM) considerations (Nüchter and Stöckhert, submitted), significant non-elastic and time-dependent deformation of the host rock must have contributed to the opening of the low aspect ratio veins.

4.5. Microfabrics

4.5.1. Primary quartz microfabrics related to sealing

Both veins are predominantly sealed by quartz, in places associated with additional minor albite and zoisite (Figs. 4a, 5a). At the vein margins, quartz tends to form elongate crystals with a shape and crystallographic preferred orientation of the c-axis about normal to the vein wall (Figs. 4, 5 b, c). Close to the vein walls, the c-axis orientation distribution of the vein sealing quartz is diffuse with multiple weak maxima (Figs. 4b, 5b). With increasing distance to the vein walls, the number of these maxima diminishes and the crystallographic preferred orientation (CPO) with a c-axis maximum about normal to the vein walls becomes more and more pronounced (Figs. 4b, 5b). With increasing distance to the vein walls, the grain size increases gradually (Figs. 4d, 5d) and reaches up to several centimetres in in the centre of the vein (Figs. 4a, 6a). Residual open vugs with crystallographically controlled faces are common. In contrast, inclusion trails parallel to the vein walls (Durney and Ramsay, 1973; Ramsay, 1980) are systematically absent. The grain size at the wall of vein EN 38 is larger compared to that in vein EN 45, and the inward increase in grain size is less pronounced (Figs. 4, 5).

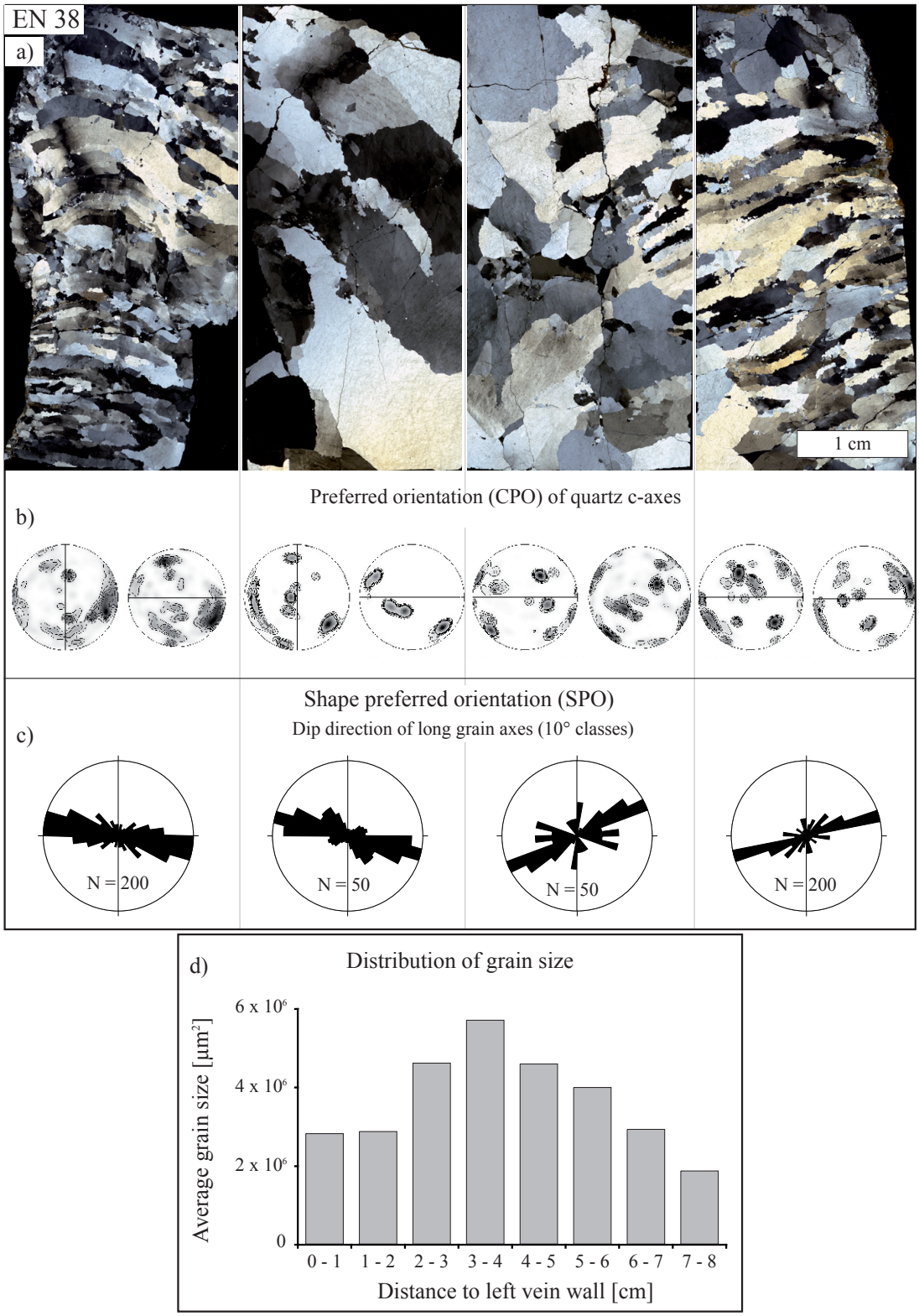

Fig. 4: Quartz microfabrics of vein EN 38, grain shape and orientation data acquired by EBSD: a) Optical microstructure (thin sections scanned with crossed polarizers). b) Development of a more pronounced quartz c-axes preferred orientation with increasing distance to the vein walls. c) Shape preferred orientation of the quartz crystals. d) Increase in quartz grain size with increasing distance to the vein walls.

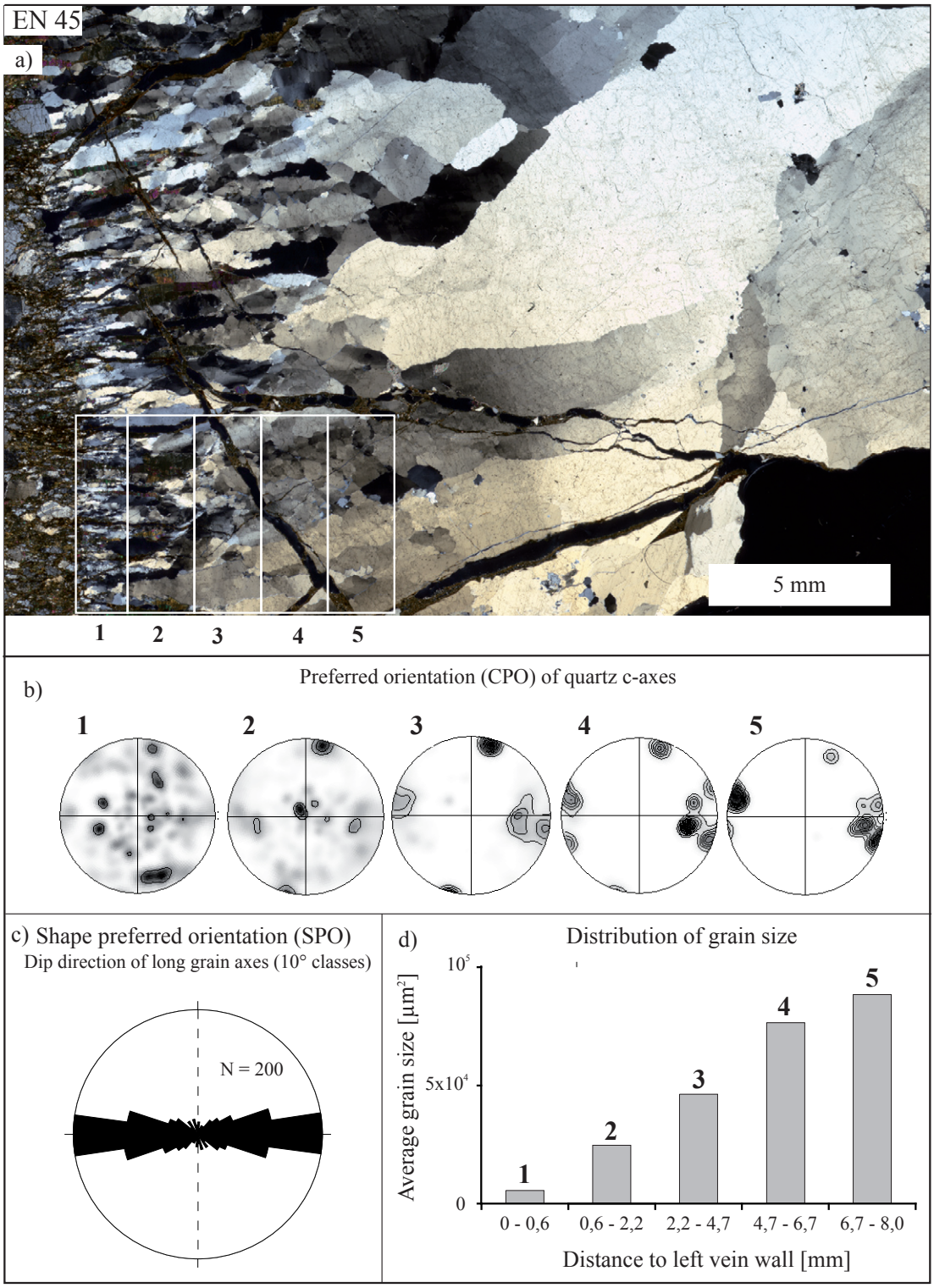

Figs. 5: Quartz microfabrics of vein EN 45, grain shape and orientation data acquired by EBSD: a) Optical microstructure (thin sections scanned with crossed polarizers). b) Development of a more pronounced quartz c-axes preferred orientation with increasing distance to the vein walls. c) Shape preferred orientation of the quartz crystals. d) Increase in quartz grain size with increasing distance to the vein walls.

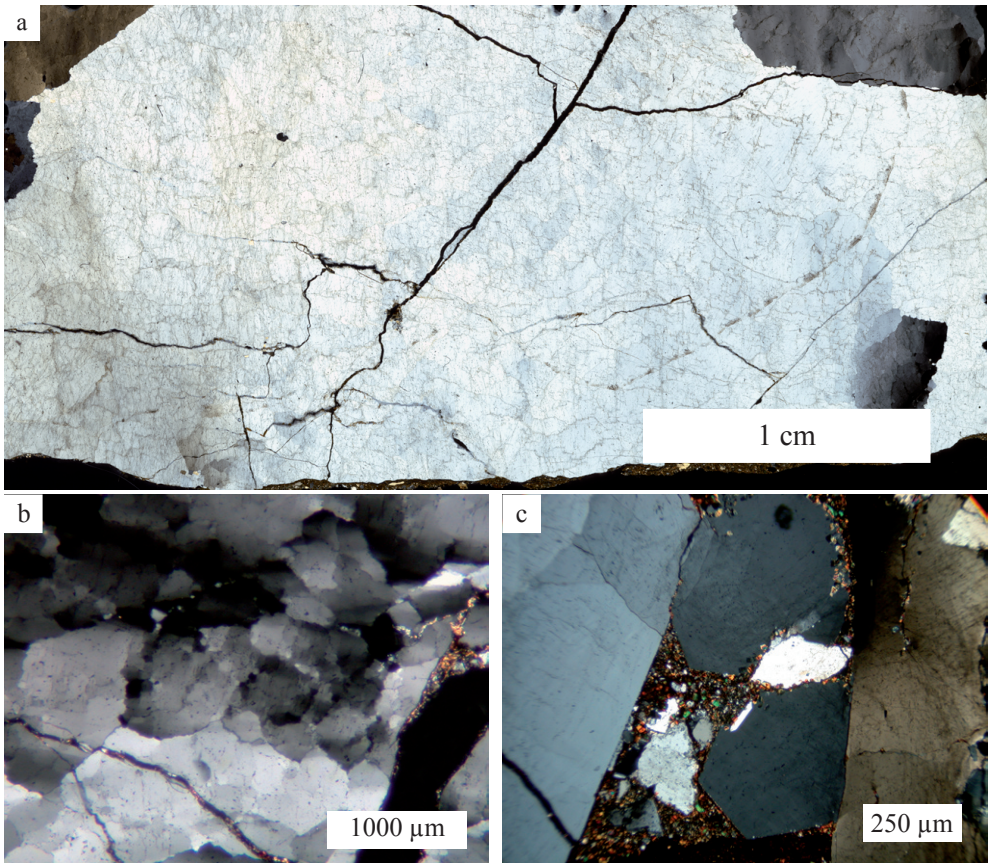

Fig. 6: a) Centimetre-sized quartz crystals at the centre of vein EN 45. The grains show undulatory extinction. Scanned thin section with crossed polarizers. b) Original grain with small subgrains and high misorientation angles at the subgrain boundaries. c) Open vug bound by euhedral facets of large quartz grains with undulatory extinction. Photomicrographs with crossed polarizers.

4.5.2. Microfabrics of vein quartz related to crystal plastic deformation

The coarse quartz grains in the veins show microstructures indicative of deformation by dislocation glide, least so in the vein centres in the vicinity of the open vugs (Fig. 6c). Inhomogeneous crystal plastic deformation is revealed by marked undulatory extinction (Figs. 4a, 5a, 6). Microstructures indicating thermally activated annealing comprise subgrains and sutured high-angle grain boundaries indicative of migration recrystallization (Fig. 6b). On the grain scale, finite strain is very low; most grains appear almost undistorted with their original shape largely preserved.

4.5.3. Description of the fluid inclusions

The vein quartz is crowded with fluid inclusions of variable size. The diameter is typically up to about 0.03 mm. Most inclusions occur isolated or in clusters and are considered as primary (Roedder, 1984). Near the vein margins, the inclusions are particularly abundant and large. Some show tendency towards a negative crystal shape. Other inclusions are arranged along healed cracks. At room temperature, all inclusions contain two phases, a liquid and a small gas bubble comprising a few percent in volume. (Fig. 7).

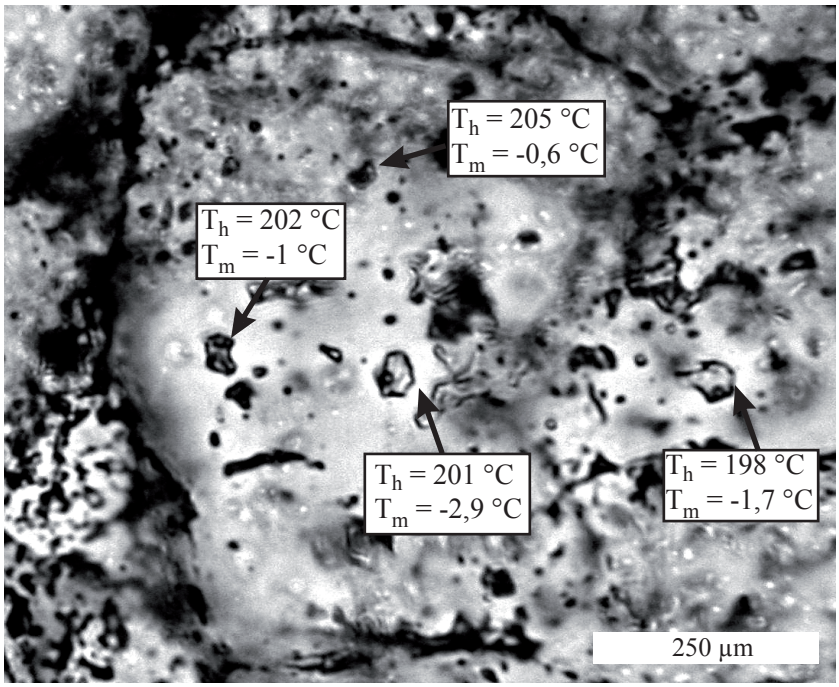

Fig. 7: Fluid inclusions trapped in quartz of vein EN 38. The diameter is typically up to about 0.03 mm. At room temperature, all inclusions contain two phases, a liquid and a small gas bubble (photomicrograph).

4.6. Fluid inclusion analysis

4.6.1. Fluid composition

Quadrupol Mass Spectrometry (QMS) (e.g. Barker and Smith, 1986) was used to determine the principal volatile components of the fluid inclusions, H_20, CO_2, CO, N_2 and CH_4. Representative mm-sized fragments of the thick sections are heated in high vacuum causing decrepation of the individual fluid inclusions. The liberated gas is analyzed by QMS. The fundamentals of the technique and the evaluation procedures are described by Röller et al. (2001).

Information on the concentration of non-volatile constituents of the fluids is obtained by low-temperature microthermometry. The sample is cooled down so that the inclusion is completely frozen. During subsequent heating, the eutect temperature T_e of the fluid is determined by the

occurrence of first melt, which yields some constraints on the chemical composition of the solutes (Crawford, 1981; Roedder, 1984; Shepherd et al., 1985). The depression of the freezing point, i.e. the temperature of complete melting T_m reflects the concentration of the solutes, which are in this case assumed to be entirely NaCl (e.g. Bodnar, 1993). As this is generally not true, the concentration is reported as wt.-% NaCl equivalent.

4.6.2. Principles of density determination of fluid inclusions

Small aliquots of the fluid in the cavity get trapped in the growing quartz grains during vein sealing (e.g. Roedder, 1984; Shepherd et al., 1985). The properties of the fluid inclusions depend on the fluid composition and on the temperature and pressure at the time of crystallization (Bodnar et al., 1985; Roedder and Howard, 1988; Sasada, 1988; Hedenquist et al., 1992; Goff and Gardner, 1994; Bargar, 1995; Sasada and Goff, 1995).

As the volume and hence the density of an inclusion can be assumed to remain approximately constant during exhumation (Roedder, 1984; Shepherd et al., 1985), the change of pressure inside the inclusion as a function of temperature must follow a line of constant volume, referred to as isochore (e.g Roedder, 1984; Shepherd et al., 1985). Upon cooling, a vapour bubble forms at the point where the isochore meets the liquid / vapour curve. Inversely, during microthermometric analysis this point is determined by heating of the inclusion until it homogenizes into a single phase, the temperature being referred to as the temperature of homogenization, T_h (e.g. Roedder, 1984; Shepherd et al., 1985). For a known fluid composition, and with PVT-data for this composition being available, an isochore can be calculated that links the pressure and the temperature of the pore fluid at the time of trapping (e.g. Bakker, 2003).

4.7. Results of fluid inclusion analysis

4.7.1. Fluid inclusion composition

At room temperature (25°C), the fluid inclusions generally contain two phases, a gas bubble and a liquid phase. Daughter crystals inside the inclusions are systematically absent. Based on QMS analysis, the only volatile component of the fluid is H_2O, while the concentration of other volatiles like CO_2, CO, N_2 and CH_4 is below the limit of detection (Fig. 8).

The eutect temperature T_e ranges between -20 and -22° C, and suggests NaCl to be the predominant non-volatile constituent of the fluid inclusion (Roedder, 1962; Potter et al., 1978; Crawford, 1981). The values for T_m average at -3 ± 1.9°C, corresponding to salinities of 4.8 ± 2.8 wt. % NaCl equivalent (Bodnar, 1993). This salinity range holds for all analyzed inclusions, independent on their position within the vein.

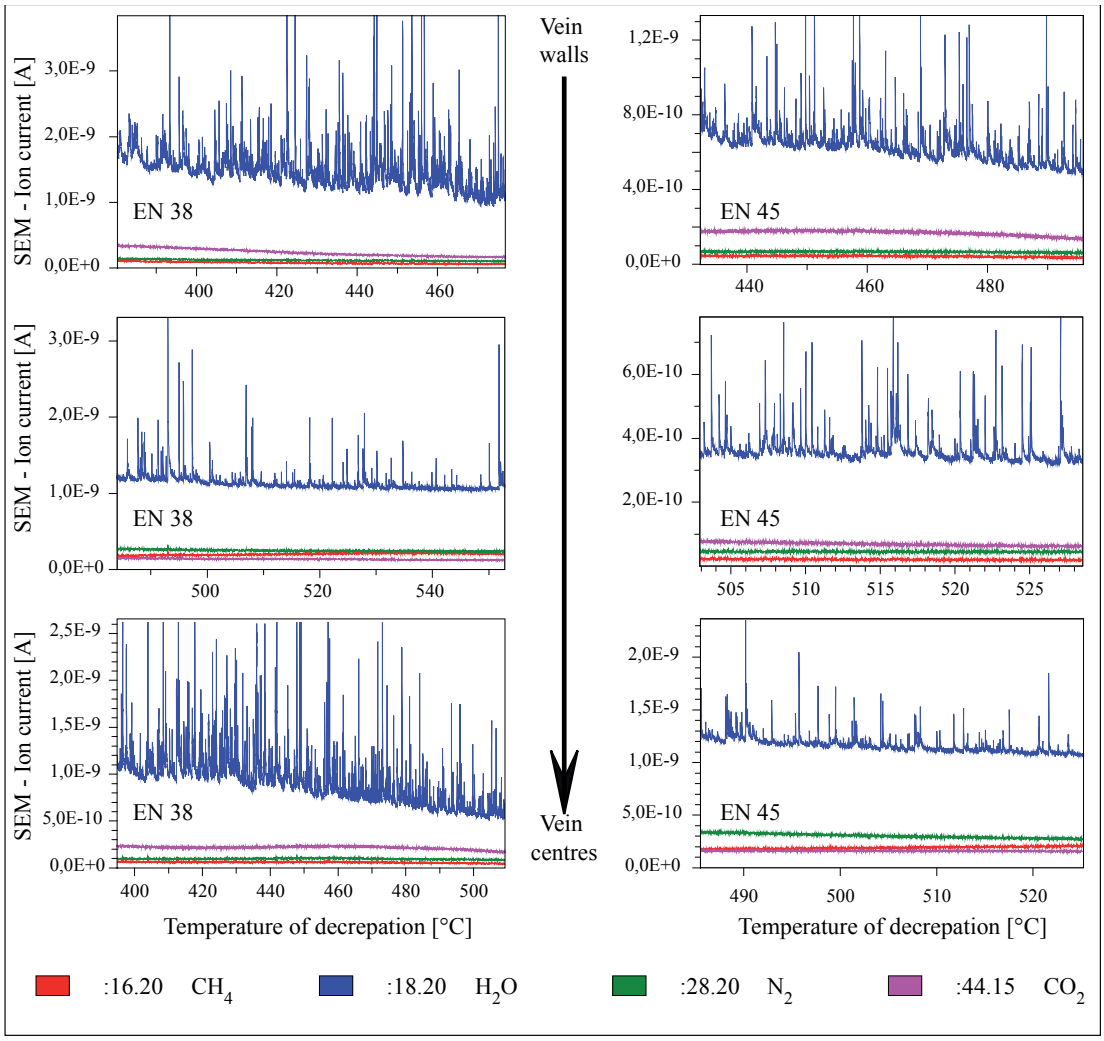

Fig. 8: Results of quadrupol mass spectrometric analysis of mm-sized specimens. The primary volatile component of the fluid is H_2O, while the concentration of other volatiles like CO_2, CO, N_2 and CH_4 is below the limit of detection.

4.7.2. Homogenization temperature T_h as a function of position within the vein

The temperature of homogenization T_h of the fluid inclusions was measured along profiles over the veins, oriented normal to the vein walls (Fig. 1) to detect changes in the density of the fluid inclusion depending on position. In vein EN 38, T_h decreases from 200 ± 6.4°C (left wall) and 203 ± 3.4°C (right wall) to 163 ± 5.8°C at the vein center. In vein EN 45, T_h decreases from 212 ± 4.1°C (left wall) and 206 ± 4.5°C (at a distance of 4 cm from the right wall) to 155 ± 3.5°C at the vein centre. In vein EN 45 the outermost 4 cm of the right vein margin could not be sampled. Based on the available data and comparison with the other veins, it can be assumed that T_h would be identical at both vein walls. The measured T_h depending on the position within the veins is listed in Tab. 1 and plotted in the T_h - X diagrams in Figs. 9a and 10a. For both veins in their outer part, the gradient in T_h is low. It becomes steep near the vein centre, resulting in a deep trough in T_h (Figs. 9a, 10a). The patterns are symmetric (Figs. 9a, 10a). In the following, the width of the central troughs are referred to as the "low homogenization temperature zones, LT_hZ", while the rims are referred to as the "high homogenization temperature zone, HT_hZ" (Figs. 9a, 10a). In both veins, the ratio between the width of the LT_hZ and the vein aperture w is the same. The percentage of the profile length made up by the LT_hZ is 15.6 % in vein EN 38 and 16.6 % in vein EN 45.

4.7.3. Density and calculation of the isochores

In the present study, all fluid inclusions homogenize into the liquid phase. There is no evidence for phase separation and trapping of an effervescent fluid (e.g. Mullis, 1976; Roedder, 1984; Shepherd et al., 1985). In this case, the temperature of the fluid at trapping, T_t, exceeds T_h. First, the density of a fluid inclusion is deduced from T_h and the fluid composition. Based on the inclusion density, an isochore is calculated that links the temperature of trapping to the fluid pressure (e.g Roedder, 1984; Shepherd et al., 1985). For both, density and isochore calculation, the software package "Fluids 1" (Bakker, 2003) was used.

In a first step, the T_h and composition data were used to determine isochores according to the empirical PVT data provided by Roedder (1984). The predictions based on the equation of state published by Anderko and Pitzer (1993a, 1993b) and Duan et al. (1995) turned out to compare well with the empirical isochores (Roedder, 1984), and were therefore used to derive the fluid pressure at the time of trapping.

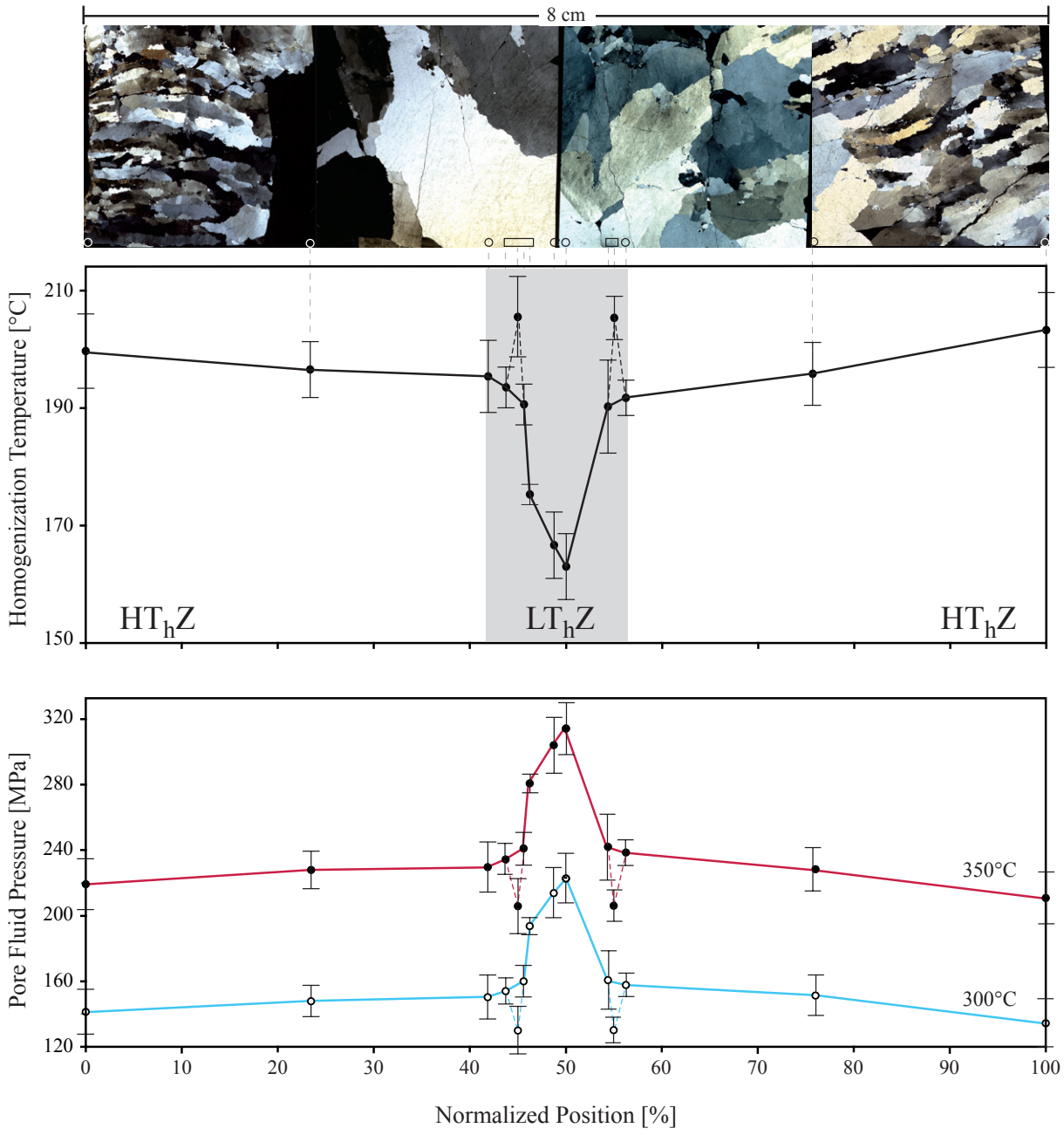

Fig. 9: Results of microthermometric analysis of fluid inclusions in quartz of vein EN 38: a) Plot of the homogenization temperature as a function of position along the profile line (see Fig. 1a). In the outer part, the gradient in Th is low, it becomes steep near the centre. b) Plot of the derived pore fluid pressure (for a given temperature) as a function of the position along the profile line.

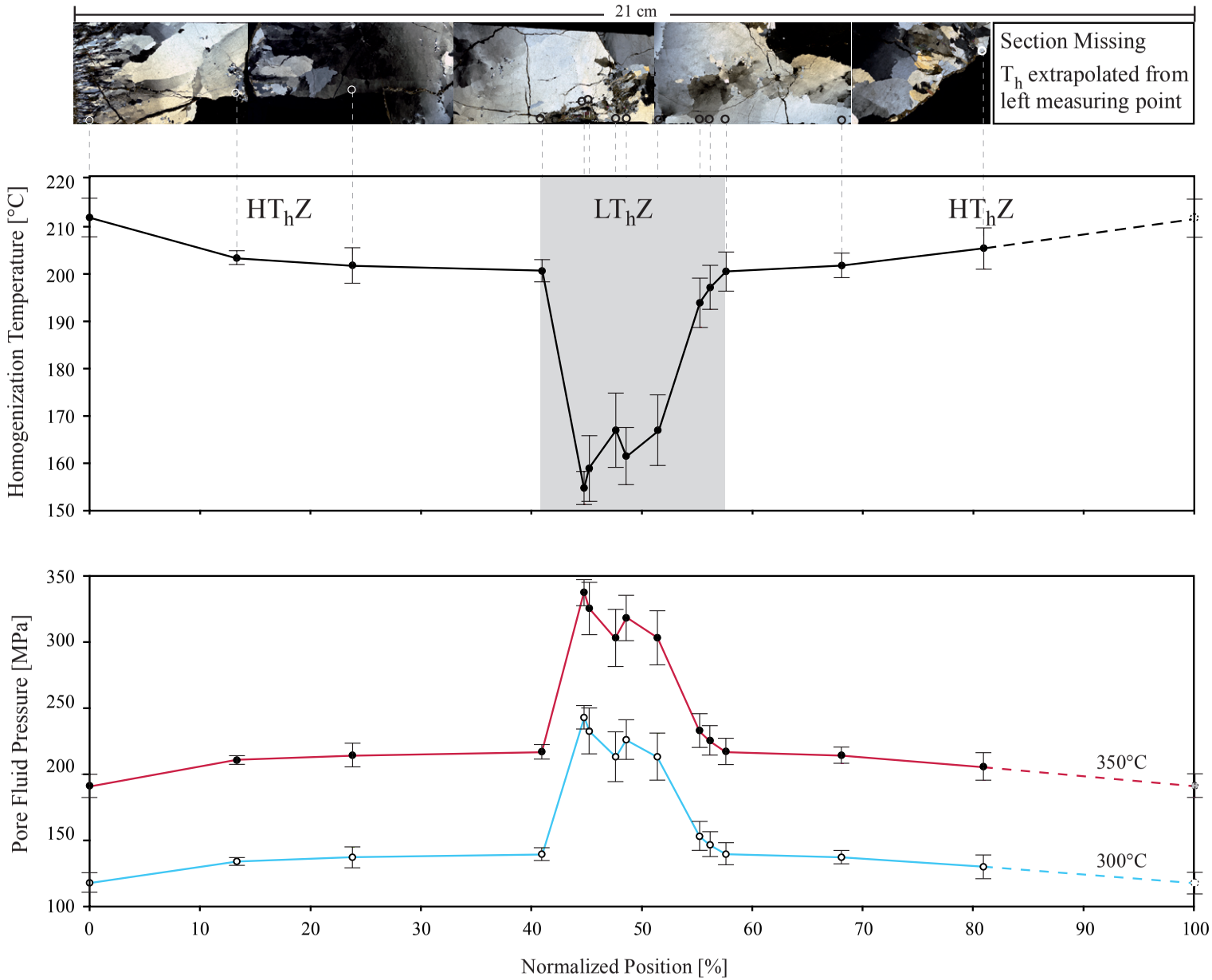

Fig. 10: Results of microthermometric analysis of fluid inclusions in quartz of vein EN 45: a) Plot of the homogenization temperature as a function of the position along the profile line (see Fig. 1a). In the outer part, the gradient in Th is low; it becomes steep near the centre. b) Plot of the derived pore fluid pressure (for a given temperature) as a function of the position along the profile line.

Vein EN 38						
Position [cm]	Position [%]	T_h [°C]	300°C P_f [MPa]	350 °C P_f [MPa]	300°C Δσ [MPa]	350°C Δσ [MPa]
0.00	0	199.7 ± 6.4	141 ± 6.5	219 ± 7.7	124 ± 6.5	90 ± 7.7
1.90	23.8	196.5 ± 4.6	148 ± 4.6	227 ± 5.5	117 ± 4.6	82 ± 5.5
3.35	41.9	195.4 ± 6.3	150 ± 6.4	230 ± 7.5	115 ± 6.4	79 ± 7.5
3.5	43.8	193.5 ± 3.5	154 ± 3.5	234 ± 4.2	111 ± 3.5	75 ± 4.2
3.6	45	205.5 ± 6.8	130 ± 6.7	206 ± 7.9	135 ± 6.7	103 ± 7.9
3.65	45.6	190.7 ± 4.1	159 ± 4.5	241 ± 5.2	105 ± 4.5	68 ± 5.2
3.7	46.3	175.3 ± 2	193 ± 2.3	281 ± 2.7	71 ± 2.3	28 ± 2.7
3.9	48.8	166.7 ± 6	214 ± 7.2	304 ± 8.3	51 ± 7.2	5 ± 8.3
4.0	50	163.0 ± 5.8	223 ± 7.1	314 ± 8.1	42 ± 7.1	-5 ± 8.1
4.35	54.4	190.3 ± 8.2	161 ± 8.8	242 ± 10.3	104 ± 8.8	67 ± 10.3
4.4	55	205.4 ± 3.9	130 ± 3.7	206 ± 4.4	135 ± 3.7	103 ± 4.4
4.5	56.3	191.8 ± 3.1	158 ± 3.3	239 ± 3.8	107 ± 3.3	70 ± 3.8
6.0	75	195.3 ± 5.5	150 ± 5.6	230 ± 6.6	115 ± 5.6	79 ± 6.6
8.0	100	203.3 ± 6.6	134 ± 6.5	210 ± 7.7	131 ± 6.5	98 ± 7.7
Vein EN 45						
0.0	0.0	211.9 ± 4.1	118 ± 7.6	192 ± 9.1	147 ± 7.6	118 ± 9.1
2.8	13.3	203.4 ± 1.4	134 ± 2.8	211 ± 3.3	131 ± 2.8	98 ± 3.3
5.0	23.8	201.8 ± 3.8	137 ± 7.6	214 ± 9.0	128 ± 7.6	95 ± 9.0
8.6	41.0	200.6 ± 2.3	140 ± 4.7	217 ± 5.5	125 ± 4.7	92 ± 5.5
9.4	44.8	154.8 ± 3.5	243 ± 8.8	338 ± 10.2	22 ± 8.8	-29 ± 10.2
9.5	45.2	159.0 ± 7.0	232 ± 17.4	326 ± 20.1	32 ± 17.4	-17 ± 20.1
10.0	47.6	167.0 ± 7.8	213 ± 18.9	303 ± 21.8	52 ± 18.9	6 ± 21.8
10.2	48.6	161.6 ± 6.1	226 ± 15.0	318 ± 17.3	39 ± 15.0	-9 ± 17.3
10.8	51.4	167.0 ± 7.4	213 ± 17.9	303 ± 20.6	52 ± 17.9	6 ± 20.6
11.6	55.2	193.9 ± 5.2	153 ± 11.0	233 ± 12.9	112 ± 11.0	76± 12.9
11.8	56.2	197.1 ± 4.6	147 ± 9.5	226 ± 11.1	118 ± 9.5	83 ± 11.1
12.1	57.6	200.6 ± 4.2	140 ± 8.5	217 ± 10.0	125 ± 8.5	92 ± 10.0
14.3	68.1	201.8 ± 2.6	137 ± 5.1	214 ± 6.2	128 ± 5.1	95 ± 6.2
17.0	81.0	205.5 ± 4.5	130 ± 8.7	206 ± 10.4	135 ± 8.7	103 ± 10.4
21.0	100.0	211.9 ± 4.1	118 ± 7.6	192 ± 9.1	147 ± 7.6	118 ± 9.1

Tab. 1: Results of microthermomety listed according to to the position in the veins.

4.8. Discussion

4.8.1. Sealing of the cavity

The microstructure of the vein-filling material provides information on the opening and sealing history of the vein (e.g. Durney and Ramsay, 1973; Ramsay, 1980). Two types of microstructures are diagnostic for the relation between the opening rate and the sealing rate:

1) If the sealing rate exceeds the opening rate, vein formation gets cyclic. Incremental widening is followed by complete sealing. The process is called the crack-seal mechanism (Durney and Ramsay, 1973; Ramsay, 1980). The indicative microfabrics comprise fibrous crystals, generally without lattice preferred orientation, and narrowly spaced inclusion trails parallel to the vein walls, marking healed fractures (Durney and Ramsay, 1973; Ramsay, 1980); each trail represents a single increment of opening.

2) If the opening rate exceeds the sealing rate, crystals grow into an open fluid filled cavity. In this case, the crystals may attain crystal facets (e.g. Durney and Ramsay, 1973; Ramsay, 1980; Ague, 1995). The growth of crystals in the open cavity is restricted only by growth competition between adjacent crystals. This leads to a selection of those grains, for which the fastest growth direction is oriented about normal to the vein wall, the growth of other grains becoming eventually terminated by impingement (Hilgers and Urai, 2002). For quartz, the direction of fastest growth is parallel to the c-axis (Iler, 1979; Fisher and Brantley, 1992). Consequently, growth competition between adjacent crystals leads to a selection of quartz crystals with a c-axis orientation about normal to the vein wall. Due to progressive elimination of grains in less favourable orientation, the grain size increases towards the centre of the vein and a crystallographic preferred orientation of c-axes normal to the vein walls develops (e.g. Fisher and Brantley, 1992; Fisher et al., 1995; Hilgers and Urai, 2002).

The microfabrics of the representative veins show no discontinuities indicative of episodic or cyclic processes of opening and sealing. In particular, the microstructures characteristic for the crack-seal vein growth mechanism (Durney and Ramsay, 1973; Ramsay, 1980) are systematically absent. Instead, the coarse-grained microfabric with elongate or blocky crystals suggests crystallization from a free fluid phase in an open cavity. This is indicated (1) by residual voids between euhedral crystals (e.g. Ague, 1995) (Fig. 6c), (2) by microstructures resulting from growth competition, which leads to impingement and inward coarsening of the grain size (Figs. 4a, d; 5a, d) (Durney and Ramsay, 1973; Ramsay, 1980; Hilgers and Urai, 2002), and (3) by the development of an increasingly pronounced crystallographic preferred orientation with increasing distance to the vein wall (Figs. 4b, 5b) (Fisher and Brantley, 1992; Hilgers and Urai, 2002). These features demonstrate that the fractures were opened in a single stage. During the early history, the opening rate was high compared to the sealing rate, leaving the fractures as

open cavities. The sealing grains nucleated at the vein walls and grew towards the vein centre. Such veins are referred to as syntaxial veins (Ramsay and Huber, 1983). Fluid inclusions trapped in such veins record a history of the fluid composition and density in the fissure.

4.8.2. Temperatures indicated by the microstructural record of the quartz veins

The crosscutting relationship between the veins and all syn-metamorphic structures indicate that the veins postdate the pervasive deformation during HP / LT metamorphism. Also, the original vein shapes appear to be at best little modified by later deformation. The orientation of the veins indicates tensile fracturing and vein formation in an extensional tectonic regime. This structural record indicates that the veins have formed at some stage during exhumation and cooling.

Within the vein, the record of deformation accompanied by thermally activated annealing processes is ubiquitous in the vein quartz microstructure. The microfabrics suggest that crystal plastic deformation took place at elevated temperatures. Based on the correlation between thermochronometry and natural quartz microstructures (e.g. Voll, 1976; Dunlap et al., 1997; Stöckhert et al., 1999; Brix et al., 2002), supported by the extrapolation of experimental flow laws to slow geological strain rates (e.g. Hirth et al., 2001), the syn-kinematic temperature can be estimated. For deformation of the vein quartz, the microfabrics point to temperatures similar or slightly above 300°C, a temperature commonly predicted for the long-term brittle ductile transition in continental crust (e.g. Strehlau and Meissner, 1987; Ranalli and Murphy, 1987). As there is no evidence for a complex thermal history, uniform cooling during exhumation indicates that formation of the parent fractures, opening, and cavity sealing must have taken place at minimum temperatures near to or somewhat above 300°C. As vein formation is expected to be a rapid process compared to geological timescales, the temperature was probably approximately constant during the stage of sealing.Transient thermal perturbations caused by rapid fluid flow cannot be excluded, however, although there is no indication for that.

4.8.3. Evolution of fluid pressure during sealing

Based on the structural record of the quartz veins, the temperature during vein sealing and hence, the trapping temperature of the fluid inclusions, T_t, is estimated to range between about 300 and 350°C. The crystal grew from the vein walls towards the vein centre. Primary fluid inclusions in crystals close to the vein walls got trapped at an early stage of sealing, while fluid inclusions close to the centre of the vein got trapped at a late stage, just before sealing of the vein went to completion. Based on this correlation between position and time of trapping, the fluid inclusions record the history of fluid composition and density. As there is no evidence for a decreasing temperature during vein sealing and as the fluid composition remains approximately constant, the decrease in the homogenization temperature with increasing distance from the vein walls (Figs. 9a, 10a) reflects an increase in the pore fluid pressure with time. Based

on T_h and the fluid inclusion composition, the fluid pressure at a temperature of 300 or 350°C is calculated for the analyzed specimens. The fluid pressure is then plotted as a function of the distance to the vein walls in the P_f – X diagrams shown in Figs. 9b and 10b (see also Tab. 1).

4.8.4 Remote stress during vein opening and sealing

Prerequisite for the formation of a monogenetic syntaxial vein is that - during the entire stage of sealing - the fissure is kept open to provide space for crystal growth into a fluid filled cavity. Therefore, the effective stress normal to the fracture wall must be tensile, i.e. negative, or at least zero. From the general law of effective stress (Rice and Cleary, 1976), the remote stress component acting normal to the fracture wall σ_n, which is the least principal stress σ_3, is counteracted by P_f, and reduced to an effective stress:

$$\sigma'_n = \sigma_3 - P_f \qquad (1)$$

To open an arrested fracture, σ'_n must be tensile (Atkinson and Cook, 1993):

$$\sigma_3 \leq P_f \qquad (2)$$

The remote tensile stress gets intensified in the vicinity of a fracture (Irwin, 1948). The magnitude of stress in the material, σ, at a distance r to a sharp crack tip under tensile load is proportional to the stress intensity factor K_I and to $1/\sqrt{r}$, with r denoting the distance to the tip (Irwin, 1948). The static tensile stress intensity factor K_I depends on the magniude of tensile stress acting normal to the fracture, here $-\sigma'_n$, and the crack length L (Irwin, 1948):

$$K_I = -\sigma'_n \sqrt{\pi L/2} \qquad (3)$$

A fracture keeps arrested as long as K_I remains below a critical value, the fracture toughness K_{IC} (Irwin, 1961). If K_I reaches K_{IC}, unstable fracture propagation gets re-initiated (Irwin, 1961), resulting in a drop of P_f due to dilantancy. According to eqs. 1 and 3, the maximum fluid pressure inside the fracture P_{fc} is limited by the fracture toughness of the host rock:

$$P_{fc} = \sigma_3 + \frac{K_{IC}}{\sqrt{\pi L/2}} \qquad (4)$$

In combination with the microstructural record of the veins, equations 1 through 4 imply that the fluid pressure is directly coupled to the remote differential stress. If the fluid pressure drops to value below σ_3, the cavity gets closed and crystal growth stalled (eqs. 1 and 2). The upper

limit of $P_f = P_{fc}$ is reached when $K_I = K_{IC}$. According to eq.1, σ'_n is the driving stress for widening of the fracture by ductile deformation of the host rock (Nüchter and Stöckhert, submitted). Therefore, the ratio between σ_3 and P_f is kept approximately constant during the entire history of vein sealing.

To keep a crack arrested and to – at the same time - widen the fissure by creep, the fluid pressure must be similar to the least principal stress, $\sigma_3 \approx P_f$. Furthermore, in the given extensional tectonic setting, the maximum principal stress is given by the overburden, $\sigma_1 = \sigma_v$. Based on these considerations, the fluid inclusions trapped in vein quartz represent an effective stress gauge. The differential stress is $\Delta\sigma = \sigma_1 - \sigma_3$. For a geothermal gradient of about 30 °C/km during exhumation (Klein-Helmkamp, 1996) and an average rock density of 2.7 g/cm^3, σ_1 is 270 MPa for T_t = 300 °C and 310 MPa for T_t = 350 °C. The magnitude of remote differential stress $\Delta\sigma$ recorded by the fluid inclusions as a function of the distance to the vein wall (which represents the opening and sealing history) is listed in Tab. 1 an plotted in the $\Delta\sigma$ -X diagram in Fig. 11. For T_t = 300°C, the decrease of remote differential stress during sealing of the veins EN 38 and EN 45 would be 93 MPa and 125 MPa, respectively, and for T_t = 350°C, the decrease of remote differential stress would be 80 MPa and 100 MPa, respectively (Fig. 11; Tab. 1).

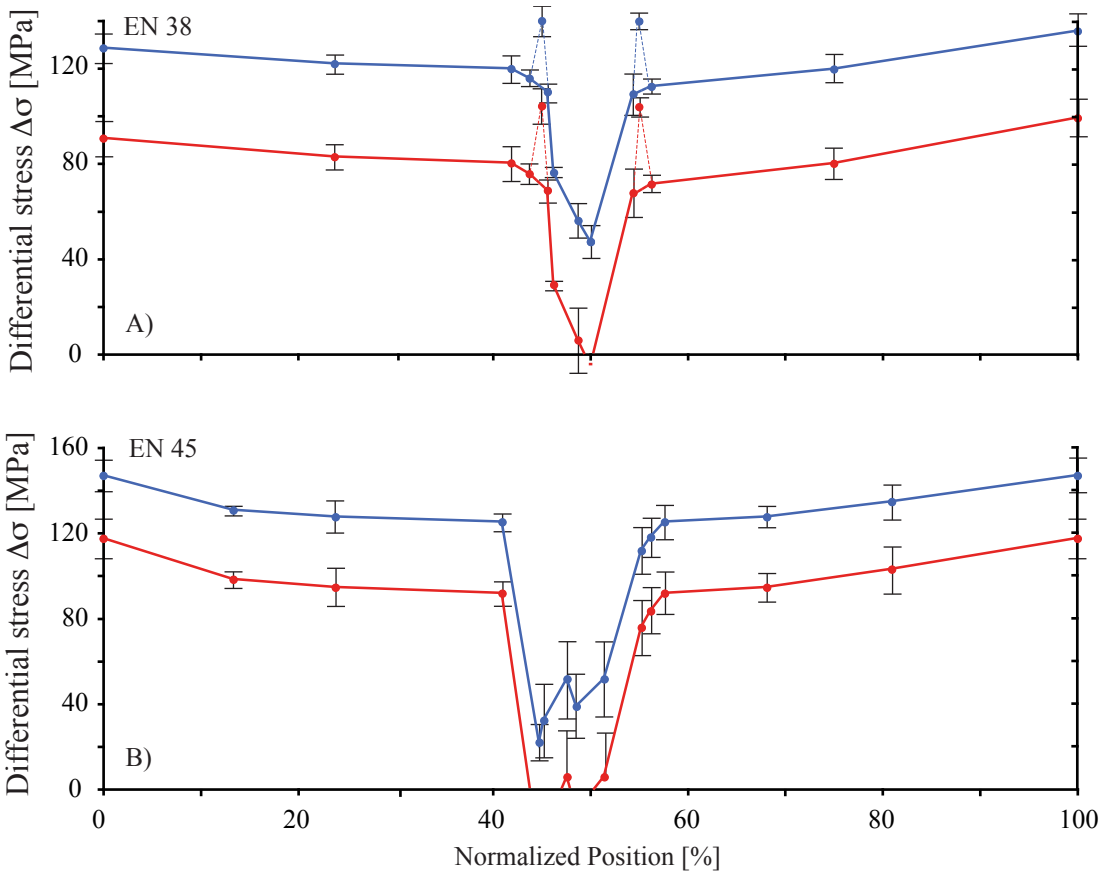

Fig. 11: Level of differential stress obtained from the fluid inclusion data based on the LEFM approach as a function of the position along the profile line (see Fig. 1) for T_t = 300°C (blue graphs) and T_t = 350°C (red graphs). a) En 38; b) EN 45.

The low pore fluid pressures recorded by the low density of the fluid inclusions trapped close to the vein walls indicate that the early stage of cavity formation and sealing proceeded within a framework of high remote stress. The stage of loading to high stress is not recorded in the vein and must have preceeded the onset of sealing. Loading of the viscous (on the long term) middle crust to high differential stress must necessarily be achieved in a very short time, most probably by stress redistribution during a major earthquake in the overlying upper crust (e.g. Sibson, 1980; Tse and Rice, 1986; Scholz, 1990; Ellis and Stöckhert, 2004a, 2004b; Ellis et al., 2006). The subsequent increase in the density of the fluid inclusions with distance to the vein walls reflects the gradual decay in the magnitude of the remote differential stress with time, i.e. postseismic stress relaxation and recovery of pore fluid pressure to a near-lithostatic value.

4.8.5. How to estimate the timescale of stress relaxation and fracture sealing

In the following, a simple model is used to get insight into the time scale of vein formation. On a local scale, coseismic loading is expected to be in a fixed grip mode: A volume element of the crust is distorted elastically by only a few percent within a few seconds. In a simple model, the imposed stress peak is then relaxed by creep of the distorted crustal volume (Ellis and Stöckhert, 2004a, 2004b; Ellis et al., 2006). If so, the timescale of relaxation depends on the magnitude of the imposed stress peak, the rheology of the rock, and the syn-kinematic temperature. To gain insight into the lifetime of the seismically induced brittle damage (e.g. Sibson, 1981; Küster and Stöckhert 1999; Baisch and Bokelmann, 2001; Trepmann and Stöckhert, 2002; Miller et al., 2004) in the uppermost plastosphere (Scholz, 1990), the timescale of vein sealing is compared to the timescale of stress relaxation for a simple model, in which it is either controlled by a non-linear powerlaw rheology (e.g. Ivins, 1996; Freed and Bürgmann, 2004) or by a linear Newtonian rheology (e.g. Gerbault et al., 2003).

From the microstructural record of the host rock, there is no evidence supporting either a powerlaw or Newtonian rheology of the host rock. The timescale of stress relaxation is therefore calculated for both a powerlaw rheology of quartz and a linear Newtonian rheology with constant viscosity.

For the powerlaw rheology of quartz, the flow law parameters obtained by Paterson and Luan (1990) are used, the pre-exponential factor $A = 6.5 \times 10^{-8}$ MPa^{-n}, the activation energy $Q = 135$ $kJmol^{-1}$, and the powerlaw stress exponent $n = 3.1$. For the Newtonian rheology, a constant viscosity $\eta = 10^{21}$ Pa s is used (e.g. Gerbault et al., 2003), independent on temperature.

Differential stress is correlated with fluid pressure in the fissure, as $\sigma_3 \approx P_f$. The decrease in stress between two positions, $\sigma_{x1} - \sigma_{x2}$, is taken to result from relaxation of the remote stress by viscous creep of the host rock. Then the stress difference $\sigma_{x1} - \sigma_{x2}$ is compared to the timescale of stress relaxation, predicted on the base of the presumed rock rheology (Fig. 12). The times required for this stress relaxation would then correspond to the time interval Δt between

crystallization of quartz and trapping of fluids at points x_1 and x_2 (Fig. 12). Summing up these time intervals, $\sum \Delta t$, gives an estimate of the time it took to seal the vein. $\sum \Delta t$ is calculated for both presumed rheologies and syn-kinematic temperatures of 300°C and 350 °C. The syn-kinematic temperature controls (1) the viscosity predicted by the powerlaw rheology, and (2) the differential stress derived from the fluid pressure, as this is a function of temperature in an isochoric system.

In the diagram in Fig. 13, $\sum \Delta t$ is plotted with distance to the vein walls. Depending on the chosen rheology and the temperature, the sealing of the HT_hZ, representing about 85% of the vein width, is predicted to take place on a timescale of 10^1 – 10^2 years. In contrast, the sealing of the LT_hZ is predicted to take place on a timescale of 10^2 – 10^4 years. In the diagrams in Fig. 14, the history of both the decrease in the remote stress and the increase in the pore fluid pressure is visualized.

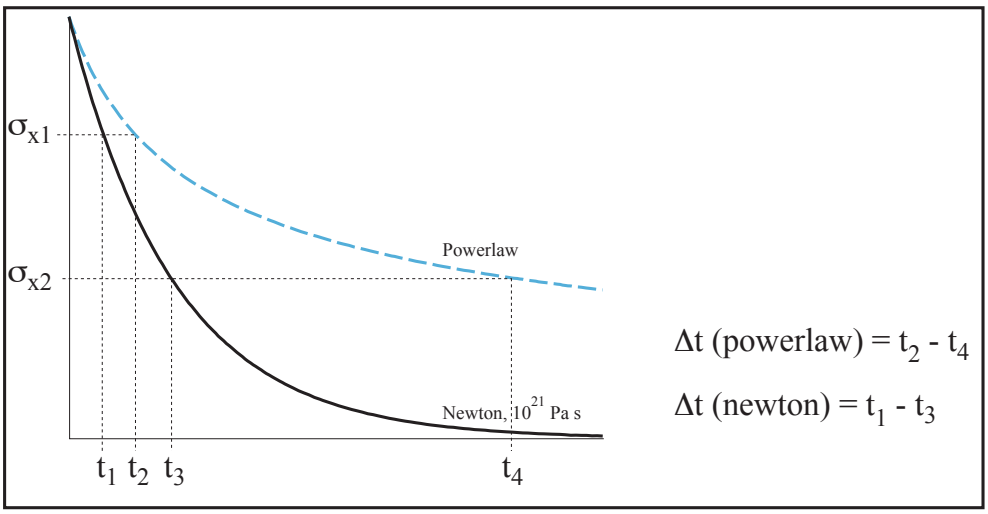

Fig. 12: Principles of the model used to estimate the timescale of stress relaxation and sealing. The timescale of vein sealing is taken to correspond to the timescale of stress relaxation, predicted for a presumed bulk rock rheology, a given temperature, and the level of differential stress obtained from the fluid inclusion data based on the LEFM approach.

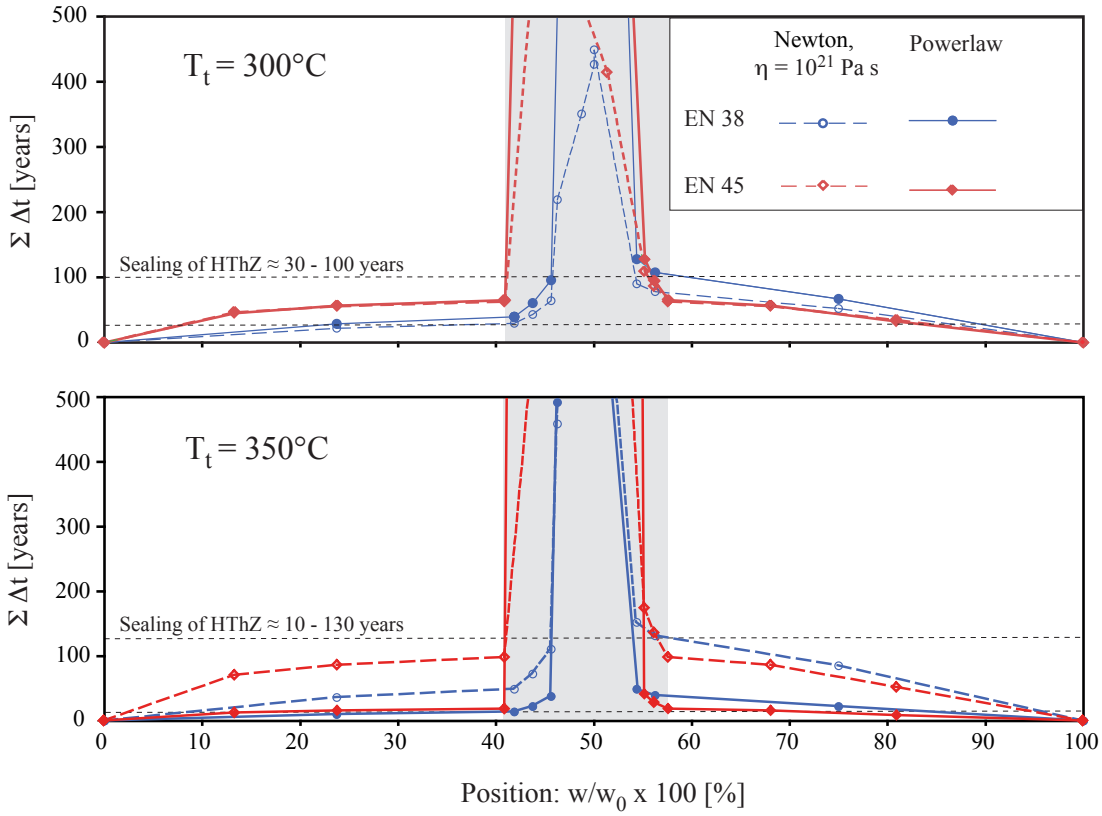

Fig. 13: Estimates of the timescale of vein sealing for a temperature of a) 300°C and b) 350°C. Sealing of the HT$_h$Z (ca. 85% of the vein width) is predicted to take place within about 10 to 130 years.

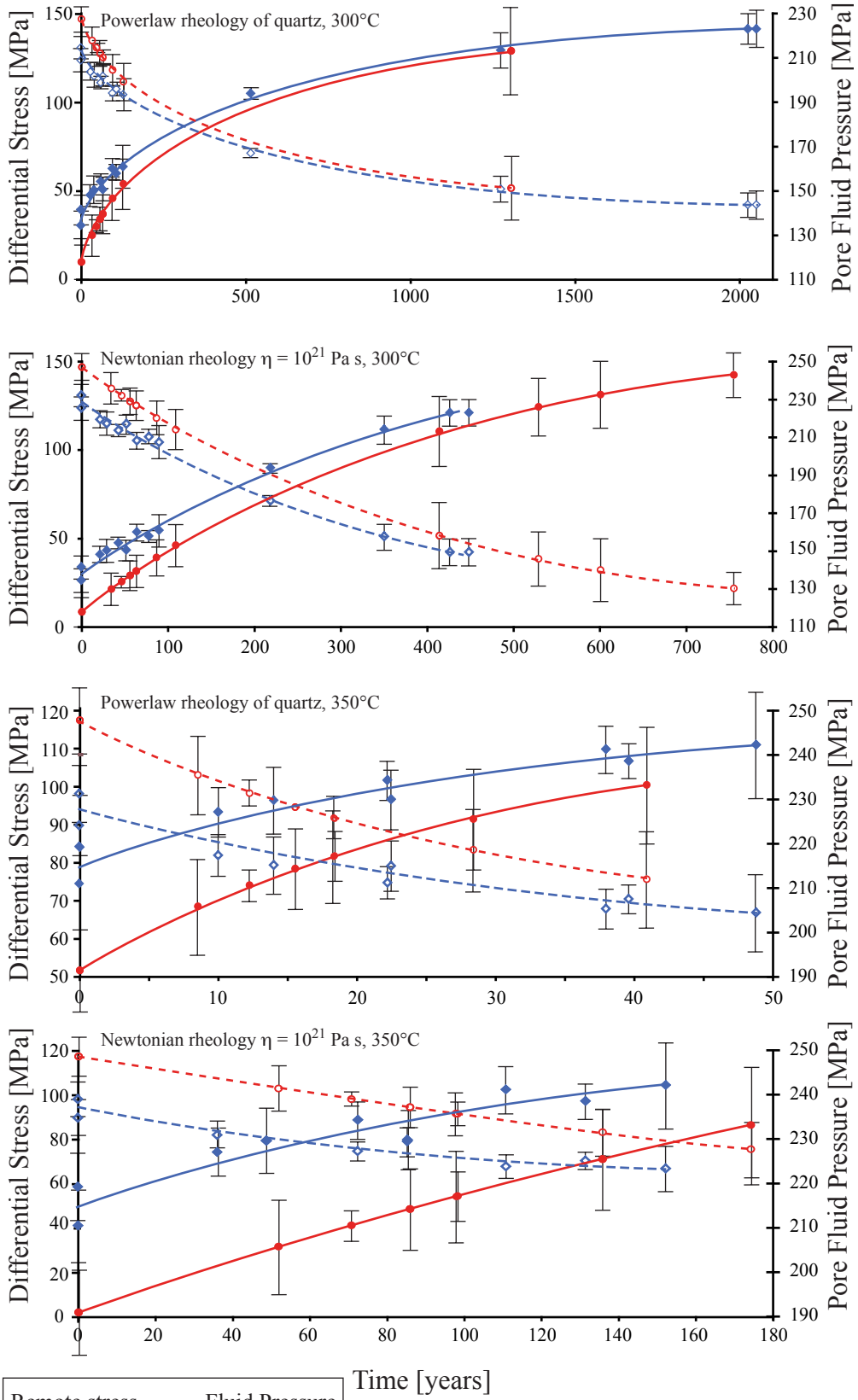

Fig. 14: History of both the decrease in the remote stress and in the increase in the pore fluid pressure.

4.8.6. Drop in pore fluid pressure in consequence to unstable crack propagation

4.8.6.1. Background

The stress intensification at a crack tip drives crack propagation. Hence, K_I (eq. 3) is also referred to as the tensile crack extension force (e.g. Atkinson, 1987; Anderson, 1995). During unstable crack propagation, K_I increases with crack length, if σ_n = const (eq. 3). According to the first law of thermodynamics, the excess in crack extension force, K_I, is converted into kinetic energy (e.g. Anderson, 1995) and controls the crack speed (e.g. Atkinson, 1987; Anderson, 1995). For high speed crack propagation, the kinetic energy may also allow crack propagation to continue when K_I has fallen to below K_{IC}. High speed fractures get arrested when K_I reaches the arrest toughness $K_{IA} < K_{IC}$ (e.g. Anderson, 1995).

The energy approach of Griffith (1920) and Irwin (1956, 1957) implies that incremental crack propagation can be described as a release of strain energy. The energy release rate, G, is correlated to the rate of crack propagation (e.g. Atkinson, 1987). The energy is dissipated by the formation of two new surface increments and the inelastic damage in the process zone around the crack tip (e.g. Anderson, 1995; Engvik et al., 2005). If a crack is accelerated to the terminal velocity, theoretically defined by the Raleigh wave speed (e.g. Kalthoff, 1973; Lawn, 1975; Atkinson, 1987; Anderson, 1995; Bertram and Kalthoff, 2003), a further increase in the energy release rate cannot be attained by further acceleration. Instead, fractures branch to increase the area of new surface and the volume of the related damage zone per growth increment. This type of fracture branching is symmetric in isotropic and homogeneous material, with a characteristic apex angle of 30° (Kalthoff, 1973).

The apparent fracture toughness at blunt voids K^*_{IC} exceeds the fracture toughness K_{IC} at sharp crack tips (e.g. Anderson, 1995; Bertram and Kalthoff, 2003). Nüchter and Stöckhert (submitted) proposed that high speed fracture propagation may be initiated from such blunt voids, which are expected to prevail over sharp microcracks in the hot and viscous middle crust in consequence to rapid crack healing (Smith and Evans, 1984; Hickman and Evans, 1987). Such blunt voids are expected to be capable to endure the stage of coseismic loading. First, K_I rises due to increase of the void length by subcritical crack growth (e.g. Broek, 1987), driven by the strong remote stress. When the stress intensification at the blunt void reaches K^*_{IC}, unstable crack propagation eventually gets initiated at $K_I = K^*_{IC} > K_{IC}$. After initiation, the tip sharpens immediately and accelerates as a consequence to the surplus energy, given by the difference between K^*_{IC} and K_{IC}. The cracks get arrested when $K_I = K_{IA}$ (e.g. Anderson, 1995).

4.8.6.2. Evidence for unstable crack growth

Early grown quartz grains trapped fluid inclusions of low density, indicating a low fluid pressure inside the juvenile vein. According to eqs. 2 – 4, the remote stress must have been high to keep the cavity open. The stage of loading to high stress is not recorded and must have preceded the onset of vein sealing. The Hubbert-Rubey ratio $\lambda = P_f / \sigma_v = P_f / \rho g z$ denotes the ratio between the pore fluid pressure and overburden stress σ_v, with ρ denoting the average rock density (~ 2,7 g cm^{-3}), g the gravitational acceleration, and z the depth (Hubbert and Rubey, 1959). At the margins of vein EN 38, λ ranges between 0.5 (assuming T_t = 300 °C) and 0.7 (assuming T_t = 350 °C); at the margins of vein EN 45, λ ranges between 0.45 (T_t = 300 °C) and 0.63 (T_t = 350 °C). The fluid pressure at incipient sealing was markedly sub-lithostatic and the differential stress was high.

In structural geology, it is a widely accepted paradigm that veins formed from tensile fractures are restricted to an environment of high pore fluid pressure and weak remote differential stress (Secor, 1965; Secor and Pollard, 1975; Sibson, 1981). Based on the Griffith failure criterion and illustrated in the Mohr diagram, formation of tensile fractures is proposed to be restricted to a differential stress not exceeding $4T_0$, with T_0 denoting tensile strength (e.g. Secor, 1965; Secor and Pollard, 1975; Sibson, 1981). If so, λ has to be similar or slightly above 0.9 to allow tensile fracturing at a depth level of about 10 km (Secor, 1965; Sibson, 1981).

It is anticipated that such hydraulic fractures advance and arrest in a cyclic process, controlled by the changing fluid pressure in the fracture (e.g. Atkinson and Cook, 1993; Renshaw and Harvey, 1994). The pressure changes arise from the volume increase related to fracture propagation (Atkinson and Cook, 1993; Renshaw and Harvey, 1994; Olson, 2003). If the rate of fluid infiltration into the fracture cannot keep up with the dilation rate, the fracture gets arrested. Fracture propagation is re-initiated, when the internal fluid pressure has sufficiently recovered, so that $K_I = K_{IC}$ (eq. 4). As such, the propagation rate is limited by the rate of fluid flow into the fracture, which in turn is governed by the permeability of the host rock (Atkinson and Cook, 1993; Renshaw and Harvey, 1994). In rocks of low permeability, particularly under metamorphic conditions (e.g. Brace, 1980, 1984; Nur and Walder, 1990; Manning and Ingebritsen, 1999), hydraulic fractures are prevented from runaway dynamic crack propagation (Atkinson and Cook, 1993; Renshaw and Harvey, 1994). As a consequence, for hydraulic fractures, the fracture driving force must remain low. Instead, they grow in a cyclic process with repeated initiation and arrest after a small increment of growth (Atkinson and Cook, 1993; Renshaw and Harvey, 1994). Crack propagation gets quasi-static at an approximately constant, slightly fluctuating stress intensity factor $K_I \approx K_{IC}$. According to eq. 3, P_f slightly decreases to keep $K_I = K_{IC}$ during crack growth. A significant drop in P_f in consequence to hydraulic fracture propagation (Secor, 1965; Sibson, 1981) is impossible. As a consequence, the fluid pressure inside an arrested hydraulic fracture is expected to be slightly below the fluid pressure at initiation, but a significant drop in P_f in consequence to hydraulic fracturing is impossible.

The stage of loading to high stress may either have followed or preceded the arrest of the original fractures. In the first case, crack initiation and arrest takes place in a framework of low remote stress and necessarily high pore fluid pressure. In this case, fluid inclusions trapped close to the vein walls should reveal a high density, corresponding to a quasi-lithostatic fluid pressure. During sealing, loading should then be reflected by a lowering of the fluid inclusion density. This scenario is in obvious contradiction with the results of the present study.

In the second case, the cracks initiate and propagate driven by high differential stress. In this case, the fluid inclusions close to the vein walls are of low density, reflecting a low fluid pressure. Atkinson and Cook (1993) have shown that the propagation rate and the finite length of cracks decreases with increasing loading rate. Therefore, the growth of the fractures (represented by veins with a length on the order of 10^{-1} to 10^{1} m) during loading to high stress is unlikely. For these cracks, the results of the present study favour initiation and arrest at a stage, when a high level of differential stress and a low pore fluid pressure were (just) attained. During crack initiation, the remote stress clearly exceeded $4T_0$ and the Hubbert - Rubey ratio was significantly below $\lambda = 0.9$.

Based on these considerations, the record of the fluid inclusions trapped in the vein quartz is in obvious conflict with an origin of the veins from hydraulic fractures (sensu Secor, 1965; Secor and Pollard, 1975; Sibson 1981). The record of the fluid inclusions indicates that crack propagation got initiated and arrested in an environment of high remote stress and low pore fluid pressure. This result is supported by the structural record: The veins are interpreted to result from fractures, which propagated driven by high remote stress (Nüchter and Stöckhert, submitted). This interpretation is based on two principal observations: First, the veins crosscut pre-existing planes of low tensile strength, e.g. schistosity, in the host rock. The crack path was exclusively controlled by the orientation of the principal stresses. Secondly, symmetrical branching of the fractures (Fig. 2) is indicative for high speed fracture propagation and requires a very high driving force (Kalthoff, 1973; Lawn, 1975; Bertram and Kalthoff, 2003). Nüchter and Stöckhert (submitted) proposed that the fractures have initiated from blunt voids at which the apparent fracture toughness allows unstable crack initiation after the loading stage and some incubation time. It is expected that the fluid pressure drops to even below σ_3 during unstable crack propagation with a high dilatancy rate In this case, fracture opening and vein sealing would start after an early stage of fluid pressure recovery to $P_f \approx \sigma_3$, so that $\sigma'_n \leq \sigma_3$ (eq. 1).

4.9. Conclusions

Monogenetic discordant quartz veins in the HP / LT – metamorphic Styra-Ochi Unit of southern Evia developed from cracks created in consequence to coseismic loading to high differential stress. These cracks were opened and sealed during subsequent time-dependent deformation of the host rock. The systematic change of the density of fluid inclusions in vein quartz as a function of position records the history of both fluid pressure and differential stress for this stage of postseismic stress relaxation. The record reflects the cyclic stress and fluid pressure changes related to the earthquake cycle, at a depth level just below the crustal scale brittle ductile transition. The following features are characteristic:

(1) Fluid inclusions trapped in the incipient stage of vein sealing are of low density and indicate a low pore fluid pressure.

(2) The fluid inclusion densities as a function of position demonstrate a continuous and gradual increase in the pore fluid pressure during the stage of vein sealing.

Based on the principles of fracture mechanics, the pore fluid pressure in an open cavity must be in equilibrium to the wall normal remote stress σ_3 and can therefore be taken as a differential stress gauge, if $\sigma_1 = \sigma_v$ is defined by the lithostatic load in an extensional regime. The spatial arrangement of the fluid inclusion densities indicate the onset of vein sealing in a framework of high stress and low pore fluid pressure, followed up by stress relaxation and restoration of the pore fluid pressure to quasi-lithostatic values upon progressive sealing. The (micro-)structural and fluid inclusion record of the discordant vein in the Styra-Ochi Unit reveals that a single vein records a single cycle of coseismic loading and postseismic creep.

References

Ague, J.J. (1995): Deep crustal growth of quartz, kyanite and garnet into large-aperture, fluid filled fractures, north-eastern Connecticut, USA.- J. metamorphic Geol., 13: 299-314.

Anderko, A. and Pitzer, K.S. (1993a): Equation-of-state representation of phase equilibria and volumetric properties of the system NaCl-H2O above 573 K.- Geochim. Cosmochim. Acta, 57: 1657-1680.

Anderko, A. and Pitzer, K.S. (1993b): Phase equilibria and volumetric properties of the systems KCl- H2O and NaCl-KCl- H2O above 573 K; equation of state representation.- Geochim. Cosmochim. Acta, 57: 4885-4897.

Anderson, T.L. (1995): Fracture mechanics- Fundamentals and Application, second edition.- CRC Press.

Atkinson, B.K. (1987): Introduction to fracture mechanics and its geophysical applications.- In: Atkinson, B.K. [ed.]: Fracture mechanics of rock (pp. 1-26). Academic Press Limited.

Atkinson, C., Cook, J. M. (1993): Effect of Loading Rate on Crack Propagation Under Compressive Stress in a Saturated Porous Material.- J. Geophys. Res, 98(B4): 6383-6395.

Baisch, S., Bokelmann, G.H.R. (2001): Seismic waveform attributes before and after the Loma Prieta earthquake: Scattering change near the earthquake and temporal recovery.- J. Geophys. Res., 106(B8): 16323-16337.

Bakker, R. J. (2003): Package FLUIDS; 1, Computer programs for analysis of fluid inclusion data and for modelling bulk fluid properties.- Chemical Geology, 194: 3-23.

Bargar, K.E. (1995): Some fluid-inclusion measurements for geothermal drill holes in California, Nevada, El Salvador, and Russia.- U.S. Geol. Surv. Open-File Rep. 95-0826, 14 pp.

Barker, C., Smith, M.P. (1986): Mass spectrometric determination of gases in individual fluid inclusions in natural minerals.- Anal. Chem., 58: 1330-1333.

Bertram, A. & Kalthoff, J.F. (2003). Crack propagation toughness of rock for the range from low to very high crack speeds.- Paper presented at the third international conference on fracture and damage mechanics, FDM 2003.

Bodnar, R.J. (1993): Revised equation and table for determining the freezing point depression of H2O-NaCl solutions.- Geochim. Cosmochim. Acta, 57: 683-684.

Bodnar, R.J., Reynolds, T.J., Kuehn, C.A. (1985): Fluid-inclusion systematics in epithermal systems.- Rev. Econ. Geol., 2: 73-97.

Bosl, W. J. & Nur, A. (2002). Aftershocks and pore fluid diffusion following the 1992 Landers earthquake. J. Geophys. Res., 107(B12), doi: 10.1029/2001JB000155.

Bouchon, M. (1997): The state of stress on some faults of the San Andreas system as inferred from near-field strong motion data.- J. Geophys. Res., 102: 11731-11744.

Bouchon, M., Campillo, M., Cotton, F. (1998): Stress field associated with the rupture of the 1992 Landers, California, earthquake and its implications concerning the fault strength at the onset of the earthquake.- J. Geophys. Res., 103: 21091-21097.

Brace, W.F. (1980): Permeability of crystalline and argillaceous rocks. Int. J. Rock Mech. Min. Sci., 17: 241-251.

Brace, W.F. (1984): Permeability of crystalline rocks: new in situ measurements. J. Geophys. Res., 89(B6): 4327-4330.

Brix, M.R., Stöckhert, B., Seidel, E., Theye, T., Thomson, S.N., Küster, M. (2002): Thermobarometric data from a fossil zircon partial annealing zone in high pressure-low temperature rocks of eastern and central Crete, Greece.- Tectonophysics, 349, 309-326.

Broek, D. (1987): Elementary Engineering fracture mechanics.- Martinus Nijhoff Publishers.

Crawford, M.L. (1981): Phase equilibria in aqueous fluid inclusions.- In: Hollister, L.S. and Crawford, M.L. (eds.): Fluid inclusions: Applications to petrology: Mineralogical Association of Canada Short Course Handbook, 6: 75-100.

Duan, Z, Moller, N. and Weare, J.W. (1995): Equation of state for the NaCl-H (sub 2) O-CO (sub 2) system; prediction of phase equilibria and volumetric properties.- Geochim. Cosmochim. Acta, 59: 2869-2882.

Dunlap, W.J., Hirth, G. and Teyssies, C. (1997): Thermomechanical evolution of a ductile duplex.- Tectonics, 16: 983-1000.

Durney, D. W., & Ramsay, J. G. (1973): Incremental strains measured by syntectonic crystal growth. In K. A. De Jong, & R. Scholten (Eds.), Gravity and Tectonics. (pp. 67-96). New York: John Wiley.

Ellis, S., Stöckhert, B. (2004a): Imposed strain localization in the lower crust on seismic timescales.- Earth Planets Space, 56(12): 1103-09.

Ellis, S., Stöckhert, B. (2004b): Elevated stresses and creep rates beneath the brittle-ductile transition caused by seismic faulting in the upper crust. J. Geophys. Res, 109(5), B05407.

Ellis, S., Beavan, J., Eberhart-Phillips, D., Stöckhert, B. (2006): Simplified models of the Alpine Fault seismic cycle: stress transfer in the mid-crust.- Geophys. J. Int., 166(1): 386-402.

Engvik, A., Bertram, A., Kalthoff, J.F., Stöckhert, B., Austrheim, H., Elvevold, S. (2005): Magma-driven hydraulic fracturing and infiltration of fluids into the damaged host rock, an example from Dronning Maud Land, Antarctica.- J. Struct. Geol., 27: 839-854.

Etheridge, M.A. (1983): Differential stress magnitudes during regional deformation and metamorphism: upper bound imposed by tensile fracturing.- Geology, 11: 231-234.

Etheridge, M.A., Wall, V.J., Cox, S.F., Vernon, R.H. (1984): High fluid pressures during regional metamorphism and deformation: implications for mass transport and deformation mechanisms.- J. Geophys. Res., 89: 4344-4358.

Faure, M., Bonneau, M. and Pons, J. (1991): Ductile deformation and syntectonic granite emplacement during the late Miocene extension of the Aegea (Greece).- Neues Jahrb. Mineral. Monatsh., 4: 145-162.

Fisher, D.M., Brantley, S.L. (1992): Models for quartz overgrowth and vein formation:

´Deformation and episodic fluid flow in an ancient subduction zone.- J. Geophys. Res., 97(B13): 20,043-20,061.

Fisher, D.M., Brantley, S.L., Everett, M., Dzvonik, J. (1995): Cyclic fluid flow through a regionally extensive fracture network within the Kodiak accretionary prism. J. Geophys. Res, 100(B7), 12.881-12.894.

Freed, A.M., Bürgmann, R. (2004). Evidence of power-law flow in th Mojave desert mantle. Nature, 430, 548-551.

Gautier, P. and Brun, J.-P. (1994): Crustal-scale geometry and kinematics of late-orogenic extension in the central Aegean (Cyclades and Evvia Island).- Tectonophysics, 238: 399-424.

Gerbault, M., Henrys, S., Davey, F. (2003): Numerical models of lithospheric deformation forming the Southern Alps of New Zealand.- J. Geophys. Res., 108: doi:10.1029/2001JB001716.

Goff, F., Gardner, J.N. (1994): Evolution of a mineralized geothermal system, Valles caldera, New Mexico.- Econ. Geol., 89: 1803-1832.

Griffith, A.A. (1920):The Phenomena of rupture and flow in solids.- Philosophical Transactions, Series A, 221:163-198.

Hedenquist, J.W., Reyes, A.G., Simmons, S.F., Taguchi, S. (1992): The thermal and geochemical structure of geothermal and epithermal systems: A framework for interpreting fluid inclusion data.- Eur. J. Mineral., 4: 989-1015.

Hickman, S.H., Evans, B. (1987): Influence of geometry upon crack healing rate in calcite. Phys. Chem. Minerals, 15, 91-102.

Hilgers, C., Urai, J. (2002): Experimental study of syntaxial vein growth during lateral fluid flow in transmitted light: first results. J. Struct. Geol, 24, 1029-43.

Hirth, G., Teyssier, C., Dunlap, W.J. (2001): An evaluation of quartzite flow laws based on comparisons between experimentally and naturally deformed rocks.- Int. J. Earth. Sci., 90(1), 77-87.

Hubbert, M.K., Rubey, W.W. (1959): Role of fluid pressure in mechanics of overthrust faulting, I, Mechanics of fluid-filled porous solids and its application to overthrust faulting.- Geol. Soc. Am. Bull., 70: 115-166.

Iler, R. (1979): The chemistry of silica.- Wiley-Interscience, New York.

Irwin, G.R. (1948): Fracture dynamics.- Fracturing of metals, American society for metals, Cleveland: 147-166.

Irwin, G.R. (1956): Onset of fast crack propagation in high strength steel and aluminium alloys.- Sagamore research conference proceedings, 2: 289-305.

Irwin, G.R. (1957): Analysis of stresses and strains near the end of a crack traversing a plate.- Journal of Applied Mechanics, 24: 361-364.

Irwin, G.R. (1961): Plastic zone near a crack and fracture toughness.- Sagamore research conference proceedings, 4.

Ivins, E.R. (1996): Transient creep of a composite lower crust 2. A polymineralic basis for rapidly evolving postseismic deformation modes.- J. Geophys. Res., 101: 28005-28028

Jolivet, L., Faccenna, C. (2000): Mediterranean extension and the Africa-Eurasia collision.- Tectonics, 19: 1095-1106.

Kalthoff, J.F. (1973): On the propagation direction of bifurcated cracks.- In: Sih, G.C. (ed.): Proc. Int. Conf. on Dynamic Crack Propagation, Bethlehem, Pa., Nordhoff Int. Publ.: 449-458.

Klein-Helmkamp, U. (1996): Metamorphose und Exhumierung der niedrigtemperierten Hochdruckmetamorphite der Styra-Ochi-Einheit in Süd-Euböa, Attisch-Kykladisches Kristallin, Griechenland.- Ruhr University Bochum, Germany.

Kohlstedt, D. L., Evans, B., & Mackwell, S. J. (1995). Strength of the lithosphere: Constraints imposed by laboratory experiments. J. Geophys. Res, 100(B9), 17,587-17,602.

Küster, M. & Stöckhert, B. (1999): High differential stress and sublithostatic pore fluid pressure in the ductile regime-microstructural evidence for short-term postseismic creep in the Sezia Zone, Western Alps. Tectonophysics, 303, 263-77.

Lawn, B. (1975): Fracture of brittle solids - second edition.- Cambridge University Press.

Le Pichon, X., Angelier, J. (1981): The Aegean Sea.- Philos. Trans. R. Soc. Lond., Ser. A, 300: 357-372.

Lister, G.S., Banga, G. and Feenstra, A. (1984): Metamorphic core complexes of Cordilleran type in the Cyclades, Aegean Sea, Greece.- Geology, 12: 221-225.

Manning, C.E., Ingebritsen, S.E. (1999): Permeability of the continental crust: implications of geothermal data and metamorphic systems.- Rev. Geophys, 37: 127-150.

Miller, S. A., Collettini, C., Chiaraluce, L., Cocco, M., Barchi, M., & Kaus, B. J. P. (2004): Aftershocks driven by a high-pressure CO2 source at depth.- Nature, 427: 714-727.

Meulenkamp, J.E., Wortel, M.J.R., Van Wamel, W.A., Spakman, W., Hoogerduyn Strating, E. (1988): On the Hellenic subduction zone and the geodynamic evolution of Crete since the late Middle Eocene.- Tectonophysics, 146: 203-215.

Mullis, J. (1975): Growth conditions of Quartz Crystals from Val d´Illiez (Valais, Switzerland).- Schweizerische Mineralogische und Petrographische Mitteilungen, 55(3): 419-429.

Mullis, J. (1976): Das Wachstumsmillieu der Quarzkristalle im Val d´lliez.- Schweizerische Mineralogische und Petrographische Mitteilungen, 56(2): 219-268.

Nüchter, J.-A., Stöckhert, B. (submitted): Fracturing and single-event vein formation in the middle crust – the record of coseismic loading and postseismic creep.- J. Geophys. Res.

Nur, A. and Walder, J. (1990): Time-dependent hydraulics of the earth´s crust.- In: Bredehoeft, J.D. and Norton, D. (eds.): The role of fluids in crustal processes, pp. 113-127, Natl. Acad.Press, Washington.

Oliver, N.H.S. (1996): Review and classification of structural controls on fluid flow during regional metamorphism.- J. Metamorph. Geol., 14: 477-492.

Olson, J. E. (2003): Sublinear scaling of fracture aperture versus length: An exception or the rule? J. Geophys. Res, 108(B9).

Paterson, M. S., Luan, F. C. (1990): Quartzite rheology under geological conditions. In R. J. Knipe, & E. H. Rutter (Eds.), Deformation Mechanisms, Rheology and Tectonics. (pp. 299-307). Geological Society Special Publications.

Potter, R.W., Clynne, M.A., Brown, D.L. (1978): Freezing point depression of aqueous sodium chloride solutions.- Econ. Geol., 73: 284-285.

Ramsay, J.G. (1980): The crack-seal mechanism of rock deformation. Nature, 284, 135-39.

Ramsay, J.G., Huber, M.I. (1983): The techniques of modern structural geology, Volume 1: Strain analysis.- Academic Press. London.

Ranalli, G., Murphy, D.C. (1987): Rheological stratification of the lithosphere.- Tectonophysics, 132: 281-295.

Renshaw, C. E., Harvey, C. F. (1994): Propagation velocity of a natural hydraulic fracture in a poroelastic medium. J. Geophys. Res, 99(B11), 21667-77.

Rice, J.R., Cleary, M. P. (1976). Some basic stress diffusion solutions for fluid-saturated elastic porous media with compressible constituents. Rev. Geoph. Space Phys, 14(2), 227-241.

Rice, J.R. and Gu, J.C. (1983): Earthquake aftereffects and triggered seismic phenomena.- Pageoph., 121: 187-219.

Roedder, E. (1962): Studies of fluid inclusions I: Low temperature application of a dual-purpose freezing and heating stage.- Econ. Geol., 57: 1045-1061.

Roedder, E. (1984): Fluid inclusions.- Rev. Mineral., 12. Mineral. Soc. Am., Washington, DC.

Roedder, E., Howard, K.W. (1988): Fluid inclusion in Salton Sea Scientific Drilling Project core: Preliminary results.- J. Geophys. Res., 93: 13159-13164.

Röller, K., Küster, M., Stöckhert, B. (2001): Quatrupol-mass-spectrometric (QMS) analysis of fluid inclusions – Applications and perspectives.- XVI ECROFI European Current Research On fluid Inclusions. Fac. Ciênc. Porto, Dep. Geol. Mem. T, Porto, pp. 383-386.

Rolandone, F., Bürgmann, R., & Nadeau, R. M. (2004): The evolution of the seismic-aseismic transition during the earthquake cycle; constraints from the time-dependent depth distribution of aftershocks. Geophys Res Lett, 31(23).

Sasada, M. (1988): Microthermometry of fluid inclusions fro the VC-1 core hole in Valles Caldera, New Mexico.- J. Geophys. Res., 93: 6091-6096.

Sasada, M., Goff, F. (1995): Fluid inclusion evidence for rapid formation of the vapor-dominated zone at Sulphur Springs, Valles Caldera, New Mexico, USA.- J. Volcanol. Geotherm. Res., 67: 161-169.

Scholz, C.H. (1990): The mechanics of earthquake and faulting.- Cambridge University press.

Shepherd, T.J., Rankin, A.H., Alderton, D.H.M. (1985): A practical guide to fluid inclusion studies.- Blackie, Glasgow.

Secor, D. T. (1965): Role of fluid pressure in jointing. Am. J. Sci, 263, 633-46.

Secor, D. T. & Pollard, D. D. (1975): On the stability of open hydraulic fractures in the earth´s crust. Geophys. Res. Lett., 2(11), 510-13.

Sibson, R. H. (1980): Transient discontinuities in ductile shear zones.- J. Struct. Geol., 2: 165-171.

Sibson, R.H. (1981). Fluid flow accompanying faulting: Field evidence and models. In D. W. Simpson, & P. G. Richards (Eds.), Earthquake Prediction: An international review. (pp. 593-603). American Geophysical Union.

Smith, D. & Evans, B. (1984): Diffusional crack healing in quartz.- J. Geophys. Res, 89(B6): 4125-4135.

Stöckhert, B., Brix, M. R., Kleinschrodt, R., Hurford, A. J., Wirth, R. (1999): Thermochronometry and microstructures of quartz; a comparison with experimental flow laws and predictions on the temperature of the brittle-plastic transition. J. Struct. Geol, 21: 351-369.

Strehlau, J., Meissner, R. (1987): Estimation of crustal viscosities and shear stresses from an extrapolation of experimental steady state flow data.- Geodynamic series, 16: 69-87.

Trepmann, C. A. & Stöckhert, B. (2001): Mechanical twinning of jadeite; an indication of synseismic loading beneath the brittle-plastic transition. Int. J.Earth Sci., 90(1), 4-13.

Trepmann, C. A. & Stöckhert, B. (2002): Cataclastic deformation of garnet; a record of synseismic loading and postseismic creep. J. Struct. Geol, 24(11), 1845-56.

Trepmann, C. A. & Stöckhert, B. (2003): Quartz microstructures developed during non-steady state plastic flow at rapidly decaying stress and strain rate. J. Struct. Geol, 25(12), 2035-51.

Tse, S.T., Rice, J.R. (1986): Crustal earthquake instability in relation to the depth variation of frictional slip properties.- J. Geophys. Res., 91(9): 9452-9472.

Urai, J., Williams, P. F., & Roermund, v. H. L. M. (1991): Kinematics of crystal growth in syntectonic fibrous veins. J. Struct. Geol, 13(7), 823-836.

Voll, G. (1976): Recrystallization of quartz, biotite and feldspars from Erstfeld to the Leventina Nappe, Swiss Alps, and ist geological significance. Schweizerische Miner. Petrog., 56, 541-647.

Wald, D. & Heaton, T. (1994): Spatial ad temporal distribution of slip for the 1992 Landers, California, earthquake.- Bull. Seismol. Soc. Am., 84: 668-691.

Yardley, B. (1984): Fluid migration and veining in the Connemara Schists, Ireland.- In: Walther, J.V., Wood, B.J. [eds.]: Fluid-rock interactions during metamorphism, pp. 109-131, Springer-Verlag, New York.

5. General Conclusions

The discordant low aspect ratio veins in the high pressure / low temperature metamorphic Styra-Ochi Unit of southern Evia / Greece formed in the middle crust in consequence to almost instantaneous coseismic loading to high stress followed up by a stage of postseismic stress relaxation. The veins yield insight into earthquake-related brittle / ductile processes at a depth level just below the crustal scale brittle ductile transition, hence in the uppermost plastosphere. The following features are characteristic:

1) The veins formed by a single stage of mineral precipitation in an open cavity at temperatures similar to 300°C during exhumation and cooling.

2) The veins formed from unstable propagating cracks, some reached the terminal velocity for crack propagation. The original cracks propagated driven by high stress in consequence to mid-crustal coseismic loading.

3) The length to aperture ratio of the veins is inconsistent with host rock distortion obeying a linear elastic fracture mechanics model. Distributed ductile deformation of the host rock has controlled the geometry of the veins.

4) Systematic gradients in the microstructural record of quartz in monogenetic veins indicate that the vein quartz crystallized during progressive widening of the cavity and shortening parallel to the crack.

5) Fluid inclusions trapped in the vein quartz recorded gradual recovery of the pore fluid pressure during the sealing stage, controlled by postseismic stress relaxation by ducile creep of the host rock.

The structural and microstructural record of the discordant veins yields insight into the boundary conditions controlling cycles of non-steady state brittle / ductile deformation of the middle crust, governed by the seismic cycle in the overlying schizosphere. Following the principle of uniformitarianism, the structural record of discordant monogenetic veins in exhumed metamorphic rocks yields insight into processes and conditions relevant for the understanding of present day earthquakes and the interpretation of related surface deformation recorded by geodesy.

Sample	Sample type	Geographic coordinates (UTM)	Study area
EN 1	Quartz vein with host rock	35 2 71264 E / 42 24979 N	Giannitsi
EN 2	Vein quartz without host rock	35 2 71264 E / 42 24979 N	Giannitsi
EN 3	Vein quartz without host rock	35 2 71264 E / 42 24979 N	Giannitsi
EN 4	Quartz vein with host rock	35 2 71264 E / 42 24979 N	Giannitsi
EN 5	Vein quartz without host rock	35 2 68050 E / 42 25151 N	Akteo
EN 6	Vein quartz without host rock	35 2 68050 E / 42 25151 N	Akteo
EN 7	Vein quartz without host rock	35 2 68050 E / 42 25151 N	Akteo
EN 8	Sample with mineralization	35 2 74344 E / 42 12475 N	North Karistos
EN 9	Vein quartz without host rock	35 2 80487 E / 42 03288 N	Cape Mandilou
EN 11	Vein quartz without host rock	35 2 79603 E / 42 03484 N	Cape Paximada
EN 12	Quartz and feldspar veins from en échelon system	35 2 79603 E / 42 03484 N	Cape Paximada
EN 13	Quartz vein with host rock	35 2 71264 E / 42 24979 N	Giannitsi
EN 14	Vein quartz without host rock	35 2 71264 E / 42 24979 N	Giannitsi
EN 15	Vein quartz and feldspar without host rock	35 2 71264 E / 42 24979 N	Giannitsi
EN 16	Quartz vein with host rock	35 2 71264 E / 42 24979 N	Giannitsi
EN 17	Quartz vein with host rock	35 2 71264 E / 42 24979 N	Giannitsi
EN 18	Quartz vein with host rock	35 2 71264 E / 42 24979 N	Giannitsi
EN 19	Quartz vein with host rock	35 2 71264 E / 42 24979 N	Giannitsi
EN 20	Vein quartz without host rock	35 2 71264 E / 42 24979 N	Giannitsi
EN 21	Quartz vein with host rock	35 2 71264 E / 42 24979 N	Giannitsi
EN 22	Vein quartz without host rock	35 2 71264 E / 42 24979 N	Giannitsi
EN 23	Quartz vein with host rock	35 2 71264 E / 42 24979 N	Giannitsi
EN 24	Quartz vein with host rock	35 2 74344 E / 42 12475 N	North Karistos
EN 25	Branching quartz and calcite vein with host rock	35 2 74605 E / 42 13760 N	Ochi
EN 26	Quartz veins with host rock	35 2 71264 E / 42 24979 N	Giannitsi
EN 27	Quartz vein with host rock	35 2 71264 E / 42 24979 N	Giannitsi
EN 28	Asymmetric branching vein with host rock	35 2 80487 E / 42 03288 N	Cape Mandilou
EN 30	Host rock with calcite vein relicts	35 2 80487 E / 42 03288 N	Cape Mandilou
EN 31	Calcite vein system with host rock	35 2 80487 E / 42 03288 N	Cape Mandilou
EN 32	Calcite vein with host rock	35 2 80487 E / 42 03288 N	Cape Mandilou
EN 34	Vein quartz without host rock	35 2 68050 E / 42 25151 N	Akteo
EN 35	Fragments of vein quartz without host rock	35 2 68050 E / 42 25151 N	Akteo
EN 36	Vein quartz without host rock	35 2 68050 E / 42 25151 N	Akteo
EN 37	Vein quartz without host rock	35 2 68050 E / 42 25151 N	Akteo
EN 38	Vein quartz without host rock	35 2 68050 E / 42 25151 N	Akteo
EN 39	Vein quartz without host rock	35 2 68050 E / 42 25151 N	Akteo
EN 40	Vein quartz without host rock	35 2 68050 E / 42 25151 N	Akteo
EN 41	Quartz vein with host rock	35 2 68050 E / 42 25151 N	Akteo
EN 42	Quartz vein with host rock	35 2 68050 E / 42 25151 N	Akteo
EN 43	Vein quartz without host rock	35 2 68050 E / 42 25151 N	Akteo
EN 44	Vein quartz without host rock	35 2 68050 E / 42 25151 N	Akteo
EN 45	Vein quartz without host rock	35 2 68050 E / 42 25151 N	Akteo
EN 46	Quartz vein with host rock	35 2 68050 E / 42 25151 N	Akteo
EN 48	Quartz vein with host rock	35 2 68050 E / 42 25151 N	Akteo
EN 49	Sample with single vein	35 2 68050 E / 42 25151 N	Akteo

Sample	Sample type	Geographic coordinates (UTM)	Study area
EN 50	Vein quartz without host rock	35 2 68050 E / 42 25151 N	Akteo
EN 53	Plate with veins	35 2 74450 E / 42 10071 N	East Karistos
EN 54	Quartz veins with host rock	35 2 74450 E / 42 10071 N	East Karistos
EN 55	Plate with veins	35 2 79603 E / 42 03484 N	Cape Paximada
EN 56	Quartz vein with host rock	35 2 71264 E / 42 24979 N	Giannitsi
EN 57	Quartz vein with host rock	35 2 71264 E / 42 24979 N	Giannitsi
EN 58	Quartz veins with host rock	35 2 71264 E / 42 24979 N	Giannitsi
EN 59	Quartz veins with host rock	35 2 65509 E / 42 19755 N	Watisi
EN 60	Calcite veins from en échelon system	25 2 78720 E / 42 24587 N	Kallianos
EN 61	Veins with host rock	25 2 78720 E / 42 24587 N	Kallianos
EN 62	Quartz veins from en échelon system	35 2 79603 E / 42 03484 N	Cape Paximada
EN 64	Quartz veins with host rock	35 2 79603 E / 42 03484 N	Cape Paximada
EN 65	Calcite veins from en échelon system	35 2 65236 E / 42 20096	Stupaioi
EN 66	Calcite veins with host rock	35 2 65240 E / 4219684 N	Watisi
EN 67	Calcite vein with host rock	35 2 65240 E / 4219684 N	Watisi
EN 68	Calcite veins from en échelon system	35 2 65240 E / 4219684 N	Watisi
EN 70	Asymmetric branching vein	35 2 81913 E / 42 03665 N	Kastri
EN 72	Asymmetric branching vein	35 2 81913 E / 42 03665 N	Kastri
EN 73	Asymmetric branching vein	35 2 81913 E / 42 03665 N	Kastri
EN 74	Asymmetric branching vein	35 2 81913 E / 42 03665 N	Kastri
EN 75	Vein tip with host rock	35 3 30519 E / 41 63439 N	Marlas / Tinos
EN 76	Calcite veins from en échelon system	35 2 71705 E / 42 25620 N	Giannitsi II
EN 77	Fragmented vein quartz	35 2 71705 E / 42 25620 N	Giannitsi II
EN 78	Vein tip with host rock	35 2 71705 E / 42 25620 N	Giannitsi II
EN 79	Quartz veins with host rock	35 2 71705 E / 42 25620 N	Giannitsi II
EN 80	Vein tip with host rock	35 2 71705 E / 42 25620 N	Giannitsi II
EN 81	Vein tip with host rock	35 2 71705 E / 42 25620 N	Giannitsi II
EN 83	Quartz vein with host rock	35 2 74344 E / 42 12475 N	North Karistos
EN 84	Veins from en échelon system	35 2 74344 E / 42 12475 N	North Karistos
EN 85	Quartz vein with host rock	35 2 71705 E / 42 25620 N	Giannitsi II
EN 86	Quartz vein with host rock	35 2 79603 E / 42 03484 N	Cape Paximada
EN 87	Vein from en échelon system	35 2 79603 E / 42 03484 N	Cape Paximada
EN 88	Quartz vein with host rock	35 2 79603 E / 42 03484 N	Cape Paximada

Length	Aperture	L / W	Length	Aperture	L / W
13,0	2,0	6,5	30,0	2,0	15,0
20,0	3,0	6,7	30,0	2,0	15,0
12,0	1,7	7,1	23,0	1,5	15,3
23,0	3,0	7,7	20,0	1,3	15,4
48,0	6,0	8,0	8,0	0,5	16,0
24,0	3,0	8,0	107,0	5,0	21,4
24,0	3,0	8,0	54,0	2,5	21,6
19,0	2,2	8,6	26,0	1,2	21,7
40,0	4,5	8,9	23,0	1,0	23,0
12,0	1,3	9,2	17,0	0,7	24,3
56,0	6,0	9,3	34,0	1,4	24,3
51,0	5,2	9,8	66,0	2,7	24,4
40,0	4,0	10,0	12,5	0,5	25,0
40,0	4,0	10,0	22,0	0,8	27,5
40,0	4,0	10,0	112,0	4,0	28,0
13,0	1,3	10,0	20,0	0,7	28,6
25,0	2,5	10,0	25,0	0,8	31,2
27,0	2,6	10,4	160,0	5,0	32,0
19,0	1,8	10,6	13,0	0,4	32,5
32,0	3,0	10,7	38,0	1,1	34,5
28,0	2,5	11,2	42,0	1,2	35,0
44,0	3,8	11,6	18,0	0,5	36,0
29,0	2,5	11,6	128,0	3,0	42,7
49,0	4,2	11,7	44,0	1,0	44,0
47,0	4,0	11,8	18,0	0,4	45,0
120,0	10,0	12,0	118,0	2,5	47,2
30,0	2,5	12,0	205,0	4,0	51,2
31,0	2,5	12,4	16,0	0,3	53,3
50,0	4,0	12,5	183,0	2,7	67,8
26,0	2,0	13,0	48,0	0,7	68,6
39,0	3,0	13,0	212,0	3,0	70,7
29,0	2,2	13,2	150,0	1,8	83,3
30,0	2,2	13,6	84,0	1,0	84,0

Acknowledgements

First of all I would like to thank Prof. Dr. Bernhard Stöckhert, who made this project possible. His valuable discussion, stimulating ideas, outstanding motivation abilities and positive thoughts are very much appreciated. Sincere thanks are extended to Prof. Dr. J. Kalthoff and Andreas Bertram for teaching, help and discussions on Fracture Mechanics. Dr. Rolf Neuser is thanked for support at the SEM. Many thanks to Dr. Klaus Röller for QMS measurements and for the help with the interpretation. I am greatful to Dr. Claudia Trepmann and Dr. Jens Steffahn for thoughtful comments on the manuscripts of the present thesis.

I am specially indepted to Antje for her inestimable help and motivation, and especially for her assistence during the last (and hardest) hours before the finishing of the present thesis!

The German Research Foundation (DFG) is greatfully acknowledged for financial support within the scope of the Collaborative Research Centre 526 “Rheology of the Earth – from the upper crust into the subduction zone”.

Curriculum Vitae

Personal Data

Date of birth	• 30.12.1975
Place of birth	• Bochum, NRW, Germany
Nationality	• German

School

1982 – 1986	• Josefs Elementary School, Essen
1986 – 1995	• Gymnasium Essen Werden

Study

10 / 1996 – 11 / 2003	• Study of Geology, Ruhr University Bochum
11 / 2003	• Graduation as “Diplom-Geologe”, Ruhr University Bochum

Employment record

12 / 2003 - recent	• Research assistant at the Ruhr University Bochum